

---

# SCALABLE VARIATIONAL BAYES METHODS FOR HAWKES PROCESSES

---

**Déborah Sulem**  
Department of Statistics  
University of Oxford  
deborah.sulem@stats.ox.ac.uk

**Vincent Rivoirard**  
Ceremade, CMRS, UMR 7534  
Université Paris-Dauphine, PSL University  
vincent.rivoirard@dauphine.fr

**Judith Rousseau**  
Department of Statistics  
University of Oxford  
judith.rousseau@stats.ox.ac.uk

December 2, 2022

## ABSTRACT

Multivariate Hawkes processes are temporal point processes extensively applied to model event data with dependence on past occurrences and interaction phenomena, e.g., neuronal spike trains, online messages, and financial transactions. In the generalised nonlinear model, *positive* and *negative* interactions between the components of the process are allowed, therefore accounting for so-called *excitation* and *inhibition* effects. In the nonparametric setting, learning the temporal dependence structure of Hawkes processes is often a computationally expensive task, all the more with Bayesian estimation methods. In general, the posterior distribution in the nonlinear Hawkes model is non-conjugate and *doubly intractable*. Moreover, existing Monte-Carlo Markov Chain methods are often slow and not scalable to high-dimensional processes in practice. Recently, efficient algorithms targeting a mean-field variational approximation of the posterior distribution have been proposed. In this work, we unify existing variational Bayes inference approaches under a general framework, that we theoretically analyse under easily verifiable conditions on the prior, the variational class, and the model. We notably apply our theory to a novel spike-and-slab variational class, that can induce sparsity through the *connectivity graph* parameter of the multivariate Hawkes model. Then, in the context of the popular sigmoid Hawkes model, we leverage existing data augmentation technique and design adaptive and sparsity-inducing mean-field variational methods. In particular, we propose a two-step algorithm based on a thresholding heuristic to select the graph parameter. Through an extensive set of numerical simulations, we demonstrate that our approach enjoys several benefits: it is computationally efficient, can reduce the dimensionality of the problem by selecting the graph parameter, and is able to adapt to the smoothness of the underlying parameter.

## 1 Introduction

Modelling point or event data with temporal dependence often implies inferring a local dependence structure between events, or estimating interaction parameters. In this context, the multivariate Hawkes model is a widely used temporal point process (TPP) model, e.g., in seismology Ogata [1999], criminology Mohler et al. [2011], finance Bacry and Muzy [2015], and social network analysis Lemonnier and Vayatis [2014]. In particular, the generalised nonlinear Hawkes model is able to account for different *types* of temporal interactions, including *excitation* and *inhibition* effects. For event data, the *excitation* phenomenon, sometimes named *contagion* or *bursting behaviour*, corresponds to empirical observation that the occurrence of an event, e.g., a post on a social media, increases the probability of observing similar events in the future, e.g., reaction comments. In contrast, the *inhibition* phenomenon refers to the opposite observation and is prominent in neuronal applications due to biological regulation mechanisms Bonnet et al. [2021], and in criminology due to the enforcement of policies Olinde and Short [2020]. In addition to its expressive

power, the multivariate Hawkes model has become popular for the interpretability of its parameter, in particular the *connectivity* or *dependence* graph parameter, which corresponds to a Granger-causal graph Eichler et al. [2017].

In general, a multivariate TPP can be described as a counting process  $N = (N_t)_{t \in \mathbb{R}} = (N_t^1, \dots, N_t^K)_{t \in \mathbb{R}}$ , where  $K \geq 1$  is the number of components (or dimensions) of the process. Each component of a TPP can represent a specific type of event (e.g., a flooding or earthquake, when modelling natural disaster events), or a particular location where events are recorded (e.g., a region or country). For each  $k = 1, \dots, K$  and time  $t$ ,  $N_t^k$  denotes the number of events that have occurred until  $t$  at component  $k$ . We note that a multivariate TPP is also equivalent to a *marked TPP* where the marks belong to the set  $\{1, 2, \dots, K\}$  Daley and Vere-Jones [2007]. Therefore, multivariate TPPs are of interest for jointly modelling the occurrences of events of distinct types, or recorded at multiple places. In TPPs, the probability distribution of events is characterised by a conditional intensity function (or, more concisely, the intensity), denoted  $(\lambda_t)_t = (\lambda_t^1, \dots, \lambda_t^K)_{t \in \mathbb{R}}$ . This function is informally the infinitesimal probability rate of event, conditionally on the history of the process, i.e.,

$$\lambda_t^k dt = \mathbb{P} \left[ N_t^k \text{ has a jump in } [t, t + dt] \middle| \mathcal{G}_t \right], \quad k = 1, \dots, K, \quad t \in \mathbb{R},$$

where  $\mathcal{G}_t = \sigma(N_s, s < t)$  denotes the history of the process until time  $t$ . In the nonlinear Hawkes model, the intensity is defined as

$$\lambda_t^k = \phi_k \left( \nu_k + \sum_{l=1}^K \int_{-\infty}^{t^-} h_{lk}(t-s) dN_s^l \right), \quad k = 1, \dots, K, \quad (1)$$

where for each  $k$ ,  $\phi_k : \mathbb{R} \rightarrow \mathbb{R}^+$  is a *link* or *activation* function,  $\nu_k > 0$  is a *background* or *spontaneous* rate of events, and for each  $l$ ,  $h_{lk} : \mathbb{R}^+ \rightarrow \mathbb{R}$  is the *interaction function* or *triggering kernel* from  $N^l$  onto  $N^k$ . On the one hand, the parameter  $\nu = (\nu_k)_k$  characterises the external influence of the environment on the process. Here, we assume that this parameter is constant over time. On the other hand, the functions  $h = (h_{lk})_{l,k}$  parametrise the endogeneous and *causal* influence of past events. In particular, for any  $l, k$ , there exists a *causal* relationship from  $N^l$  to  $N^k$ , or in other words,  $N^k$  is *locally-dependent* of  $N^l$ , if and only if  $h_{lk} \neq 0$  Eichler et al. [2017]. Moreover, defining for each  $l, k$ ,  $\delta_{lk} := \mathbb{1}_{h_{lk} \neq 0}$ , the parameter  $\delta := (\delta_{lk})_{l,k} \in \{0, 1\}^{K \times K}$  defines a Granger-causal graph, called the *connectivity* graph. Finally, the link functions  $\phi = (\phi_k)_k$ 's are in general nonlinear and monotone non-decreasing. They are an essential part of the model chosen by the practitioner, and frequently set as ReLU functions  $\phi_k(x) = \max(x, 0) = (x)_+$  Hansen et al. [2015], Chen et al. [2017], Costa et al. [2020], Lu and Abergel [2018], Bonnet et al. [2021], Deutsch and Ross [2022], sigmoid-type functions, e.g.,  $\phi_k(x) = \theta_k(1 + e^x)^{-1}$  with a scale parameter  $\theta_k > 0$  Zhou et al. [2021b,a], Malem-Shinitski et al. [2021], softplus functions  $\phi_k(x) = \log(1 + e^x)$  Mei and Eisner [2017], or clipped exponential functions, i.e.,  $\phi_k(x) = \min(e^x, \Lambda_k)$  with a clip parameter  $\Lambda_k > 0$  Gerhard et al. [2017], Carstensen et al. [2010]. When all the interaction functions are non-negative and  $\phi_k(x) = x$  for every  $k$ , the intensity (1) corresponds to the linear Hawkes model. Defining the *underlying* or *linear* intensity as

$$\tilde{\lambda}_t^k = \nu_k + \sum_{l=1}^K \int_{-\infty}^{t^-} h_{lk}(t-s) dN_s^l, \quad k = 1, \dots, K, \quad (2)$$

for any  $t \in \mathbb{R}$ , the nonlinear intensity (1) can be re-written as  $\lambda_t^k = \phi_k(\tilde{\lambda}_t^k)$ .

Estimating the parameter of the Hawkes model, denoted  $f = (\nu, h)$ , and the graph parameter  $\delta$ , has been theoretically studied in the Bayesian nonparametric framework and the linear model by Donnet et al. [2020] and in general nonlinear models in Sulem et al. [2021]. Moreover, the properties of nonparametric penalised projection estimators have been analysed in the linear model by Hansen et al. [2015] and Bacry et al. [2020] for high-dimensional linear processes, and by Cai et al. [2021] in nonlinear models. Yet, in practice, most methods rely on a parametric framework. In particular, a popular approach in the ReLU Hawkes model consists in setting an exponential form of the interaction functions, i.e.,  $h_{lk}(x) = \alpha_{lk} e^{-\beta_{lk} x}$ . Then, the estimation of  $(\alpha, \beta) = (\alpha_{lk}, \beta_{lk})_{l,k}$  can be performed via the maximum likelihood estimate (MLE) Bonnet et al. [2021], Wang et al. [2016], or a Monte-Carlo Markov Chain (MCMC) method Deutsch and Ross [2022]. Besides, a nonparametric approximated MLE is proposed in Lemonnier and Vayatis [2014] for the ReLU model. In sigmoid models, a data augmentation strategy derived from Donner and Opper [2019] and Adams et al. [2009] for Poisson point processes, allows to design Gibbs sampling algorithms. Such MCMC sampler has been notably proposed in a time-varying Hawkes model and semi-parametric estimation framework Zhou et al. [2021a], and in a Gaussian process framework in Malem-Shinitski et al. [2021]. However, these algorithms rely on a computationally expensive sampling strategy and are not efficient enough in practice for multivariate processes.

Recently, data augmentation strategies have also been used to derive variational Bayes algorithms in Hawkes models. These novel methods leverage the conjugacy of an augmented mean-field variational posterior distribution with certain families of Gaussian priors. In the linear univariate model (i.e.,  $K = 1$ ), the *self-exciting* function  $h := h_{11}$  is estimated via a transformation of a Gaussian process, e.g., a quadratic function in Zhang et al. [2020], or a sigmoid function in

Zhou et al. [2019, 2020], and an iterative mean-field variational inference (MF-VI) algorithm. In the sigmoid Hawkes model, Zhou et al. [2021b] propose an efficient variational EM algorithm, then Zhou et al. [2021a] develop a related iterative MF-VI algorithm in a time-varying and semi-parametric multivariate model. A similar type of algorithm is introduced by Malem-Shinitzki et al. [2021] in a Gaussian process framework. Nonetheless, these variational approaches have not been yet theoretically analysed. Moreover, the estimation of the graph  $\delta$  has not been considered in the variational framework, although this parameter can be of interest for scaling up these methods to high-dimensional Hawkes processes. In fact, the connectivity graph also determines the dimensionality and the sparsity of the estimation problem, similarly to the structure parameter in high-dimensional regression Ray and Szabó [2021].

In this work, we first provide a general variational Bayes estimation framework for multivariate Hawkes processes that unifies existing approaches, and theoretically analyse variational methods in this context. We notably derive concentration rates for variational posterior distributions, leveraging the general methodology of Zhang and Gao [2017] based on verifying a prior mass, a testing, and a variational class condition. We apply our general results to two variational classes of interest in the Hawkes model, namely the mean-field family and a novel spike-and-slab family, and two families of nonparametric priors. Then, we propose a novel adaptive and sparsity-inducing variational approach, based on the general methods of Zhang and Gao [2017] and Ohn and Lin [2021] for variational inference with model selection.

Next, building on existing data augmentation strategy, we design two adaptive and sparsity-inducing MF-VI algorithms in the sigmoid Hawkes model. In particular, we propose a two-step procedure based on a thresholding heuristic to select the connectivity graph parameter, which allows to reduce the computational cost for high-dimensional processes. We empirically demonstrate the effectiveness of our algorithms in an extensive set of simulations. We notably show that our adaptive variational algorithms are more computationally efficient than MCMC methods, while enjoying comparable estimation performance. Finally, our algorithms can also correctly infer the connectivity graph parameter, therefore uncovering the causality structure of the true generating process.

Additionally, we note that in the context of sigmoid Hawkes models with link function  $\phi_k(x) = \theta_k(1 + e^{-x})^{-1}$  with  $\theta_k > 0, k \in [K]$ , existing algorithms also aim at estimating the scale parameter  $\theta = (\theta_k)_k$  Apostolopoulou et al. [2019], Zhou et al. [2021b], Malem-Shinitzki et al. [2021], Zhou et al. [2021a]. However, the latter estimation problem has not been thoroughly analysed yet, neither in the Bayesian nor the frequentist frameworks. Therefore, we also extend the posterior concentration results of Sulem et al. [2021] to the latter model with unknown scale parameter  $\theta$ , and validate the use of Bayesian methods in this setup.

**Outline** We first introduce some useful notation. Then, in Section 2, we describe our model and inference setup. Section 3 contains our general results, and their applications to prior and variational families of interest in the Hawkes model. In Section 4, we focus on the sigmoid Hawkes model and present our novel adaptive and sparsity-inducing variational algorithms. Finally, Section 5 contains the results of our numerical experiments. The proofs of our main results are reported in Appendix A.

**Notations.** For a function  $h$ , we denote  $\|h\|_1 = \int_{\mathbb{R}} |h(x)| dx$  the  $L_1$ -norm,  $\|h\|_2 = \sqrt{\int_{\mathbb{R}} h^2(x) dx}$  the  $L_2$ -norm,  $\|h\|_\infty = \sup_{x \in \mathbb{R}} |h(x)|$  the supremum norm, and  $h^+ = \max(h, 0)$ ,  $h^- = \max(-h, 0)$  its positive and negative parts. For a  $K \times K$  matrix  $A$ , we denote  $r(A)$  its spectral radius,  $\|A\|$  its spectral norm, and  $\text{tr}(A)$  its trace. For a vector  $u \in \mathbb{R}^K$ ,  $\|u\|_1 = \sum_{k=1}^K |u_k|$ . The notation  $k \in [K]$  is used for  $k \in \{1, \dots, K\}$ . For a set  $B$  and  $k \in [K]$ , we denote  $N^k(B)$  the number of events of  $N^k$  in  $B$  and  $N^k|_B$  the point process measure restricted to the set  $B$ . For random processes, the notation  $\stackrel{\mathcal{L}}{=}$  corresponds to equality in distribution. We also denote  $\mathcal{N}(u, \mathcal{H}_0, d)$  the covering number of a set  $\mathcal{H}_0$  by balls of radius  $u$  w.r.t. a metric  $d$ . For any  $k \in [K]$ , let  $\mu_k^0 = \mathbb{E}_0[\lambda_i^k(f_0)]$  be the mean of  $\lambda_i^k(f_0)$  under the stationary distribution  $\mathbb{P}_0$ . For a set  $\Omega$ , its complement is denoted  $\Omega^c$ . We also use the notations  $u_T \lesssim v_T$  if  $|u_T/v_T|$  is bounded when  $T \rightarrow \infty$ ,  $u_T \gtrsim v_T$  if  $|v_T/u_T|$  is bounded and  $u_T \asymp v_T$  if  $|u_T/v_T|$  and  $|v_T/u_T|$  are bounded. We recall that a function  $\phi$  is  $L$ -Lipschitz, if for any  $(x, x') \in \mathbb{R}^2$ ,  $|\phi(x) - \phi(x')| \leq L|x - x'|$ . We denote  $\mathbb{1}_n$  and  $\mathbf{0}_n$  the all-ones and all-zeros vectors of size  $n$ . Finally, we denote  $\mathcal{H}(\beta, L_0)$  the class of  $\beta$ -smooth functions with radius  $L_0$ .

## 2 Model and inference setup

In this section, we first recall the formal definition of multivariate Hawkes processes and our main assumptions. Then, we describe our general variational Bayes inference framework.

## 2.1 Multivariate Hawkes processes

Let  $(\mathcal{X}, \mathcal{G}, \mathbb{P})$  be a probability space,  $N = (N_t)_{t \in \mathbb{R}} = (N_t^1, \dots, N_t^K)_{t \in \mathbb{R}}$  be a  $K$ -dimensional temporal point process, and  $\{\mathcal{G}_t\}_{t \in \mathbb{R}}$  be the filtration such that  $\mathcal{G}_t = \sigma(N_s, s \leq t) \subset \mathcal{G}$ .

**Definition 2.1** (Multivariate nonlinear Hawkes process). *A TPP  $(N_t)_t$  is a Hawkes process adapted to  $\mathcal{G}$  if*

- i) *almost surely,  $\forall k, l \in [K]$ ,  $(N_t^k)_t$  and  $(N_t^l)_t$  never jump simultaneously;*
- ii) *for all  $k \in [K]$ , the  $\mathcal{G}_t$ -predictable conditional intensity function of  $N^k$  at  $t \in \mathbb{R}$  is given by (1).*

An alternative definition of Hawkes processes can be formulated via a system of stochastic equations (see for instance Bremaud and Massoulié [1996]).

**Definition 2.2.** *Let  $Q$  be a  $K$ -dimensional Poisson point process on  $(0, +\infty) \times (0, +\infty)^K$  with unit intensity and  $N_0$  a point process measure on  $\mathbb{R}_-$ . If  $N$  is the pathwise unique strong solution of the following system of equations*

$$\begin{cases} N^k = N_0^k + \int_{(0, +\infty) \times (0, +\infty)^K} \delta(u) \mathbb{1}_{\theta \leq \lambda^k(u)} Q^k(du, d\theta), \\ \lambda^k(u) = \phi_k \left( v_k + \sum_{l=1}^K \int_{u-A}^u h_{lk}(u-s) dN_s^l \right), \quad u > 0, \quad k \in [K] \end{cases}$$

with  $\delta(\cdot)$  the Dirac delta function, then  $N$  is a Hawkes process with parameter  $v = (v_k)$ ,  $h = (h_{lk})_{lk}$ , link functions  $(\phi_k)_k$  and initial measure  $N_0$  on  $\mathbb{R}_-$  driven by  $(Q_t)_{t \geq 0}$

We consider finite-memory and stationary Hawkes processes. More precisely, we assume that the interaction functions  $(h_{lk})_{l,k}$  have a bounded support included in  $[0, A]$ , where  $A > 0$  is known. We also assume that the activation functions  $(\phi_k)_k$  are monotone non-decreasing,  $L$ -Lipschitz,  $L > 0$ , and that one of the two following conditions is satisfied (see for instance Bremaud and Massoulié [1996], Deutsch and Ross [2022], or Sulem et al. [2021]):

- (C1) The matrix  $S^+ = (S_{lk}^+)_{l,k} \in \mathbb{R}_+^{K \times K}$  with  $S_{lk}^+ = L \|h_{lk}^+\|_1$ ,  $\forall l, k$ , satisfies  $\|S^+\| < 1$ ;
- (C2) For any  $k \in [K]$ , the link function  $\phi_k$  is bounded, i.e.,  $\exists \Lambda_k > 0, \forall x \in \mathbb{R}, 0 \leq \phi_k(x) \leq \Lambda_k$ .

## 2.2 Bayesian inference framework

We assume that we observe a stationary  $K$ -dimensional Hawkes process  $N$  with unknown parameter  $f_0 = (v_0, h_0)$  and known link functions  $(\phi_k)_k$  such that  $(\phi, h_0)$  verifies condition (C1), i.e.,  $\|S_0^+\| < 1$  with  $S_0^+ = (L \|h_{lk}^{0+}\|_1)_{l,k}$ . Given an observation of  $N$  over a time window  $[-A, T]$ , with  $T > 0$ , the log-likelihood function for a parameter  $f = (v, h)$  is given by

$$L_T(f) := \sum_{k=1}^K L_T^k(f), \quad L_T^k(f) = \left[ \int_0^T \log(\lambda_t^k(f)) dN_t^k - \int_0^T \lambda_t^k(f) dt \right]. \quad (3)$$

We then denote  $\mathbb{P}_f(\cdot | \mathcal{G}_0)$  the conditional distribution of  $N$  defined as

$$d\mathbb{P}_f(\cdot | \mathcal{G}_0) = e^{L_T(f) - L_T(f_0)} \mathbb{P}_0(\cdot | \mathcal{G}_0).$$

We also denote  $\mathbb{E}_0$  and  $\mathbb{E}_f$  the expectations associated to  $\mathbb{P}_0(\cdot | \mathcal{G}_0)$  and  $\mathbb{P}_f(\cdot | \mathcal{G}_0)$ . With a slight abuse of notation, we will drop the notation  $\mathcal{G}_0$ . Let  $\mathcal{F}$  be the parameter space and  $\Pi$  be a prior distribution on  $\mathcal{F}$ . The posterior distribution for any subset  $B \subset \mathcal{F}$  is defined as

$$\Pi(B|N) = \frac{\int_B \exp(L_T(f)) d\Pi(f)}{\int_{\mathcal{F}} \exp(L_T(f)) d\Pi(f)} =: \frac{N_T(B)}{D_T}, \quad D_T := \int_{\mathcal{F}} \exp(L_T(f)) d\Pi(f). \quad (4)$$

The posterior distribution (4) is often said to be *doubly intractable*, because of the integrals in the log-likelihood function (3) and in the denominator  $D_T$ . In general, it is expensive to compute since the parameter  $f$  includes  $K^2$  functions.

**Remark 2.3.** *Let, for each component  $k \in [K]$ ,  $f_k = (v_k, (h_{lk})_{l=1, \dots, K}) \in \mathcal{F}_k$  so that  $f = (f_k)_k$  and  $\mathcal{F} = \mathcal{F}_1 \times \dots \times \mathcal{F}_K$ . If the prior distribution verifies  $\Pi(f) = \prod_k \Pi_k(f_k)$ , then, given the expressions of the log-likelihood function (3) and the intensity (1), we have that  $L_T^k(f) = L_T^k(f_k)$  and the posterior distribution can be written as*

$$\Pi(B|N) = \prod_k \Pi_k(B_k|N), \quad \Pi_k(B_k|N) = \frac{\int_{B_k} \exp(L_T^k(f_k)) d\Pi_k(f_k)}{\int_{\mathcal{F}_k} \exp(L_T^k(f_k)) d\Pi_k(f_k)}, \quad B_k \subset \mathcal{F}_k, \quad \forall k \in [K].$$

The latter factorisation implies that each factor  $\Pi_k(\cdot | N)$  of the posterior distribution can be independently computed - nonetheless, given the whole data  $N$ .

For the prior distribution  $\Pi$ , we use a construction similar to Donnet et al. [2020] and Sulem et al. [2021]. For ease of exposition, we consider link functions  $(\phi_k)_k$  that are injective on  $\mathbb{R}$  (see Assumption 3.1 in Section 3.1), however, our construction can be easily adapted if for each  $k$ ,  $\phi_k$  is injective on a subset of  $\mathbb{R}$ . We define a prior on  $f$  of the form

$$d\Pi(f) = d\Pi_h(h) \prod_k d\Pi_v(v_k).$$

We use a distribution  $\Pi_v$  absolutely continuous with respect to the Lebesgue measure, with positive and continuous probability density on  $\mathbb{R}^+ \setminus \{0\}$ , e.g., a gamma distribution. For  $h = (h_{lk})_{l,k}$ , we use the hierarchical spike-and-slab prior of Donnet et al. [2020] based on the connectivity graph parameter  $\delta$ . For each  $l, k$ , we consider the following reparametrisation

$$h_{lk} = \delta_{lk} \bar{h}_{lk}, \quad \delta_{l,k} \in \{0, 1\}, \quad \bar{h}_{lk} \in \mathcal{H}',$$

so that  $\delta = (\delta_{lk})_{l,k}$  is the connectivity graph. We then consider  $\delta \sim \Pi_\delta$ , where  $\Pi_\delta$  is a prior distribution on  $\{0, 1\}^{K^2}$ . Next, conditionally on  $\delta$ , we use a truncated distribution on  $h|\delta$  of the form

$$d\Pi_h(h|\delta) = \left( \prod_{l,k} d\tilde{\Pi}_{h|\delta}(h_{lk}) \right) \mathbb{1}_{\|S^+\| < 1}(h),$$

or simply  $d\Pi_h(h) = \prod_{l,k} d\tilde{\Pi}_h(h_{lk})$  if  $(\phi_k)_k$  satisfies **(C2)**, with

$$\tilde{\Pi}_{h|\delta}(h_{lk}) = \delta_{lk} \tilde{\Pi}_h(\bar{h}_{lk}) + (1 - \delta_{lk}) \delta_{\{0\}}(\bar{h}_{lk}),$$

where  $\delta_{\{0\}}$  is the Dirac measure at  $h_{lk} = 0$  and  $\tilde{\Pi}_h$  is a nonparametric prior distribution on  $\mathcal{H}'$ , e.g., a Gaussian process, random histogram, or spline prior (see Sulem et al. [2021]).

**Remark 2.4.** From the previous construction, one can see that the graph parameter  $\delta \in \{0, 1\}^{K^2}$  defines the sparsity structure of  $h$ . Besides, one can also use a soft-sparse (or shrinkage) prior distribution for  $\tilde{\Pi}_h$ .

### 2.3 Variational Bayes framework

Previous work on Hawkes processes underlines the difficulty of computing the nonparametric posterior distribution (4) Donnet et al. [2020], Zhou et al. [2021a], Malem-Shinitzki et al. [2021], and scaling up Bayesian methods to high-dimensional processes. Alternatively, variational Bayes methods consist in approximating the posterior distribution within a *variational* class of “convenient” distributions. We first recall the definition of the Kullback-Leibler divergence. For any two distributions  $Q$  and  $Q'$  on  $\mathcal{F}$ , it is defined as

$$KL(Q||Q') := \begin{cases} \int \log \frac{dQ}{dQ'} dQ, & \text{if } Q \ll Q' \\ +\infty, & \text{otherwise} \end{cases}.$$

Let  $\mathcal{V}$  be an approximating family of distributions on  $\mathcal{F}$ . The *variational posterior* distribution, denoted  $\hat{Q}$ , is defined as the best approximation of the posterior distribution within  $\mathcal{V}$ , with respect to the Kullback-Leibler divergence, i.e.,

$$\hat{Q} := \arg \min_{Q \in \mathcal{V}} KL(Q||\Pi(\cdot|N)). \quad (5)$$

From Remark 2.3, we note that the variational distribution also factorises in  $K$  factors,  $\hat{Q} = \prod_k \hat{Q}_k$  where each factor  $\hat{Q}_k$  approximates  $\Pi_k(\cdot|N)$ . Therefore, one can choose a variational class  $\mathcal{V}'$  of distributions on  $\mathcal{F}_1$  and define  $\mathcal{V} = \mathcal{V}'^{\otimes K}$ .

**Mean-field variational inference** When the parameter of interest, say  $\vartheta$ , is multi-dimensional, i.e.,  $\vartheta = (\vartheta_1, \dots, \vartheta_D)$  with  $D > 1$ , a common choice of variational class is a mean-field family Zhang and Gao [2017], Ohn and Lin [2021], that can be defined as

$$\mathcal{V}_{MF} = \left\{ Q; dQ(\vartheta) = \prod_{d=1}^D dQ_d(\vartheta_d) \right\}.$$

Then, the mean-field variational posterior distribution corresponds to  $\hat{Q} = \arg \min_{Q \in \mathcal{V}_{MF}} KL(Q||\Pi(\cdot|N)) = \prod_{d=1}^D \hat{Q}_d$ . Note that the mean-field family removes correlation between coordinates of the parameter. From now on, we assume that the mean-field variational posterior distribution has a density with respect to a dominating measure  $\mu = \prod_d \mu_d$ , and with a slight abuse of notation, we denote  $\hat{Q}$  both the distribution and density with respect to  $\mu$ . An interesting

result from Bishop and Nasrabadi [2006], Donnet et al. [2020] is that the mean-field variational posterior distribution verifies, for each  $d \in [D]$ ,

$$\hat{Q}_d(\vartheta_d) \propto \exp\left\{\mathbb{E}_{\hat{Q}_{-d}}[\log p(\vartheta, N)]\right\}, \quad (6)$$

where  $p(\vartheta, N)$  is the joint density of the observations and the parameter with respect to  $\prod_d \mu_d \times \mu_N$  with  $\mu_N$  the data density, and  $\hat{Q}_{-d} := \prod_{d' \neq d} \hat{Q}_{d'}$ . This property (6) can be used to design efficient algorithms for computing the variational posterior, such as the coordinate-ascent variational inference algorithm. In the sigmoid Hawkes model, for which  $\phi_k(x) = \theta_k(1 + e^x)^{-1}, \forall k$ , a mean-field approximating class is used within a latent variable augmentation scheme, by breaking only the correlation between the original parameter and the latent variable Malem-Shinitzki et al. [2021], Zhou et al. [2021a]. We therefore consider a general setting where the log-likelihood function of the nonlinear Hawkes model can be augmented with some latent variable  $z \in \mathcal{Z}$  and denoted  $L_T^A(f, z)$ . Then, an augmented posterior distribution can be defined as

$$\Pi_A(B|N) = \frac{\int_B \exp(L_T^A(f, z)) d(\Pi(f) \times \mathbb{P}_A(z))}{\int_{\mathcal{F} \times \mathcal{Z}} \exp(L_T^A(f, z)) d(\Pi(f) \times \mathbb{P}_A(z))}, \quad B \subset \mathcal{F} \times \mathcal{Z},$$

where  $\mathbb{P}_A$  is a prior distribution on  $z$  which has a density with respect to a dominating measure  $\mu_z$ . The approximating mean-field family of  $\Pi_A(\cdot|N)$  is then defined as

$$\mathcal{V}_{AMF} = \{Q : \mathcal{F} \times \mathcal{Z} \rightarrow [0, 1]; Q(f, z) = Q_1(f)Q_2(z)\}.$$

Thus, using property (6), the (augmented) mean-field variational posterior defined as

$$\hat{Q}_{AMF}(f, z) := \arg \min_{Q \in \mathcal{V}_{AMF}} KL(Q(f, z) || \Pi_A(f, z|N)) =: \hat{Q}_1(f)\hat{Q}_2(z), \quad (7)$$

also verifies

$$\begin{aligned} \hat{Q}_1(f) &\propto \exp\left\{\mathbb{E}_{\hat{Q}_2}[\log p(f, z, N)]\right\}, \\ \hat{Q}_2(z) &\propto \exp\left\{\mathbb{E}_{\hat{Q}_1}[\log p(f, z, N)]\right\}, \end{aligned}$$

where  $p(f, z, N)$  is the joint density of the parameter, the latent variable, and the observations with respect to the measure  $\prod_d \mu_d \times \mu_z \times \mu_N$ .

**Spike-and-slab variational inference** Another variational class of interest in the context of sparse and high-dimensional models is the spike-and-slab variational family. In the multivariate Hawkes model, we introduce the following spike-and-slab variational family, inspired by the spike-and-slab prior from Section 2.2.

**Definition 2.5** (Spike-and-slab variational class). *In the Hawkes model with parameter  $f = (v, h)$  and connectivity graph  $\delta$ , the spike-and-slab variational family can be defined as*

$$\mathcal{V}_{SAS} = \left\{Q; dQ(f) = dQ_\delta(\delta)dQ_{f|\delta}(f) = dQ_\delta(\delta)dQ_{f|\delta}(v, \delta h)\right\}.$$

We note that if  $Q_\delta$  is deterministic, i.e.,  $Q_\delta$  is the Dirac measure at some  $\delta' \in \{0, 1\}^{K \times K}$ , then  $\mathcal{V}_{SAS}$  corresponds to a variational family where the graph parameter is fixed, i.e., the variational posterior has a certain sparsity structure. Moreover, if  $Q_\delta$  is given a factorised form, i.e.,  $Q_\delta(\delta) = \prod_{l,k} \tilde{Q}_\delta(\delta_{lk})$ , then  $\mathcal{V}_{SAS}$  corresponds to a mean-field variational family. While standard MCMC methods using spike-and-slab priors are generally untractable, it is sometimes possible to design spike-and-slab variational inference algorithms that enjoy good computational properties (see for instance Titsias and Lázaro-Gredilla [2011], Ray and Szabó [2021] in sparse linear regression).

**Variational inference with model selection** More generally, variational inference algorithms aim at optimising a lower bound of the marginal log-likelihood, called the evidence lower bound (ELBO), and defined as

$$ELBO(Q) := \mathbb{E}_Q \left[ \log \frac{p(f, N)}{Q(f)} \right], \quad Q \in \mathcal{V}, \quad (8)$$

where  $p(f, N)$  is the joint distribution of the parameter and the data. The ELBO can also be used within a model-selection variational methodology, and we recall here the two related approaches of Zhang and Gao [2017] and Ohn and Lin [2021]. Let  $\mathcal{M}$  be a set of models and for each  $m \in \mathcal{M}$ , let  $\Pi_m$  be a prior distribution on  $\mathcal{M}$  and  $\mathcal{V}^m$  be a variational class. The variational posterior in model  $m$  is defined  $\hat{Q}^m = \arg \min_{Q \in \mathcal{V}^m} KL(Q || \Pi(\cdot|N))$ . Then, a *model-selection* variational posterior, which lies in a selected model, is defined by Zhang and Gao [2017] as

$$\hat{Q} := \hat{Q}_{\hat{m}}, \quad \hat{m} := \arg \max_{m \in \mathcal{M}} ELBO(\hat{Q}^m). \quad (9)$$

We note that the approximating variational family in this case is  $\mathcal{V} = \bigcup_{m \in \mathcal{M}} \mathcal{V}^m$ . Another possibility is to construct an *adaptive* variational posterior as a mixture of distributions over the different models Ohn and Lin [2021], i.e.,

$$\hat{Q}(f) = \sum_{m \in \mathcal{M}} \hat{\gamma}_m \hat{Q}_m, \quad (10)$$

where  $\{\hat{\gamma}_m\}_{m \in \mathcal{M}}$  are marginal probabilities defined as

$$\hat{\gamma}_m = \frac{\Pi_m(m) \exp\{ELBO(\hat{Q}_m)\}}{\sum_{m \in \mathcal{M}} \Pi_m(m) \exp\{ELBO(\hat{Q}_m)\}}, \quad \forall m \in \mathcal{M}. \quad (11)$$

In this case, the variational family is

$$\mathcal{V} = \left\{ \sum_{m \in \mathcal{M}} \alpha_m Q_m; \sum_m \alpha_m = 1, \alpha_m \geq 0, Q_m \in \mathcal{V}^m, \forall m \right\}.$$

In Section 3.2.2, we will use this approach to induce sparsity and achieve adaptivity in our variational method. In our context of multivariate Hawkes processes, a ‘‘model’’  $m$  will correspond to the sparsity structure and dimensionality of  $h$ , i.e., a graph parameter  $\delta$  and the truncation level in a basis decomposition for each non-null function  $h_{lk}$ .

### 3 Main results

In this section, we provide theoretical guarantees for using variational Bayes methods to estimate the parameter of nonlinear Hawkes processes. We first derive the concentration rate of the variational posterior distribution (5), under general conditions on the model, the prior distribution, and the variational family. Then, we apply our results to variational methods of practical interest.

#### 3.1 Variational posterior concentration rates

We recall that in our setting, the link functions  $\phi = (\phi_k)_k$  in the nonlinear intensity (1) are fixed by the statistician and therefore known *a priori*. To analyse the variational posterior distribution, we first state a general assumption that guarantees the concentration of the posterior distribution (4) in the nonlinear Hawkes model (see Sulem et al. [2021]).

**Assumption 3.1.** *For a parameter  $f$ , we assume that there exists  $\varepsilon > 0$  such that for each  $k \in [K]$ , the link function  $\phi_k$  restricted to  $I_k = (v_k - \max_{l \in [K]} \|h_{lk}^-\|_\infty - \varepsilon, v_k + \max_{l \in [K]} \|h_{lk}^+\|_\infty + \varepsilon)$  is bijective from  $I_k$  to  $J_k = \phi_k(I_k)$  and its inverse is  $L'$ -Lipschitz on  $J_k$ , with  $L' > 0$ . We also assume that at least one of the two following conditions is satisfied.*

i) *For any  $k \in [K]$ ,  $\inf_{x \in \mathbb{R}} \phi_k(x) > 0$ .*

ii) *For any  $k \in [K]$ ,  $\phi_k > 0$ , and  $\sqrt{\phi_k}$  and  $\log \phi_k$  are  $L_1$ -Lipschitz with  $L_1 > 0$ .*

Assumption 3.1 is needed in Sulem et al. [2021] to prove the posterior concentration rates, and is verified for commonly used link functions (see Example 1 in Sulem et al. [2021]). We also need this assumption to obtain the concentration of the variational posterior distribution since our proofs leverage this existing theory.

We define the parameter space  $\mathcal{F}$  as follows

$$\mathcal{H}' = \{h : [0, A] \rightarrow \mathbb{R}; \|h\|_\infty < \infty\}, \quad \mathcal{H} = \left\{ h = (h_{lk})_{l,k=1}^K \in \mathcal{H}'^{K^2}; (h, \phi) \text{ satisfy (C1) or (C2)} \right\},$$

$$\mathcal{F} = \left\{ f = (v, h) \in (\mathbb{R}_+ \setminus \{0\})^K \times \mathcal{H}; (f, \phi) \text{ satisfies Assumption 3.1} \right\},$$

and the  $L_1$ -distance for any  $f, f' \in \mathcal{F}$  as

$$\|f - f'\|_1 := \|v - v'\|_1 + \|h - h'\|_1, \quad \|h - h'\|_1 := \sum_{l,k=1}^K \|h_{lk} - h'_{lk}\|_1, \quad \|v - v'\|_1 := \sum_k |v_k - v'_k|.$$

In our main assumptions, we will consider the following neighbourhood around  $f_0$  in supremum norm

$$B_\infty(\varepsilon) = \left\{ f \in \mathcal{F}; v_k^0 \leq v_k \leq v_k^0 + \varepsilon, h_{lk}^0 \leq h_{lk} \leq h_{lk}^0 + \varepsilon, (l, k) \in [K]^2 \right\}, \quad \varepsilon > 0.$$

Finally, we define

$$\kappa_T := 10(\log T)^r, \quad (12)$$

with  $r = 0$  if  $(\phi_k)_k$  satisfies Assumption 3.1 (i), and  $r = 1$  if  $(\phi_k)_k$  satisfies Assumption 3.1 (ii).

**Theorem 3.2.** Let  $N$  be a Hawkes process with link functions  $\phi = (\phi_k)_k$  and parameter  $f_0 = (v_0, h_0)$  such that  $(\phi, f_0)$  satisfy Assumption 3.1. Let  $\epsilon_T = o(1/\sqrt{\kappa_T})$  be a positive sequence verifying  $\log^3 T = O(T\epsilon_T^2)$ ,  $\Pi$  be a prior distribution on  $\mathcal{F}$  and  $\mathcal{V}$  be a variational family of distributions on  $\mathcal{F}$ . We assume that the following conditions are satisfied for  $T$  large enough.

(A0) There exists  $c_1 > 0$  such that  $\Pi(B_\infty(\epsilon_T)) \geq e^{-c_1 T \epsilon_T^2}$ .

(A1) There exist  $\mathcal{H}_T \subset \mathcal{H}$ ,  $\zeta_0 > 0$ , and  $x_0 > 0$  such that  $\Pi(\mathcal{H}_T^c) = o(e^{-(\kappa_T + c_1)T \epsilon_T^2})$  and  $\log \mathcal{N}(\zeta_0 \epsilon_T, \mathcal{H}_T, \|\cdot\|_1) \leq x_0 T \epsilon_T^2$ .

(A2) There exists  $Q \in \mathcal{V}$  such that  $\text{supp}(Q) \subset B_\infty(\epsilon_T)$  and  $KL(Q|\Pi) = O(\kappa_T T \epsilon_T^2)$ .

Then, for any  $M_T \rightarrow \infty$  and  $\hat{Q}$  defined in (5), we have that

$$\hat{Q}(\|f - f_0\|_1 > M_T \sqrt{\kappa_T} \epsilon_T) \xrightarrow{T \rightarrow \infty} 0 \quad \mathbb{P}_0 - a.s.,$$

or equivalently,

$$\mathbb{E}_0 \left[ \hat{Q}(\|f - f_0\|_1 > M_T \sqrt{\kappa_T} \epsilon_T) \right] \xrightarrow{T \rightarrow \infty} 0.$$

**Remark 3.3.** Similarly to Donnet et al. [2020] Sulem et al. [2021], Theorem 3.2 also holds when the neighborhoods  $B_\infty(\epsilon_T)$  around  $f_0$  in supremum norm, considered in assumptions (A0) and (A2), are replaced by the following  $L_2$ -balls

$$B_2(\epsilon_T, B) = \left\{ f \in \mathcal{F}; \max_k |v_k - v_k^0| \leq \epsilon_T, \max_{l,k} \|h_{lk} - h_{lk}^0\|_2 \leq \epsilon_T, \max_l v_l + \max_k \|h_{kl}\|_\infty < B \right\},$$

with  $B > 0$  and  $\kappa_T$  replaced by  $\kappa'_T = 10(\log \log T)(\log T)^r$ .

**Remark 3.4.** Theorem 3.2 also holds under a more general condition on the variational family

(A2') The variational family  $\mathcal{V}$  verifies  $\min_{Q \in \mathcal{V}} KL(Q|\Pi(\cdot|N)) = O(\kappa_T T \epsilon_T^2)$ .

However, in practice, one often verifies condition (A2) and deduces (A2') using the following steps from Zhang and Gao [2017]. For any  $Q \in \mathcal{V}$ , we have that

$$KL(Q|\Pi(\cdot|N)) \leq KL(Q|\Pi) + Q(KL(d\mathbb{P}_0, d\mathbb{P}_f)) = KL(Q|\Pi) + Q(KL(\mathbb{P}_{T,f_0}, \mathbb{P}_{T,f})),$$

where we denote  $\mathbb{P}_{T,f_0} = e^{L_T(f_0)}$  and  $\mathbb{P}_{T,f} = e^{L_T(f)}$ . Using Lemma S6.1 from Sulem et al. [2021], for any  $f \in B_\infty(\epsilon_T)$ , we also have that

$$\mathbb{E}_0 [L_T(f_0) - L_T(f)] \leq \kappa_T T \epsilon_T^2.$$

Therefore, under (A2), there exists  $Q \in \mathcal{V}$  such that  $KL(Q|\Pi(\cdot|N)) = O(\kappa_T T \epsilon_T^2)$ , which implies (A2').

**Remark 3.5.** On the one hand, Assumptions (A0) and (A1) are similar to the ones of Theorem 3.2 in Sulem et al. [2021]. They are sufficient conditions for proving that the posterior concentration rate is at least as fast as  $\sqrt{\kappa_T} \epsilon_T$ . On the other hand, condition (A2) (or (A2')), is the only condition on the variational class, and informally states that this family of distributions can approximate well enough the true posterior. Nonetheless, as previously noted by Nieman et al. [2021], we could well have  $\min_{Q \in \mathcal{V}} KL(Q|\Pi(\cdot|N)) \xrightarrow{T \rightarrow \infty} \infty$  under (A2).

The proof of Theorem 3.2 is reported in Section A.2.

### 3.2 Applications to variational classes of interest

In this section, we apply our previous result to variational inference methods of interest in nonlinear Hawkes models. We consider the mean-field and spike-and-slab variational families introduced in Section 2.3, and verify our general conditions on two nonparametric prior families, namely the random histogram prior and the Gaussian process prior. We then obtain explicit concentration rates for the variational posterior distribution and for Hölder-smooth classes of functions.

We recall from Sulem et al. [2021] that in the spike-and-slab prior construction from Section 2.2, we can in fact replace assumption (A0) by

(A0\*) There exists  $c_1 > 0$  such that  $\Pi(B_\infty(\epsilon_T)|\delta = \delta_0) \geq e^{-c_1 T \epsilon_T^2/2}$  and  $\Pi_\delta(\delta = \delta_0) \geq e^{-c_1 T \epsilon_T^2/2}$ ,

and that one can choose for instance,  $\Pi_\delta = \mathcal{B}(p)^{K^2}$  with  $0 < p < 1$ , implying that the  $\delta_{jk}$ 's are i.i.d. Bernoulli random variables. Then, for any fixed  $p$ , one only needs to verify  $\Pi_{h\delta}(B_\infty(\epsilon_T)|\delta = \delta_0) \geq e^{-c_1 T \epsilon_T^2/2}$ .



### 3.2.1 Mean-field variational family

We consider the mean-field variational inference method within a latent variable augmentation scheme from Section 2.2. We recall our notation  $\mathcal{V}_{AMF}$ ,  $\hat{\mathcal{Q}}_{AMF}$  and  $\mathbb{P}_A$ , for respectively the (augmented) mean-field variational family and variational posterior, and the prior distribution on the latent variable. In this section, we apply Theorem 3.2 to  $\hat{\mathcal{Q}}_{AMF}$  and two nonparametric prior distributions of interest. Practical algorithms in this context will also be designed in Section 4 for the sigmoid Hawkes model. We first note in this scheme, the augmented prior distribution  $\Pi \times \mathbb{P}_A \in \mathcal{V}_{AMF}$ , therefore assumption **(A2)** is automatically satisfied for  $\mathcal{V}_{AMF}$ , therefore, we only need to verify conditions **(A0')** and **(A1)** on the prior distribution.

**Random histogram prior** We consider a random histogram prior for  $\tilde{\Pi}_h$ , the prior on the slabs from Section 2.2. This prior family is notably used in Donnet et al. [2020], Sulem et al. [2021], and is similar to the basis decomposition prior in Zhou et al. [2021b,a]. We consider a regular partition of  $(0, A]$ ,  $(t_j)_{j=0, \dots, J}$  with  $t_j = jA/J$  and  $J \geq 0$ , and define piecewise-constant functions as

$$h_{lk}^w(x) = \sum_{j=1}^J w_{lk}^j e_j(x), \quad e_j(x) = \frac{J}{A} \mathbb{1}_{(t_{j-1}, t_j]}(x), \quad \forall j \in [J],$$

with  $w_{lk}^j \in \mathbb{R}$ ,  $\forall l, k = 1, \dots, K$  and  $j = 1, \dots, J$ . We then consider a prior on the number of pieces  $J$ ,  $J \sim \mathcal{P}(\lambda)$  with  $\lambda > 0$ , then a normal prior distribution on each  $w_{lk}$  given  $J$ , i.e.,

$$w_{lk} | J \stackrel{\text{i.i.d.}}{\sim} \mathcal{N}(0_J, K_J), \quad K_J = \sigma_0^2 I_J, \quad \sigma_0 > 0.$$

With this prior construction, assumptions **(A0')** and **(A1)** are directly satisfied. For instance, this Gaussian random histogram prior is a particular case of the spline prior family in Sulem et al. [2021], with a spline basis of order  $q = 0$ . It would also be straightforward to verify that these conditions also hold for the shrinkage prior of Zhou et al. [2021b] based on the Laplace distribution  $p_{Lap}(w_{lk}^j; 0, b) = (2b)^{-1} \exp\{-|w_{lk}^j|/b\}$  with  $b > 0$ , and for a ‘‘locally spike-and-slab’’ prior inspired by the prior of Donnet et al. [2020], Sulem et al. [2021] such as

$$w_{lk}^j | J \stackrel{\text{i.i.d.}}{\sim} p\delta_0 + (1-p)p_{Lap}(\cdot; 0, b), \quad p \in (0, 1), \quad b > 0,$$

where  $\delta_0$  is the Dirac measure at 0.

**Proposition 3.6.** *Let  $N$  be a Hawkes process with link functions  $\phi = (\phi_k)_k$  and parameter  $f_0 = (v_0, h_0)$  such that  $(\phi, f_0)$  verify Assumption 3.1. Assume that for any  $l, k \in [K]$ ,  $h_{lk}^0 \in \mathcal{H}(\beta, L_0)$  with  $\beta \in (0, 1)$  and  $L_0 > 0$ . Then, under the above Gaussian random histogram prior, the mean-field variational distribution  $\hat{\mathcal{Q}}_1$  defined in (7) satisfies, for any  $M_T \rightarrow +\infty$ ,*

$$\hat{\mathcal{Q}}_1 \left( \|f - f_0\|_1 > M_T (\log T)^q T^{-\beta/(2\beta+1)} \right) \xrightarrow{T \rightarrow \infty} 0 \quad \mathbb{P}_0 - a.s.,$$

with  $q = 0$  if  $\phi$  verifies Assumption 3.1(i) and  $q = 1/2$  if  $\phi$  verifies Assumption 3.1(ii).

The proof of Proposition 3.6 is omitted since it is a direct application of Theorem 3.2 to mean-field variational families in the context of a latent variable augmentation scheme.

**Gaussian process prior** Gaussian process priors are commonly used for nonparametric estimation of Hawkes processes Zhang et al. [2020], Zhou et al. [2020], Malem-Shinitski et al. [2021]. We consider  $\tilde{\Pi}_h$  a centered Gaussian process distribution with covariance function  $k_{GP}$ , i.e., for each  $l, k \in [K]$  and for any  $n \geq 1$ ,  $x_1, \dots, x_n \in [0, A]$ ,

$$(h_{lk}(x_i))_{i=1, \dots, n} \sim \mathcal{N} \left( 0_n, (k_{GP}(x_i, x_j))_{i, j=1, \dots, n} \right).$$

Here, we verify assumptions **(A0')** and **(A1)** using the  $L_2$ -neighborhoods (see Remark 3.3), i.e., we check that there exist  $\mathcal{H}_T \subset \mathcal{H}$  and  $c_1, x_0, \zeta_0 > 0$  such that

$$\Pi(\mathcal{H}_T^c) \leq e^{-(\kappa_T + c_1)T\epsilon_T^2}, \quad \log \mathcal{N}(\zeta_0 \epsilon_T, \mathcal{H}_T, \|\cdot\|_1) \leq x_0 T \epsilon_T^2, \quad \Pi(B_2(\epsilon_T, B)) \geq e^{-c_1 T \epsilon_T^2}.$$

It is therefore enough to find  $\mathcal{B}_T \subset L_2([0, A])$  such that

$$\tilde{\Pi}_h(\mathcal{B}_T^c) \leq e^{-(\kappa_T + c_1)T\epsilon_T^2}, \quad \log \mathcal{N}(\zeta_0 \epsilon_T, \mathcal{B}_T, \|\cdot\|_1) \leq x_0 T \epsilon_T^2 / 2, \quad \tilde{\Pi}_h(\|h - h_{lk}^0\|_2 < \epsilon_T) \geq e^{-c_2 T \epsilon_T^2 / K^2},$$

and define  $\mathcal{H}_T = \mathcal{B}_T^{\otimes K^2}$ , since

$$\Pi(\mathcal{H}_T^c) \leq \tilde{\Pi}(\mathcal{B}_T^c), \quad \log \mathcal{N}(\zeta \epsilon_T, \mathcal{H}_T, \|\cdot\|_1) \leq 2 \log K + \mathcal{N}(\zeta_2 \epsilon_T, \mathcal{B}_T, \|\cdot\|_1), \quad \Pi(B_2(\epsilon_T, B)) \geq \prod_{l, k} \tilde{\Pi}_h(\|h - h_{lk}^0\|_2 < \epsilon_T).$$

These conditions are easily deduced from Theorem 2.1 in van der Vaart and van Zanten [2009b] that we recall here. Let  $\mathbb{H}$  be the Reproducing Kernel Hilbert Space of  $k_{GP}$  and  $\phi_{h_0}(\varepsilon)$  be the concentration function associated to  $\tilde{\Pi}_h$  defined as

$$\phi_{h_0}(\varepsilon) = \inf_{h \in \mathbb{H}, \|h - h_0\|_2 \leq \varepsilon} \|h - h_0\|_{\mathbb{H}} - \log \tilde{\Pi}(\|h\|_2 \leq \varepsilon), \quad \varepsilon > 0.$$

For any  $\varepsilon_T > 0$  such that  $\phi_{h_0}(\varepsilon_T) \leq T\varepsilon_T^2$ , there exists  $\mathcal{B}_T \subset L_2([0, A])$  satisfying

$$\tilde{\Pi}_h(\mathcal{B}_T^c) \leq e^{-CT\varepsilon_T^2}, \quad \log \mathcal{N}(3\varepsilon_T, \mathcal{B}_T, \|\cdot\|_2) \leq 6CT\varepsilon_T^2, \quad \tilde{\Pi}_h(\|h - h_{h_0}^0\|_{\infty} < 2\varepsilon_T) \geq e^{-T\varepsilon_T^2},$$

for any  $C > 1$  such that  $e^{-CT\varepsilon_T^2} < 1/2$ . Since  $\|h\|_1 \leq \sqrt{A}\|h\|_2$ , we then obtain that

$$\log \mathcal{N}(3\sqrt{A}\varepsilon_T, \mathcal{B}_T, \|\cdot\|_1) \leq \log \mathcal{N}(3\varepsilon_T, \mathcal{B}_T, \|\cdot\|_2) \leq 6CT\varepsilon_T^2,$$

and finally, that  $\log \mathcal{N}(\zeta_0\varepsilon_T, \mathcal{H}_T, \|\cdot\|_1) \leq 2\log K + 6CT\varepsilon_T^2 \leq x_0T\varepsilon_T^2$  with  $\zeta_0 = 3\sqrt{A}$ ,  $x_0 = 12C$ .

Although more general kernel functions  $k_{GP}$  could be considered, we focus on squared exponential kernels for which

$$\forall x, y \in \mathbb{R}, \quad k_{GP}(x, y; \ell) = \exp\left\{-\frac{(x - y)^2}{\ell^2}\right\}, \quad \ell \sim IV(\ell; a_0, a_1), \quad a_0, a_1 > 0,$$

where  $IV(\cdot; a_0, a_1)$  with  $a_0, a_1 > 0$  is the Inverse Gamma distribution. The squared exponential kernel is notably chosen in the variational method of Malem-Shinitski et al. [2021], and its adaptivity and near-optimality has been proved by van der Vaart and van Zanten [2009a].

**Proposition 3.7.** *Let  $N$  be a Hawkes process with link functions  $\phi = (\phi_k)_k$  and parameter  $f_0 = (v_0, h_0)$  such that  $(\phi, f_0)$  verify Assumption 3.1. Assume that for any  $l, k \in [K]$ ,  $h_{lk}^0 \in \mathcal{H}(\beta, L_0)$  with  $\beta > 0$  and  $L_0 > 0$ . Let  $\tilde{\Pi}$  be a Gaussian Process prior with squared exponential kernel  $k_{GP}$ . Then, under the above Gaussian process and inverse Gamma prior, the mean-field variational distribution  $\hat{Q}_1$  defined in (7) satisfies, for any  $M_T \rightarrow +\infty$ ,*

$$\hat{Q}_1\left(\|f - f_0\|_1 > M_T(\log \log T)^{1/2}(\log T)^q T^{-\beta/(2\beta+1)}\right) \xrightarrow{T \rightarrow \infty} 0 \quad \mathbb{P}_0 - a.s.,$$

with  $q = 1$  if  $\phi$  verifies Assumption 3.1(i) and  $q = 3/2$  if  $\phi$  verifies Assumption 3.1(ii).

Proposition 3.7 is also a direct consequence of Theorem 3.2 and van der Vaart and van Zanten [2009a], therefore its proof is omitted. In practice, the Gaussian process prior is used in variational methods for Hawkes processes when there exists a conjugate form of the mean-field variational posterior distribution, i.e.,  $\hat{Q}_1$  is itself a Gaussian process with mean function  $m_{VP}$  and kernel function  $k_{VP}$ . For nonlinear Hawkes models, this is notably the case in the sigmoid model, under the latent variable augmentation scheme recalled in Section 4.2 Malem-Shinitski et al. [2021]. Nonetheless, the computation of the Gaussian process variational distribution is often expensive for large data set, therefore Malem-Shinitski et al. [2021] further approximate the posterior distribution using the sparse Gaussian process approximation via inducing variables Titsias and Lázaro-Gredilla [2011]. This leads to an ‘‘inducing variable’’ mean-field variational posterior, which is itself a variational approximation of the original mean-field variational posterior Nieman et al. [2021]. Using the results of Nieman et al. [2021], we conjecture that we could also show that our result in Proposition 3.7 also holds for the ‘‘inducing variable’’ mean-field variational posterior.

### 3.2.2 Spike-and-slab variational family

In this section, we consider the spike-and-slab variational family  $\mathcal{V}_{SAS}$  from Definition 2.5 and first assume that the true connectivity graph parameter  $\delta_0$  is known. Then, the variational distribution on  $\delta$  reduces to a Dirac measure at  $\delta_0$ . One can then use any family of distributions for  $f|\delta_0$ , e.g., the augmented mean-field and prior families and our results in Section 3.2.1, directly apply to this context.

Now, if  $\delta_0$  is unknown, since the spike-and-slab variational posterior may not be tractable for general distributions  $Q_{\delta}(\delta)$ , we propose to infer the graph within a variational Bayes approach with model selection (see Section 2.2). To avoid ambiguity with the Hawkes *model*, we use the term *graph selection*. We then adapt the general results of Zhang and Gao [2017] and Ohn and Lin [2021] to obtain the concentration rates of the *graph selection* variational posterior and the *adaptive* variational posterior, respectively defined in (9) and (10). We recall that the graph  $\delta \in \{0, 1\}^{K \times K}$  belongs to a set of cardinality  $2^K$  for any fixed  $K \geq 1$ .

From Theorem 4.1 in Zhang and Gao [2017], the prior mass conditions are enough in this case to ensure the concentration of the variational posterior (9). More precisely, we define a *graph-selection* variational posterior as follows. For any  $\delta \in \{0, 1\}^{K^2}$ , we denote

$$\mathcal{V}_{SAS}^{(\delta)} = \{Q = Q_{f|\delta}\}, \quad \hat{Q}^{(\delta)} = \arg \min_{Q \in \mathcal{V}_{SAS}^{(\delta)}} KL(Q|\Pi(\cdot|N)), \quad \hat{\delta} = \arg \max_{\delta \in \{0, 1\}^{K \times K}} ELBO(\hat{Q}^{(\delta)}),$$

where the ELBO is defined in (8). The graph selection variational posterior distribution is then defined as

$$\hat{Q}_{GS} := \hat{Q}^{(\delta)}. \quad (13)$$

**Proposition 3.8.** *Let  $N$  be a Hawkes process with link functions  $\phi = (\phi_k)_k$ , parameter  $f_0 = (v_0, h_0)$  such that  $(\phi, f_0)$  verify Assumption 3.1. Let  $\epsilon_T = o(1/\sqrt{\kappa_T})$  be a positive sequence verifying  $\log^3 T = O(T\epsilon_T^2)$  and  $\Pi$  be a prior distribution on  $\mathcal{F}$  satisfying **(A0')** and **(A1)**. Then, for the graph selection variational posterior (13), we have that*

$$\hat{Q}_{GS} \left( \|f - f_0\|_1 > M_T \sqrt{\kappa_T} \epsilon_T \right) \xrightarrow{T \rightarrow \infty} 0 \quad \mathbb{P}_0 - a.s.$$

We note that explicit concentration rates for Hölder-smooth functions can then be derived when using the prior families of Section 3.2.1. Proposition 3.8 is a direct consequence of Theorem 3.2 and Theorem 4.1 in Zhang and Gao [2017], therefore its proof is omitted. Finally, we also obtain a similar result for the adaptive variational posterior, defined in this context as

$$\hat{Q}_{AD}(f) = \sum_{\delta \in \{0,1\}^{K \times K}} \hat{\gamma}_\delta \hat{Q}^{(\delta)}, \quad (14)$$

where  $\hat{\gamma}_\delta$  are the marginal probabilities defined as

$$\hat{\gamma}_\delta = \frac{\Pi_\delta(\delta) \exp\{ELBO(\hat{Q}^{(\delta)})\}}{\sum_{\delta \in \{0,1\}^{K \times K}} \Pi_\delta(\delta) \exp\{ELBO(\hat{Q}^{(\delta)})\}}, \quad \forall \delta \in \{0,1\}^{K \times K}.$$

We note that from Theorem 2.1 of Ohn and Lin [2021], the adaptive variational posterior can be alternatively defined as  $\hat{Q}_{AD} = \arg \min_{Q \in \mathcal{V}_{SAS}} KL(Q \parallel \Pi(\cdot | N))$  with

$$\mathcal{V}_{SAS} := \left\{ Q = \sum_{\delta \in \{0,1\}^{K \times K}} \gamma_\delta Q_{f|\delta}, \sum_{\delta} \gamma_\delta = 1, \gamma_\delta \geq 0, \forall \delta \right\}.$$

The following result is adapted from Theorem 3.6 in Ohn and Lin [2021] and directly holds under the same assumptions as Proposition 3.8.

**Proposition 3.9.** *Let  $N$  be a Hawkes process with link functions  $\phi = (\phi_k)_k$ , parameter  $f_0 = (v_0, h_0)$  such that  $(\phi, f_0)$  verify Assumption 3.1, and connectivity graph  $\delta_0$ . Let  $\epsilon_T = o(1/\sqrt{\kappa_T})$  be a positive sequence verifying  $\log^3 T = O(T\epsilon_T^2)$  and  $\Pi$  be a distribution on  $\mathcal{F}$  satisfying **(A0')** and **(A1)**. Then, for the adaptive variational posterior (14), we have that*

$$\hat{Q}_{AD} \left( \|f - f_0\|_1 > M_T \sqrt{\kappa_T} \epsilon_T \right) \xrightarrow{T \rightarrow \infty} 0 \quad \mathbb{P}_0 - a.s.$$

## 4 Adaptive mean-field variational algorithms in the sigmoid model

In this section, we consider the Hawkes model with sigmoid link functions, for which an efficient mean-field variational methodology based on data augmentation and Gaussian priors has been previously proposed Malem-Shinitski et al. [2021], Zhou et al. [2021b,a]. Here, we consider the following parametrisation of this model with link functions

$$\phi_k(x) = \theta_k \tilde{\sigma}(x), \quad \tilde{\sigma}(x) = \sigma(\alpha(x - \eta)), \quad \sigma(x) = (1 + e^{-x})^{-1}, \quad \alpha, \eta, \theta_k > 0, \quad k \in [K]. \quad (15)$$

We note that for  $\alpha = 0.1, \eta = 10$  and  $\theta_k = 20$ , the nonlinearity  $\phi_k$  is similar to the ReLU and softplus functions on  $[-\infty, 20]$  (see Figure 1 in Section 5). For this model, we first prove new concentration results for the posterior distribution, when the true scale parameter, denoted  $\theta_0 = (\theta_k^0)_k$ , is unknown. Secondly, we recall the latent variable augmentation scheme from Malem-Shinitski et al. [2021], Zhou et al. [2021b,a] and, building on this prior work, we propose a novel adaptive and sparsity-inducing mean-field variational method. In particular, our approach consists in reducing the dimensionality of the problem by inferring the connectivity graph parameter using the graph selection approach described in Section 3.2.2.

### 4.1 Posterior concentration rates with unknown scale parameter

First, we state a lemma that ensures the identifiability of the sigmoid Hawkes model with link functions (15) and unknown scale. We will use the following assumption.

**Assumption 4.1.** *For  $f = (v, h)$ , we assume that*

$$\forall k \in [K], \exists l \in [K], \exists x_2 > x_1 > 0, \exists c_* > 0, \forall x \in [x_1, x_2], h_{lk}^+(x) > c_*.$$

**Remark 4.2.** Assumption 4.1 requires that every component  $N^k$  receives some excitation effect from at least one other component. This assumption ensures that the intensity function  $\lambda_i^k(f)$  can approach its upper bound  $\theta_k$  with non-zero probability.

**Lemma 4.3.** Let  $N$  be a sigmoid Hawkes process with link functions  $(\phi_k)_k$  defined in (15), scale  $\theta$ , and parameter  $f = (\nu, h)$  satisfying Assumption 4.1. If  $N'$  is a sigmoid Hawkes process with scale  $\theta'$ , parameter  $f' = (\nu', h')$  satisfying Assumption 4.1, then

$$N \stackrel{\mathcal{L}}{=} N' \implies \nu = \nu' \quad \text{and} \quad h = h' \quad \text{and} \quad \theta = \theta'.$$

The proof of this lemma is reported in Appendix B. We now consider the problem of estimating both  $f = (\nu, h)$  and the scale parameter  $\theta$  of the link functions (15), and study the concentration properties of the posterior distribution on  $(f, \theta)$ . In this context, our parameter space is now defined as  $\mathcal{F} \times \Theta$  with  $\mathcal{F} = \mathbb{R}^K \times \mathcal{H}$  and  $\Theta = (\mathbb{R}_+ \setminus \{0\})^K$ . We note that for the sigmoid model, we do not need the background rates  $(\nu_k)$  to be positive. With  $\Pi$  a prior distribution on  $\mathcal{F} \times \Theta$ , the posterior distribution is defined as

$$\Pi(B|N) = \frac{\int_B \exp(L_T(f)) d\Pi(f, \theta)}{\int_{\mathcal{F} \times \Theta} \exp(L_T(f, \theta)) d\Pi(f, \theta)}, \quad B \subset \mathcal{F} \times \Theta. \quad (16)$$

We define the  $L_2$ -neighbourhoods around  $(f_0, \theta_0)$ , for  $B > 0$ , as

$$\tilde{B}_2(\epsilon_T, B) = \left\{ (f, \theta) \in \mathcal{F} \times \Theta; \max_k |\nu_k - \nu_k^0| \leq \epsilon_T, \max_k |\theta_k - \theta_k^0| \leq \epsilon_T, \max_{l,k} \|h_{lk} - h_{lk}^0\|_2 \leq \epsilon_T, \max_{l,k} \|h_{lk}\|_\infty < B \right\},$$

and a truncated  $L_1$ -distance on  $\mathcal{F}$ , as

$$\|f - f'\|_{1,B} = \|\nu - \nu'\|_1 + \sum_{l,k} \|h_{lk} \wedge B - h'_{lk} \wedge B\|_1, \quad f, f' \in \mathcal{F}.$$

We note that if, for  $f, f' \in \mathcal{F}$ , we have for any  $l, k$ ,  $\|h_{lk}\|_\infty \wedge \|h'_{lk}\|_\infty < B$ , then it holds that  $\|f - f'\|_{1,B} = \|f - f'\|_1$ .

**Remark 4.4.** We introduce the truncated  $L_1$ -distance to satisfy the Lipschitz condition on the inverse of the link functions in Assumption 3.1. In fact, the sigmoid inverse, i.e., the logit function  $\sigma^{-1}(x) = \log \frac{x}{x-1}$ , is not Lipschitz on  $(0, 1)$ . Therefore, this assumption does not hold in the sigmoid Hawkes model, unless the parameter space is bounded in supremum norm so that one can obtain the Lipschitz condition on a bounded domain (since, in this case, the linear intensity  $\tilde{\lambda}_i(f)$  defined in (2) is also bounded). Nevertheless, we can obtain the posterior concentration in the sigmoid model wrt to the truncated norm.

We now state our concentration result on the posterior distribution (16).

**Proposition 4.5.** Let  $N$  be a sigmoid Hawkes process with link functions  $(\phi_k)_k$  defined in (15), scale parameter  $\theta_0$ , and parameter  $f_0 = (\nu_0, h_0)$  such that  $f_0$  satisfies Assumption 4.1. Let  $\kappa_T = 10(\log \log T) \log T$  and  $\epsilon_T = o(1/\sqrt{\kappa_T})$  be a positive sequence verifying  $\log^3 T = O(T\epsilon_T^2)$ . Let  $\Pi = \Pi_\nu \times \Pi_\theta \times \Pi_h$  be a prior distribution on  $\mathcal{F} \times \Theta$ . We assume that for  $T$  large enough, assumption (A1) of Theorem 3.2 and the following assumptions hold.

(A0'') There exists  $c_1 > 0$  such that  $\Pi(\tilde{B}_2(\epsilon_T, B)) \geq e^{-c_1 T \epsilon_T^2}$ .

(A3) There exists  $c_2 > 0$  such that  $\Pi_\nu(\min_k \nu_k < -e^{c_2 T \epsilon_T^2}) + \Pi_\theta(\max_k \theta_k > e^{c_2 T \epsilon_T^2}) = o(e^{-(\kappa_T + c_1) T \epsilon_T^2})$ .

Then, for any  $M_T \rightarrow \infty$ , we have that

$$\mathbb{E}_0 \left[ \Pi(\|f - f_0\|_{1,B} + \|\theta - \theta_0\|_1 > M_T \sqrt{\kappa_T} \epsilon_T | N) \right] = o(1). \quad (17)$$

The previous result is an extension of Theorem 3.2 of Sulem et al. [2021], and provides guarantess for Bayesian methods that estimate the scale parameter in the sigmoid model. Moreover, from Proposition 4.5, the concentration rates of a variational posterior on  $(f, \theta)$  can then be deduced, using similar construction and arguments as for Theorem 3.2. The proof of Proposition 4.5 is reported in Appendix ??.

## 4.2 Augmented mean-field variational inference

In this section, we recall existing latent variable augmentation strategy in the sigmoid Hawkes model, and the definition of the augmented mean-field variational distribution in this context Malem-Shinitski et al. [2021], Zhou et al. [2021a]. From now on, we consider that the scale parameter  $\theta$  is known, however, our methodology can be directly extended to estimate an unknown  $\theta$ .

The first step consists in re-writing the sigmoid function as a mixture of Polya-Gamma random variables Polson et al. [2012], i.e.,

$$\sigma(x) = \mathbb{E}_{\omega \sim p_{PG}(\cdot; 1, 0)} \left[ e^{g(\omega, x)} \right] = \int_0^{+\infty} e^{g(\omega, x)} p_{PG}(\omega; 1, 0) d\omega, \quad g(\omega, x) = -\frac{\omega x^2}{2} + \frac{x}{2} - \log 2, \quad (18)$$

with  $p_{PG}(\cdot; 1, 0)$  the Polya-Gamma density. We recall that  $p_{PG}(\cdot; 1, 0)$  is the density of the random variable

$$\frac{1}{2\pi^2} \sum_{k=1}^{\infty} \frac{g_k}{(k-1/2)^2}, \quad g_k \stackrel{\text{i.i.d.}}{\sim} \text{Gamma}(1, 1),$$

and that the *tilted* Polya-Gamma distribution is defined as

$$p_{PG}(\omega; 1, c) = \cosh\left(\frac{c}{2}\right) \exp\left\{-\frac{c^2\omega}{2}\right\} p_{PG}(\omega; 1, 0), \quad c \geq 0,$$

where  $\cosh$  denotes the hyperbolic cosine function. With a slight abuse of notation, we re-define the linear intensity (2) as

$$\tilde{\lambda}_i^k(f) = 0.1 \left( \nu_k + \sum_{l=1}^K \int_{-\infty}^{t^-} h_{lk}(t-s) dN_s^l - 10.0 \right),$$

so that we have  $\lambda_i^k(f) = \theta_k \sigma(\tilde{\lambda}_i^k(f))$ ,  $t \in \mathbb{R}$ . For any  $k \in [K]$ , let  $N_k := N^k[0, T]$  and  $T_1^k, \dots, T_{N_k}^k \in [0, T]$  be the times of events at component  $N^k$ . Now, let  $\omega = (\omega_i^k)_{k \in [K], i \in [N_k]}$  be a set of latent variables such that

$$\omega_i^k \stackrel{\text{i.i.d.}}{\sim} p_{PG}(\omega_i^k; 1, 0), \quad i \in [N_k], \quad k \in [K].$$

Then, using (18), an *augmented* log-likelihood function can be defined as

$$\begin{aligned} L_T(f, \omega; N) &= \sum_{k \in [K]} \left\{ \sum_{i \in [N_k]} \left( \log \theta_k + g(\omega_i^k, \tilde{\lambda}_{T_i^k}(f)) + \log p_{PG}(\omega_i^k; 1, 0) \right) - \int_0^T \theta_k \sigma(\tilde{\lambda}_i^k(f)) dt \right\} \\ &= \sum_{k \in [K]} \left\{ \sum_{i \in [N_k]} \left( \log \theta_k + g(\omega_i^k, \tilde{\lambda}_{T_i^k}(f)) + \log p_{PG}(\omega_i^k; 1, 0) \right) - \int_0^T \int_0^{\infty} \theta_k e^{g(\bar{\omega}, \tilde{\lambda}_i^k(f))} p_{PG}(\bar{\omega}; 1, 0) d\bar{\omega} dt \right\}. \end{aligned} \quad (19)$$

Secondly, Campbell's theorem Daley and Vere-Jones [2007], Kingman [1993] is used to re-write the integral term on the RHS in (19). We first recall here its general formulation. For a Poisson point process  $\tilde{N}$  on a space  $\mathcal{X}$  with intensity measure  $\Lambda : \mathcal{X} \rightarrow \mathbb{R}^+$ , and for any function  $\zeta : \mathcal{X} \rightarrow \mathbb{R}$ , it holds true that

$$\mathbb{E} \left[ \prod_{x \in \tilde{N}} e^{\zeta(x)} \right] = \exp \left\{ (e^{\zeta(x)} - 1) \Lambda(dx) \right\}. \quad (20)$$

Therefore, using that  $\sigma(x) = 1 - \sigma(-x)$ , and considering for each  $k$  a marked Poisson point process  $\tilde{N}^k$  on  $\mathcal{X} = ([0, T], \mathbb{R}^+)$  with intensity measure  $\Lambda^k(t, \omega) = \theta_k p_{PG}(\omega; 1, 0)$ , and distribution  $\mathbb{P}_{\tilde{N}}$ , applying Campbell's theorem with  $\zeta(t, \omega) := g(\omega, -\tilde{\lambda}_t^k(f))$ , one obtains that

$$\mathbb{E} \left[ \prod_{(\tilde{T}_j^k, \bar{\omega}_j^k) \in \tilde{N}^k} e^{g(\bar{\omega}_j^k, -\tilde{\lambda}_{\tilde{T}_j^k}(f))} \right] = \exp \left\{ \int_0^T \int_0^{\infty} \theta_k \left( e^{g(\bar{\omega}, -\tilde{\lambda}_t^k(f))} - 1 \right) p_{PG}(\bar{\omega}; 1, 0) d\bar{\omega} dt \right\}.$$

Conditionally on  $N$ , let  $\tilde{N} := (\tilde{N}^1, \dots, \tilde{N}^K)$  be an observation of the previous Poisson process on  $[0, T]$ . We denote  $\tilde{N}_k := \tilde{N}^k[0, T]$  and  $(\tilde{T}_1^k, \bar{\omega}_1^k), \dots, (\tilde{T}_{N_k}^k, \bar{\omega}_{N_k}^k) \in [0, T] \times \mathbb{R}_+$  the times and marks of  $\tilde{N}_k$  for each  $k$ . Then, a *doubly augmented* log-likelihood function can be defined as

$$L_T(f, \omega, \tilde{N}; N) = \sum_{k \in [K]} \left\{ \sum_{i \in [N_k]} \left[ \log \theta_k + g(\omega_i^k, \tilde{\lambda}_{T_i^k}(f)) + \log p_{PG}(\omega_i^k; 1, 0) \right] + \sum_{j \in [N_k]} \left[ \log \theta_k + g(\bar{\omega}_j^k, -\tilde{\lambda}_{\tilde{T}_j^k}(f)) + \log p_{PG}(\bar{\omega}_j^k; 1, 0) - \theta_k T \right] \right\}.$$

This construction allows to define *augmented* posterior distribution as

$$\Pi(f, \omega, \tilde{N} | N) \propto \prod_k \left\{ \prod_{i \in [N_k]} \theta_k e^{g(\omega_i^k, \tilde{\lambda}_{T_i^k}(f))} p_{PG}(\omega_i^k; 1, 0) \times \prod_{j \in [N_k]} \theta_k e^{g(\bar{\omega}_j^k, -\tilde{\lambda}_{\tilde{T}_j^k}(f))} p_{PG}(\bar{\omega}_j^k; 1, 0) \right\} \times \Pi(f). \quad (21)$$

Then, in this context, an augmented mean-field variational family can be defined as

$$\mathcal{V}_{AMF} = \left\{ Q; dQ(f, \omega, \bar{N}) = dQ_1(f)dQ_2(\omega, \bar{N}) \right\}, \quad (22)$$

leading to the following variational posterior

$$\hat{Q}_{AMF}(f, \omega, \bar{N}) = \arg \min_{Q \in \mathcal{V}_{AMF}} KL(Q(f, \omega, \bar{N}) || \Pi(f, \omega, \bar{N} | N)) = \hat{Q}_1(f) \hat{Q}_2(\omega, \bar{N}).$$

Using (6), it then holds that

$$\hat{Q}_1(f) \propto \exp \left\{ \mathbb{E}_{\hat{Q}_2} [\log p(f, \omega, \bar{N}, N)] \right\}, \quad (23)$$

$$\hat{Q}_2(\omega, \bar{N}) \propto \exp \left\{ \mathbb{E}_{\hat{Q}_1} [\log p(f, \omega, \bar{N}, N)] \right\}. \quad (24)$$

For certain families of Gaussian priors, the variational factors  $\hat{Q}_1$  and  $\hat{Q}_2$  of the augmented mean-field distribution are conjugate to the prior  $\Pi$  and augmented distribution  $P_A = p_{PG}(\cdot | 1, 0) \times P_{\bar{N}}$ , which allows to design iterative algorithms with closed-forms updates of (23) and (24). In the next section, we derive a mean-field variational inference algorithm for a fixed dimensionality of the parameter  $f$ , a method related to the algorithm of Zhou et al. [2021a].

### 4.3 Fixed-dimension mean-field variational algorithm

We consider a modification of the random histogram prior family, where the graph parameter  $\delta = (\delta_{lk})_{l,k} \in \{0, 1\}^{K \times K}$  and the size of the partition  $J = 2^D$  are fixed, with  $D \geq 0$  the partition's depth. We denote  $s = (\delta, D)$  and call  $D$  the dimensionality of  $h$ . We recall our notation from Section 3.2.1 of the basis functions on  $(0, A]$ ,

$$e_j(x) = \frac{J}{A} \mathbb{1}_{I_j}(x), \quad I_j = \left[ \frac{J}{A}(j-1), \frac{J}{A}j \right), \quad j \in [J].$$

We also define

$$\mathcal{H}_{histo}^D = \left\{ h = (h_{lk})_{l,k} \in \mathcal{H}; h_{lk}(x) = \sum_{j=1}^J h_{lk}^j e_j(x), x \in [0, A], \underline{h}_{lk}^D = (h_{lk}^1, \dots, h_{lk}^J) \in \mathbb{R}^J, \forall l, k \in [K] \right\}.$$

For each  $l, k \in [K]$  such that  $\delta_{lk} = 1$ , we consider a normal prior for the distribution on  $\underline{h}_{lk}^D$ , with mean vector  $\mu_D$  and covariance matrix  $\Sigma_D$ , i.e.,

$$\underline{h}_{lk}^D \sim \mathcal{N}(\mu_D, \Sigma_D).$$

For each  $l, k$  such that  $\delta_{lk} = 0$ , we set  $\underline{h}_{lk}^D = \mathbf{0}_J$ , and define  $\mu_s = (\delta_{lk} \mu_D)_{l,k} \in \mathbb{R}^{JK^2}$  and  $\Sigma_s = \text{Diag}((\delta_{lk} \Sigma_D)_{l,k}) \in \mathbb{R}^{JK^2 \times JK^2}$ . We also consider a normal prior on the background rates, i.e.,  $v_k \sim \mathcal{N}(\mu_v, \sigma_v^2), k \in [K]$ . We denote  $f_s := (f_k^s)_k \in \mathcal{F}_s$  where for each  $k$ ,

$$f_k^s = (v_k, \underline{h}_{1k}^D, \dots, \underline{h}_{kk}^D) \in \mathbb{R}^{KJ+1}.$$

We then consider the data augmentation strategy described in Section 4.2 and an augmented mean-field variational family with fixed  $s = (\delta, D)$ , i.e.,

$$\mathcal{V}_{AMF}^s = \left\{ Q = Q_{f_s, \delta, s} : \mathcal{F}_s \rightarrow [0, 1]; dQ(f, \omega, \bar{N}) = dQ_1(f_s) dQ_2(\omega, \bar{N}) \right\},$$

and we denote  $\hat{Q}_s(f_s, \omega, \bar{N}) = \hat{Q}_{1s}(f_s) \hat{Q}_{2s}(\omega, \bar{N})$  the corresponding variational posterior. Following the same strategy as Donner and Oppor [2019], Zhou et al. [2021a], Malem-Shinitiski et al. [2021], we can derive analytic forms for  $\hat{Q}_{1s}$  and  $\hat{Q}_{2s}$ .

Introducing the notation  $H(t) = (H^0(t), H^1(t), \dots, H^K(t)) \in \mathbb{R}^{KJ+1}$ , where  $H_0(t) = 1$  and for  $k \in [K]$ ,  $H^k(t) = (H_j^k(t))_{j=1, \dots, J}$  with

$$H_j^k(t) := \int_{t-A}^t e_j(t-s) dN_s^k, \quad j \in [J], \quad (25)$$

we can prove that with  $\hat{Q}_{1s}(f_s) = \prod_k \hat{Q}_{1s}^k(f_k^s)$ , for each  $k$ ,  $\hat{Q}_{1s}^k(f_k^s)$  is a normal distribution with mean vector  $\tilde{\mu}_k^s \in \mathbb{R}^{KJ+1}$  and covariance matrix  $\tilde{\Sigma}_k^s \in \mathbb{R}^{(KJ+1) \times (KJ+1)}$  given by

$$\tilde{\Sigma}_k^s = \left[ \alpha^2 \sum_{i \in [N_k]} \mathbb{E}_{\hat{Q}_{2s}^k} [\omega_i^k] H(T_i^k) H(T_i^k)^T + \alpha^2 \int_0^T \int_0^{+\infty} \bar{\omega}_i^k H(t) H(t)^T \Lambda^k(t, \bar{\omega}) d\bar{\omega} dt + \Sigma_s^{-1} \right]^{-1},$$

$$\tilde{\mu}_k^s = \frac{1}{2} \tilde{\Sigma}_k^s \left[ \alpha \sum_{i \in [N_k]} (2 \mathbb{E}_{\hat{Q}_{2s}^k} [\omega_i^k] \alpha \eta + 1) H(T_i^k) + \alpha \int_0^T \int_0^{+\infty} (2 \bar{\omega}^k \alpha \eta - 1) H(t) \Lambda^k(t, \bar{\omega}) d\bar{\omega} dt + 2 \Sigma_s^{-1} \mu_s \right],$$

where

$$\Lambda^k(t, \bar{\omega}) := \theta_k \frac{\exp\left\{-\frac{1}{2}\mathbb{E}_{\hat{Q}_{1s}^k}[\tilde{\lambda}_i^k(f_k^s)]\right\}}{2 \cosh\left(\frac{c_i^k}{2}\right)} p_{PG}(\bar{\omega}|1, c_i^k), \quad c_i^k := \sqrt{\mathbb{E}_{\hat{Q}_{1s}^k}[\tilde{\lambda}_i^k(f)^2]}.$$

Besides,  $\hat{Q}_{2s}(\omega, \bar{N}) = \hat{Q}_{21s}(\omega)\hat{Q}_{22s}(\bar{N})$  where

$$\hat{Q}_{21s}(\omega) = \prod_k \prod_{i \in [N_k]} p_{PG}(\omega_i^k | 1, c_{T_i^k}^k),$$

and  $\hat{Q}_{22s} = \prod_k \hat{Q}_{22s}^k$ , where for each  $k$ ,  $\hat{Q}_{22s}^k$  is the probability distribution of a marked Poisson point process on  $[0, T] \times \mathbb{R}^+$  with intensity measure  $\Lambda^k(t, \bar{\omega})$ . The derivation of these formulas is reported in Appendix C.1.

Therefore, given an estimate of  $\hat{Q}_{1s}$ , one can compute  $\hat{Q}_{2s}$ , and reciprocally, and the variational posterior distribution can be computed by updating each factor iteratively. This procedure is reported in Algorithm 1. We note that in the updates of  $\tilde{\mu}_k^s$  and  $\tilde{\Sigma}_k^s$ , we need to compute an integral, which we perform using the Gaussian quadrature Golub and Welsch [1969] with  $n_{GQ}$  points in our implementation. We also note that in this algorithm, the outer ‘‘for’’ loop that computes each factor  $\hat{Q}_k^s$  could be run in parallel.

We additionally note that, similarly to Zhou et al. [2021a], Malem-Shinitski et al. [2021], we can derive analytic forms of the conditional distributions of the augmented posterior distribution (21) and design a Gibbs sampler to compute the latter distribution (see Algorithm 4 in Appendix C.3).

---

**Algorithm 1** Fixed-dimension mean-field variational inference algorithm

---

**Input:**  $N, \delta, D, \mu_D, \Sigma_D, n_{iter}, n_{GQ}$ .

**Output:**  $\tilde{\mu}_D, \tilde{\Sigma}_D$ .

Precompute  $(H(T_i^k))_{i,k}$ .

Precompute  $(p_q, v_q)_{q \in [n_{GQ}]}$  the points and weights of the Gaussian quadrature method, and  $(H(p_q))_{q \in [n_{GQ}]}$ .

**for**  $k \leftarrow 1$  to  $K$  **do**

    Initialise  $\tilde{\mu}_k^s \leftarrow \mu_s, \tilde{\Sigma}_k^s \leftarrow \Sigma_s$ .

**for**  $t \leftarrow 1$  to  $n_{iter}$  **do**

**for**  $i \leftarrow 1$  to  $N_k$  **do**

$$\mathbb{E}_{\hat{Q}_{1s}}[\tilde{\lambda}_{T_i^k}^k(f_k^s)^2] = \alpha \left( H(T_i^k)^T \tilde{\Sigma}_k^s H(T_i^k) + (H(T_i^k)^T \tilde{\mu}_k^s)^2 - 2\eta H(T_i^k)^T \tilde{\mu}_k^s + \eta^2 \right)$$

$$\mathbb{E}_{\hat{Q}_{2s}}[\omega_i^k] \leftarrow \tanh\left(\frac{\sqrt{\mathbb{E}_{\hat{Q}_{1s}}[\tilde{\lambda}_{T_i^k}^k(f_k^s)^2]}}{2\sqrt{\mathbb{E}_{\hat{Q}_{1s}}[\tilde{\lambda}_{T_i^k}^k(f_k^s)^2]}}\right)$$

**end for**

**for**  $q \leftarrow 1$  to  $n_{GQ}$  **do**

$$\mathbb{E}_{\hat{Q}_{1s}}[\tilde{\lambda}_{p_q}^k(f_k^s)^2] = \alpha \left( H(p_q)^T \tilde{\Sigma}_k^s H(p_q) + (H(p_q)^T \tilde{\mu}_k^s)^2 - 2\eta H(p_q)^T \tilde{\mu}_k^s + \eta^2 \right)$$

$$\mathbb{E}_{\hat{Q}_{2s}}[\omega_q^k] \leftarrow \tanh\left(\frac{\sqrt{\mathbb{E}_{\hat{Q}_{1s}}[\tilde{\lambda}_{p_q}^k(f_k^s)^2]}}{2\sqrt{\mathbb{E}_{\hat{Q}_{1s}}[\tilde{\lambda}_{p_q}^k(f_k^s)^2]}}\right)$$

$$\mathbb{E}_{\hat{Q}_{1s}}[\tilde{\lambda}_{p_q}^k(f_k^s)] = \alpha \left( (\tilde{\mu}_k^s)^T H(p_q) - \eta \right)$$

**end for**

$$\tilde{\Sigma}_k^s = \left[ \alpha^2 \sum_{i \in [N_k]} \mathbb{E}_{\hat{Q}_{2s}}[\omega_i^k] H(T_i^k) H(T_i^k)^T + \alpha^2 \theta_k \sum_{q \in [n_{GQ}]} v_q \mathbb{E}_{\hat{Q}_{2s}}[\omega_q^k] \frac{\exp(-\frac{1}{2}\mathbb{E}_{\hat{Q}_{1s}}[\tilde{\lambda}_{p_q}^k(f_k^s)])}{2 \cosh\left(\frac{1}{2}\mathbb{E}_{\hat{Q}_{1s}}[\tilde{\lambda}_{p_q}^k(f_k^s)^2]\right)} H(p_q) H(p_q)^T + \Sigma_s^{-1} \right]^{-1}.$$

$$\tilde{\mu}_k^s = \frac{1}{2} \tilde{\Sigma}_k^s \left[ \alpha \sum_{i \in [N_k]} (2\mathbb{E}_{\hat{Q}_{2s}}[\omega_i^k] \alpha \eta + 1) H(T_i^k)^T + \alpha \theta_k \sum_{q \in [n_{GQ}]} v_q (2\mathbb{E}_{\hat{Q}_{2s}}[\omega_q^k] \alpha \eta - 1) \frac{\exp(-\frac{1}{2}\mathbb{E}_{\hat{Q}_{1s}}[\tilde{\lambda}_{p_q}^k(f_k^s)])}{2 \cosh\left(\frac{1}{2}\mathbb{E}_{\hat{Q}_{1s}}[\tilde{\lambda}_{p_q}^k(f_k^s)^2]\right)} H(p_q)^T + 2\Sigma_s^{-1} \mu_s \right].$$

**end for**

**end for**

---

#### 4.4 Adaptive mean-field variational algorithms

Using the fixed-dimension approach from Section 4.2, we can now design an adaptive and sparsity-inducing variational method, that infers the graph parameter  $\delta$  and the dimensionality of  $h$ . In fact, we propose two algorithms. The first one, Algorithm 2, explores all  $s = (\delta, D)$ , and outputs an *averaged* or *mode* variational posterior analog to (14) and (9). However, considering the  $2^K$  graphs  $\delta$  is computationally expensive for moderate  $K$ . Therefore, we also propose a more efficient two-step algorithm, Algorithm 3, which first estimates the graph  $\hat{\delta}$ , then computes an adaptive variational posterior that is a mixture on the restricted set  $(\hat{\delta}, D)_D$ .

#### 4.4.1 Fully-adaptive mean-field variational algorithm

Given a maximum depth  $D_T$ , we first define the set

$$\mathcal{S}_T = \{s = (\delta, D); \delta \in \{0, 1\}^{K \times K}, 1 \leq D \leq D_T\}.$$

For simplicity, given a graph  $\delta$ , we assume that the depth is kept the same for all non-null  $h_{lk}$ , therefore,  $|\mathcal{S}_T| \sim 2^{K^2} D_T$ , and for any  $s = (\delta, D) \in \mathcal{S}_T$ ,  $|s| = (D + 1) \sum_{l,k} \delta_{lk} + 1$ . Let  $\Pi_s$  be a prior distribution on  $\mathcal{S}_T$  of the form  $\Pi_s(s) = \Pi_\delta(\delta) \Pi_D(D)$ . Then, we define the *averaged* variational posterior as

$$\hat{Q}_{AV} = \sum_{s \in \mathcal{S}_T} \hat{\gamma}_s \hat{Q}_s, \quad (26)$$

where for each  $s$ ,  $\hat{Q}_s$  is the variational posterior defined in Section 4.3, and  $\hat{\gamma}_s$  is the marginal probability on  $s$  defined as

$$\tilde{\gamma}_s = \Pi_\delta(\delta) \Pi_D(D) \exp\{ELBO(\hat{Q}_s)\}, \quad \hat{\gamma}_s = \tilde{\gamma}_s / \sum_{s \in \mathcal{S}_T} \tilde{\gamma}_s, \quad (27)$$

with

$$ELBO(Q) := \mathbb{E}_Q \left[ \log \frac{p(f, \omega, \bar{N}, N)}{Q_1(f) Q_2(\omega, \bar{N})} \right]. \quad (28)$$

We also define a *mode* variational posterior as

$$\hat{Q}_{MV} = \hat{Q}_{\hat{s}}, \quad \hat{s} = \arg \max_{s \in \mathcal{S}_T} ELBO(\hat{Q}_s). \quad (29)$$

To obtain  $\hat{Q}_{AV}$  or  $\hat{Q}_{MV}$ , we then compute  $\hat{Q}_s$  for every  $s \in \mathcal{S}_T$  using Algorithm 1 and the corresponding ELBO (see Appendix C.2 for the latter derivation). We call this procedure the *fully-adaptive mean-field* algorithm, which is summarised in Algorithm 2.

---

#### Algorithm 2 Fully-adaptive mean-field variational inference

---

**Input:**  $N, \mathcal{S}_T, \sigma, n_{iter}, n_{GQ}$ .

**Output:**  $\hat{Q}_{AV}$  (or  $\hat{Q}_{MV}$ )

**for**  $s = (\delta, D) \in \mathcal{S}_T$  **do**

    Compute the variational posterior  $\hat{Q}_s$  using Algorithm 1 with  $\sigma, n_{iter}$  and  $n_{GQ}$ .

    Compute  $\tilde{\gamma}_s$  using (27).

**end for**

    Compute  $\{\hat{\gamma}_s\}_{s \in \mathcal{S}_T}$  and  $\hat{Q}_{AV}$  (or  $\hat{Q}_{MV}$ ) using (26) and (27) (or (29)).

---

#### 4.4.2 Two-step adaptive mean-field algorithm

For the multivariate setting  $K > 1$ , we propose a variant of the previous algorithm that reduces the computational time by avoiding to compute  $\hat{Q}_s$  for all possible  $s \in \mathcal{S}_T$ . We first define the set  $\mathcal{S}_T^{\delta_c}$  as

$$\mathcal{S}_T^{\delta_c} = \{s = (\delta_c, D); 1 \leq D \leq D_T\},$$

where  $\delta_c = \mathbb{1}\mathbb{1}^T$  is the complete graph. The first step of our method consists in computing the mode variational distribution  $\hat{Q}^{\delta_c}$  using Algorithm 2, replacing  $\mathcal{S}_T$  by  $\mathcal{S}_T^{\delta_c}$ . Then, we use  $\hat{Q}^{\delta_c}$  to estimate the norms  $(\|h_{lk}\|_1)_{l,k}$  and the graph parameter. We denote  $\hat{D}_C$  the selected dimensionality in  $\hat{Q}^{\delta_c}$  and  $J_C = 2^{\hat{D}_C}$ . We then define  $\tilde{S} = (\tilde{S}_{lk})_{l,k} \in \mathbb{R}_+^{K \times K}$ , where for any  $l, k$ ,

$$\begin{aligned} \tilde{S}_{lk} &= \mathbb{E}_{\hat{Q}_1^{\delta_c}} [\|h_{lk}\|_1] = \sum_{j=1}^{J_C} \mathbb{E}_{\hat{Q}_1^{\delta_c}} [h_{lk}^j] \\ &= \sum_{j=1}^{J_C} \sqrt{\frac{2}{\pi} [\Sigma_{lk}^{D_c}]_{jj}} \exp \left\{ -\frac{[\tilde{\mu}_{lk}^{D_c}]_j^2}{[\Sigma_{lk}^{D_c}]_{jj}} \right\} - [\tilde{\mu}_{lk}^{D_c}]_j \left[ 1 - 2\Phi \left( -\frac{[\tilde{\mu}_{lk}^{D_c}]_j}{\sqrt{[\Sigma_{lk}^{D_c}]_{jj}}} \right) \right], \end{aligned}$$



Given a pre-specified threshold  $\eta_0$ , we then compute our graph estimator  $\hat{\delta} = (\hat{\delta}_{lk})_{l,k}$  as

$$\hat{\delta}_{lk} = \mathbb{1}_{S_{lk} > \eta_0}, \quad \forall l, k. \quad (30)$$

Secondly, with

$$\mathcal{S}_T^{\hat{\delta}} = \{s = (\hat{\delta}, D); 1 \leq D \leq D_T\},$$

we compute our *two-step adaptive* variational distribution  $\hat{Q}_{TSA}$  using Algorithm 2, replacing  $\mathcal{S}_T$  by  $\mathcal{S}_T^{\hat{\delta}}$ . This procedure is summarised in Algorithm 3.

Moreover, our thresholding procedure to construct an estimator of the graph in (30) can be theoretically justified. From our theory, we know that  $\hat{Q}^{\delta^c}$  concentrates at the rate  $\varepsilon_T = \sqrt{\kappa_T} \varepsilon_T$ . Therefore, if there exists  $\epsilon_0 > 0$  such that  $\forall l, k$ ,  $\|h_{lk}^0\|_1 \geq \epsilon_0$ , then for any  $M_T \rightarrow \infty$  and sequence of thresholds  $(\eta_T)_T$  such that  $M_T \varepsilon_T \leq \eta_T \leq \epsilon_0 - M_T \varepsilon_T$ , we can show that

$$\mathbb{P}_0 \left[ \hat{\delta} = \delta_0 \right] \xrightarrow{T \rightarrow \infty} 1.$$

This comes from the fact that with

$$\begin{aligned} \hat{Q}^{\delta^c}(\{f; \exists l, k, \hat{\delta}_{lk}(\eta_T) = 1 \text{ and } \delta_{lk}^0 = 0\}) &= \hat{Q}^{\delta^c}(\{f; \exists l, k, \|h_{lk}\|_1 > \eta_T \text{ and } \|h_{lk}^0\|_1 = 0\}) \\ &\leq \hat{Q}^{\delta^c}(\{f; \exists l, k, \|h_{lk} - h_{lk}^0\|_1 > M_T \varepsilon_T \text{ and } \delta_{lk}^0 = 0\}) = o_{\mathbb{P}_0}(1). \end{aligned}$$

Similarly, it holds that

$$\hat{Q}^{\delta^c}(\{f; \exists l, k, \hat{\delta}_{lk}(\eta_T) = 0 \text{ and } \delta_{lk}^0 = 1\}) = \hat{Q}^{\delta^c}(\{f; \exists l, k, \|h_{lk}\|_1 < \eta_T \leq \|h_{lk}^0\|_1 - M_T \varepsilon_T\}) = o_{\mathbb{P}_0}(1).$$

An alternative to setting a threshold  $\eta_0$  is to select it in a data-driven way after the first step of Algorithm 3. One heuristic is to sort the entries of the matrix  $\tilde{S}$  in increasing order of magnitude, to spot a ‘‘gap’’ in this list, and to choose somewhere mid-way in this gap. The latter is visible in our simulation study, as can be seen in the plots in Figure 20.

---

### Algorithm 3 Two-step adaptive mean-field variational inference

---

**Input:**  $N, \{(\mu_D, \Sigma_D)\}_D, n_{iter}, n_{GQ}, \eta_0$ .

**Output:**  $\hat{Q}_{TSA}$

Compute  $\hat{Q}^{\delta^c}$  using Algorithm 2 with input set  $\mathcal{S}_T^{\delta^c}$ .

Compute  $\hat{\delta}$  using (30).

Compute  $\hat{Q}_{TSA}$  using Algorithm 2 with input set  $\mathcal{S}_T^{\hat{\delta}}$ .

---

## 5 Numerical results

In this section, we perform a simulation study and evaluate (variational) Bayesian methods in the context of nonlinear Hawkes processes. We first test a MCMC method in commonly used nonlinear models (Simulation 1), and then, our adaptive variational algorithms derived for the sigmoid model (Simulations 2, 3 and 4). In each setting, we sample one observation of a Hawkes process with dimension  $K$ , link functions  $(\phi_k)_k$  and parameter  $f_0 = (\nu_0, h_0)$  on  $[0, T]$  using the thinning algorithm Adams et al. [2009]. In most settings, the true interaction functions  $(h_{lk}^0)_{l,k}$  will be piecewise-constant and we will use the random histogram prior described in Section 4.3. For  $D \geq 1$ , we define

$$\mathcal{H}_{histo}^D = \left\{ h = (h_{lk})_{l,k}; h_{lk}(x) = \sum_{j=1}^{2^D} w_{lk}^j e_j(x), x \in [0, A], l, k \in [K] \right\}.$$

We report the following set of simulations:

- **Simulation 1: MCMC method in univariate nonlinear Hawkes models.** This experiment aims at evaluating a Metropolis-Hasting sampler (MH) in several nonlinear Hawkes models, with ReLU, sigmoid, and softplus link functions, and in a setting where  $h_0 \in \mathcal{H}_{histo}^{D_0}$  and the dimensionality  $D_0$  is known. Since this MCMC sampler is quite computationally expensive to run, we only test the univariate setting  $K = 1$  in this simulation.

- **Simulation 2: Comparison of MH sampler, Gibbs sampler, and fixed-dimension variational algorithm in the univariate sigmoid model.** In this simulation, we also consider a univariate setting where  $h_0 \in \mathcal{H}_{histo}^{D_0}$  and the dimensionality  $D_0$  is known. We compare two MCMC methods, namely the MH sampler and a Gibbs sampler (Algorithm 4), and the fixed-dimension mean-field variational inference algorithm (Algorithm 1).
- **Simulation 3: Adaptive mean-field variational algorithm in the univariate and bivariate sigmoid models.** In this experiment, we test our fully-adaptive variational algorithm (Algorithm 2) for sigmoid Hawkes processes with  $K = 1$  and  $K = 2$ , in nonparametric settings where the true interaction functions are piecewise-constant functions or continuous.
- **Simulation 4: Two-step variational algorithm for multivariate sigmoid models** In this simulation, we test our two-step adaptive mean-field algorithm (Algorithm 3) for sigmoid Hawkes processes with  $K = 2, 4, 8, 32$ , in sparse settings of the true parameter  $h_0$ .

In all simulations, we set  $A = 0.1$ . Additional details on these experiments are reported in Appendix D.

### 5.1 Simulation 1: MCMC method in univariate nonlinear Hawkes models

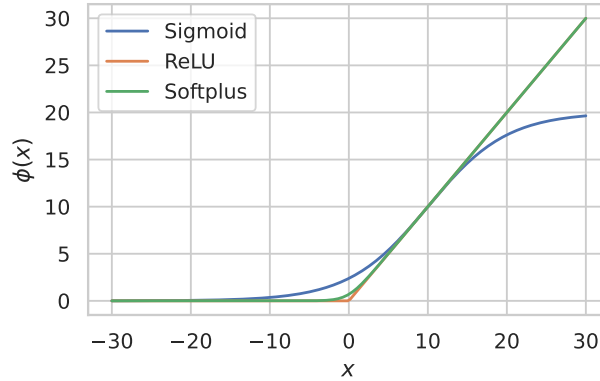


Figure 1: Link functions  $\phi$  considered in Simulation 1, corresponding to our sigmoid, ReLU, and softplus Hawkes models.

In this simulation, we set  $K = 1$  and consider a link function  $\phi$  of the form

$$\phi(x) = \theta + \Lambda\psi(\alpha(x - \eta)), \quad (31)$$

where  $\xi = (\theta, \Lambda, \alpha, \eta)$  and  $\psi : \mathbb{R} \rightarrow \mathbb{R}^+$  are known. We consider the following models:

- Sigmoid:  $\psi(x) = (1 + e^{-x})^{-1}$  and  $\xi = (0.0, 20.0, 0.1, 10.0)$ ;
- ReLU:  $\psi(x) = \max(x, 0)$  and  $\xi = (0.001, 1.0, 1.0, 0.0)$ ;
- Softplus:  $\psi(x) = \log(1 + e^x)$  and  $\xi = (0.0, 40.0, 0.1, 20.0)$ .

The corresponding link functions  $\phi$  are plotted in Figure 1. In all models, we set  $\nu_0 = 6$  and  $h_0 = h_{11}^0 \in \mathcal{H}_{histo}^{D_0}$  with  $D_0 = 2$ , and consider three scenarios:

- *Excitation only*:  $h_0$  is non-negative.
- *Mixed effect*:  $h_0$  is signed.
- *Inhibition only*:  $h_0$  is non-positive.

In this simulation, we assume that  $D_0$  is known and consider a normal prior on  $\mathcal{H}_{histo}^{D_0}$  on  $w_{11}$ ,  $w_{11} \sim \mathcal{N}(0, \sigma^2 I)$ , and on  $\nu_1$ ,  $\nu_1 \sim \mathcal{N}(0, \sigma^2)$ , with  $\sigma = 5.0$ . We set  $T = 500$  and report the number of events and excursions (see Lemma A.1 in Appendix A.1 for the definition of this concept), observed in each simulation and model in Table 1. As expected, more events and less excursions are observed in the *Excitation only* scenario than in the *Mixed effect* and *Inhibition only* scenarios.

We run a Metropolis-Hasting sampler implemented via the Python package PyMC<sup>1</sup> with 4 chains, 40 000 iterations and with a burning time of 4000 iterations. The log-likelihood is evaluated using the Gaussian quadrature method Golub and Welsch [1969] for numerical integration, except in the ReLU model and *Excitation only* scenario where the integral is computed exactly. The posterior distribution on  $f = (\nu_1, h_{11})$  in the three models and scenarios are plotted in Figure 2, Figure 3, and Figure 4.

We note that in almost all settings, the ground-truth parameter  $f_0$  is included in the 95% credible sets of the posterior distribution, except in the Excitation scenario in the softplus model. Nonetheless, the posterior mean is sometimes biased, in particular in the Excitation scenario, possibly due to the numerical integration errors. One conjecture is that the estimation quality depends on the number of events and the number of excursions, which could explain the differences between the Excitation, Mixed, and Inhibition scenarios. In particular, the credible sets seem consistently smaller for the Mixed scenario, which realisations have more excursions than the Excitation scenario and more events than the Inhibition scenario.

This simulation can be seen as an illustration of the theoretical results of Sulem et al. [2021] for general nonlinear Hawkes models. Moreover, the MH sampler provides a baseline method to compare our variational algorithms in low-dimensional settings, i.e., for  $K = 1$  (Simulations 2 and 3) and  $K = 2$  (Simulations 3). We note that we also tested a Hamiltonian Monte-Carlo sampler in this simulation, and obtained similar posterior distributions, but in a much larger computational time.

Scenario		Sigmoid	ReLU	Softplus
Excitation only	# events	5250	5352	4953
	# excursions	1558	1436	1373
Mixed effect	# events	3876	3684	3418
	# excursions	1775	1795	1650
Inhibition only	# events	3047	2724	2596
	# excursions	1817	1693	1588

Table 1: Number of events and excursions in the simulated data of Simulation 1. The definition of the concept of excursion in the Hawkes model is recalled in Lemma A.1 in Appendix A.1.

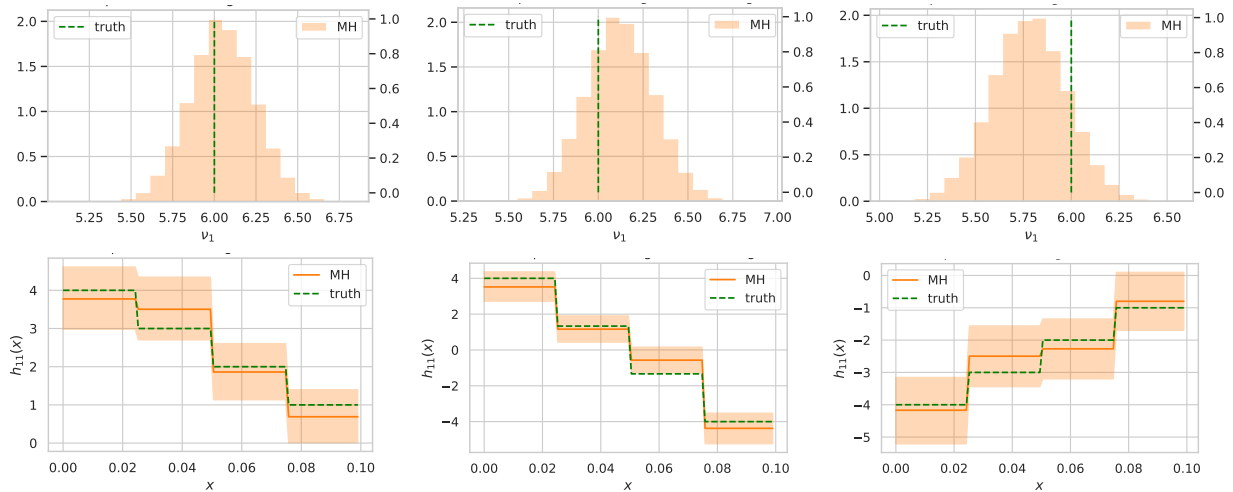


Figure 2: Posterior distribution on  $f = (\nu_1, h_{11})$  obtained with the MH sampler in the sigmoid model, in the three scenarios of Simulation 1 ( $K = 1$ ). The three columns correspond to the *Excitation only* (left), *Mixed effect* (center), and *Inhibition only* (right) scenarios. The first row contains the marginal distribution on the background rate  $\nu_1$ , and the second row represents the posterior mean (solid line) and 95% credible sets (colored areas) on the (self) interaction function  $h_{11}$ . The true parameter  $f_0$  is plotted in dotted green line.

<sup>1</sup><https://www.pymc.io/welcome.html>

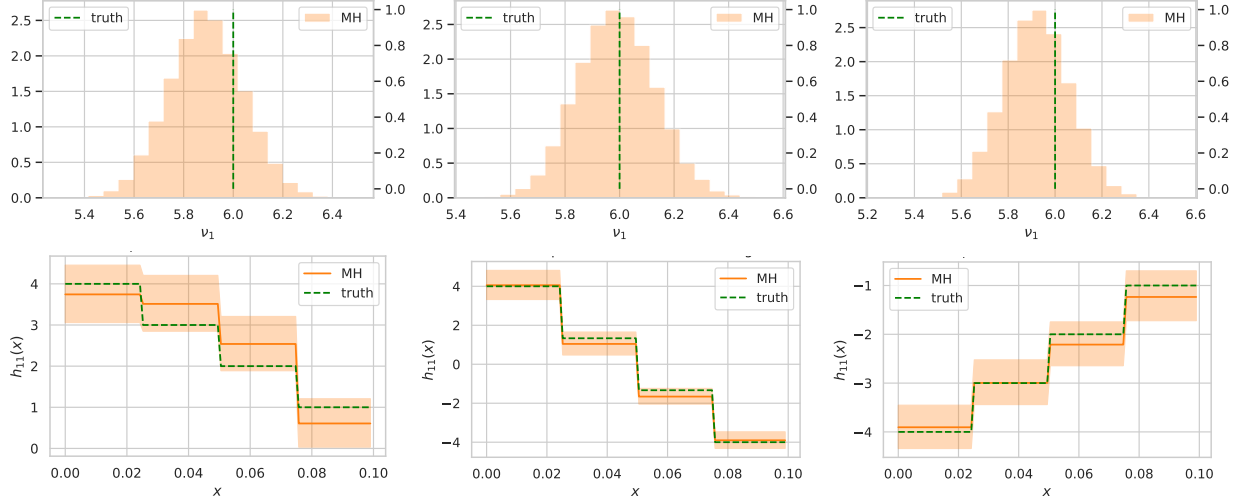


Figure 3: Posterior distribution on  $f = (\nu_1, h_{11})$  obtained with the MH sampler in the ReLU model, in the three scenarios of Simulation 1 ( $K = 1$ ). The three columns correspond to the *Excitation only* (left), *Mixed effect* (center), and *Inhibition only* (right) scenarios. The first row contains the marginal distribution on the background rate  $\nu_1$ , and the second row represents the posterior mean (solid line) and 95% credible sets (colored areas) on the (self) interaction function  $h_{11}$ . The true parameter  $f_0$  is plotted in dotted green line.

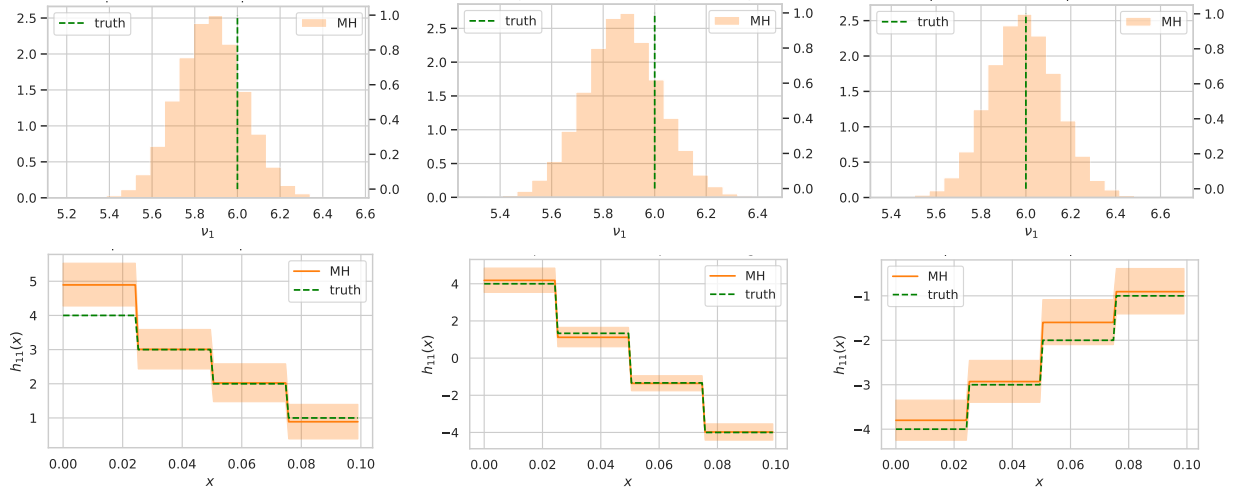


Figure 4: Posterior distribution on  $f = (\nu_1, h_{11})$  obtained with the MH sampler in the softplus model, in the three scenarios of Simulation 1 ( $K = 1$ ). The three columns correspond to the *Excitation only* (left), *Mixed effect* (center), and *Inhibition only* (right) scenarios. The first row contains the marginal distribution on the background rate  $\nu_1$ , and the second row represents the posterior mean (solid line) and 95% credible sets (colored areas) on the (self) interaction function  $h_{11}$ . The true parameter  $f_0$  is plotted in dotted green line.

## 5.2 Simulation 2: Comparison of MH sampler, Gibbs sampler, and fixed-dimension mean-field variational algorithm in the univariate sigmoid model

In this simulation, we consider the sigmoid Hawkes model with  $K = 1$  and the three estimation scenarios of Simulation 1, where the dimensionality  $D_0$  is known. We compare the performance of the previous MH sampler, the Gibbs sampler of the latent variable augmentation scheme (Algorithm 4 in Appendix C.3), and our fixed-dimension mean-field variational algorithm (Algorithm 1). We run 4 chains for 40 000 iterations for the MH sampler, 3000 iterations of the Gibbs sampler, and 30 iterations of the mean-field variational algorithm.

The (variational) distributions on the parameter  $f = (\nu_1, h_{11})$  are plotted in Figure 5. We note that the variational posterior mean is close to the posterior mean, nonetheless, the credible sets of the variational posterior are smaller

than the ones of the posterior distribution. This is not uncommon empirical observation in mean-field variational inference, and one potential solution is to post-process the variational credible bands to obtain better coverage of the truth. Moreover, in spite of the small number of Gibbs iterations, the Gibbs sampler seems slightly more precise than the other two algorithms; it is about 6 (resp. 40) times longer to run than the MH sampler (resp. our mean-field algorithm), due to the expensive latent variable sampling scheme (see the computational times in Table 2). Besides, the three algorithms seem to be similarly biased, e.g., in the Inhibition scenario. One could therefore test if this bias decreases with more data observations, i.e., larger  $T$ . Finally, we also compare the estimated intensity function on a sub-window in Figure 6 and note that all three methods provide fairly equivalent estimates.

From this simulation, we conclude that, in the univariate and parametric sigmoid Hawkes model, the fixed-dimension mean-field variational algorithm provides a good approximation of the posterior distribution. Moreover, we note that although the Gibbs sampler is slightly better than MH, it is too slow to be applied to multivariate Hawkes processes in practice. Therefore, in the next simulations, we only compare to the posterior distribution computed with the MH sampler.

Scenario	MH	Gibbs	MF-VI
Excitation only	2169	16 092	416
Mixed effect	2181	13 097	338
Inhibition only	2222	9 318	400

Table 2: Computational times (in seconds) of the Gibbs sampler (Algorithm 4), the fixed-dimension mean-field variational (MF-VI) algorithm (Algorithm 1), and the MH sampler in each scenario of Simulation 2 (with  $K = 1$ ). The Gibbs sampler is much slower than the MH sampler, which is also much slower than the MF-VI algorithm.

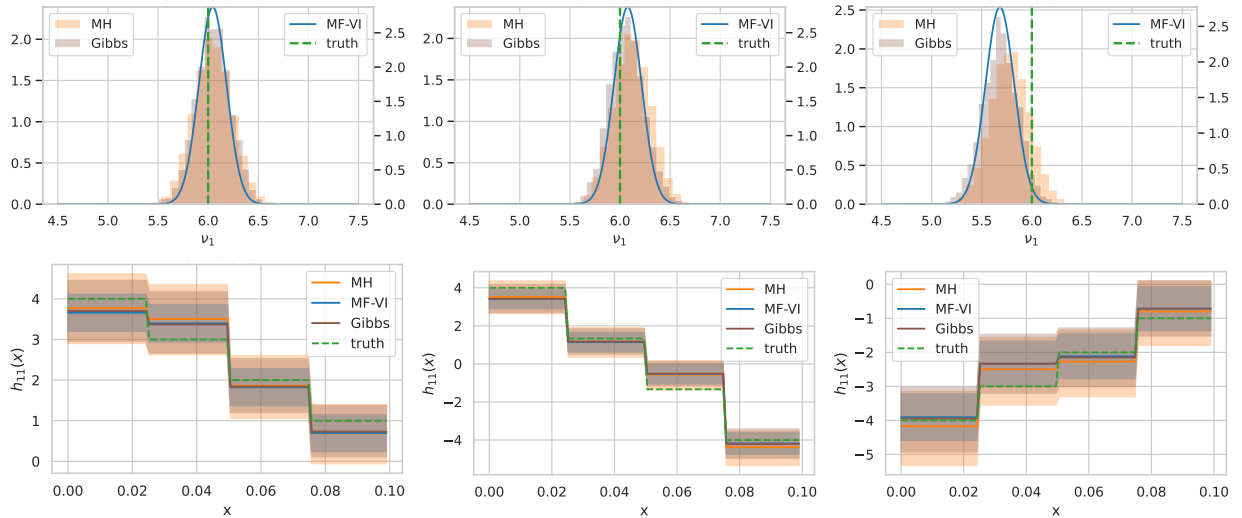
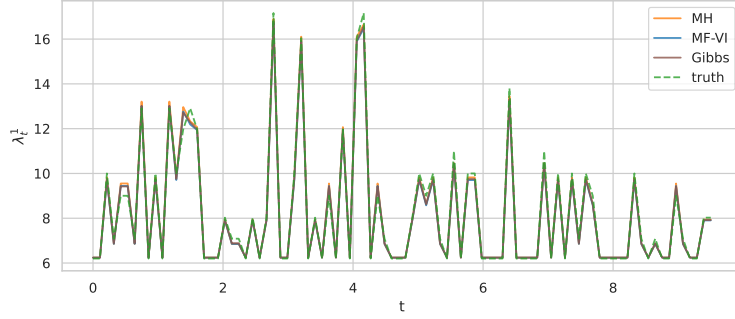


Figure 5: Posterior and variational posterior distributions on  $f = (\nu_1, h_{11})$  in the sigmoid model and in the three scenarios of Simulation 2 ( $K = 1$ ), evaluated by the MH sampler, the fixed-dimension mean-field variational (MF-VI) algorithm (Algorithm 1) and the Gibbs sampler (Algorithm 4). The three columns correspond to the *Excitation only* (left), *Mixed effect* (center), and *Inhibition only* (right) scenarios. The first row contains the marginal distribution on the background rate  $\nu_1$ , and the second row represents the (variational) posterior mean (solid line) and 95% credible sets (colored areas) on the (self) interaction function  $h_{11}$ . The true parameter  $f_0$  is plotted in dotted green line.

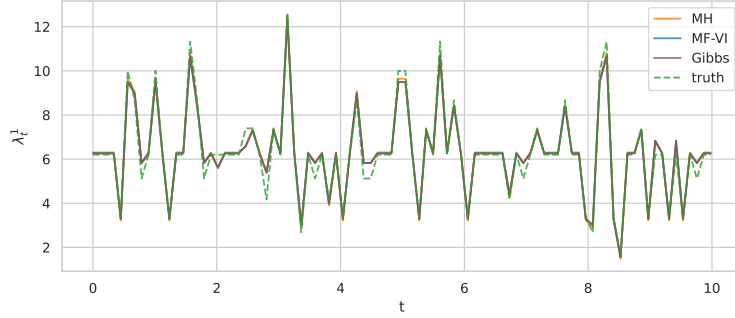
### 5.3 Simulation 3: Adaptive variational algorithm in the univariate and bivariate sigmoid models

In this simulation, we test our fully-adaptive variational Bayes algorithm (Algorithm 2) in the one-dimensional ( $K = 1$ ) and two-dimensional ( $K = 2$ ) sigmoid model. Here, we consider two nonparametric estimation settings:

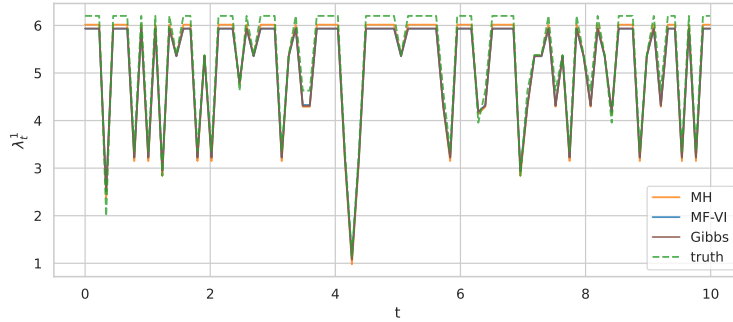
1. *Well-specified*:  $h_0 \in \mathcal{H}_{hist}^{D_0}$  with  $D_0 = 2$ . In this setting, we compare our variational posterior with the posterior distribution obtained with an “optimal” MH sampler run with the true  $s_0 = (\delta_0, D_0)$ ;



(a) *Excitation only*



(b) *Mixed effect*



(c) *Inhibition only*

Figure 6: Estimated intensity function using the (variational) posterior mean, in each scenario of Simulation 2 on  $[0, 10]$ . The true intensity  $\lambda_l^1(f_0)$  is plotted in dotted green line, while the MH, Gibbs, and mean-field variational (MF-VI) estimates are plotted in solid orange (resp., red and blue) lines.

# dimensions	Scenario	FA-MF-VI	MH
$K = 1$	Excitation	2094	3430
	Inhibition	1058	1046
$K = 2$	Excitation	3258	5777
	Inhibition	2616	4679

Table 3: Computational times (in seconds) of Algorithm 2 (FA-MF-VI) and MCMC method in the well-specified settings of Simulation 3.

2. *Mis-specified*:  $h_0 \notin \mathcal{H}_{hist}^{D_0}$ , and for all  $l, k$ ,  $h_{lk}^0$  is a continuous function.

Here,  $D_0 \geq 1$  is unknown and we set  $T = 1500$ . In the bivariate model, we pick a graph parameter  $\delta_0$  with one zero entry (see Figure 12 (a)), i.e., three of the four interaction functions are non-null. We consider an Excitation excitation

where  $h_0$  is non-negative and a Self-inhibition scenario where  $h_{kk}^0 \leq 0$ ,  $k = 1, 2$ . We note that the self-inhibition phenomenon is often observed in neuronal spiking data due to their refractory period Bonnet et al. [2021]. In our algorithm, we set a maximum depth  $D_1 = 5$  for  $K = 1$ , so that the set of dimensions has cardinality  $|\mathcal{S}_1| = 7$  and  $D_1 = 4$  for  $K = 2$ , so that  $|\mathcal{S}_2| = 76$ .

In Figure 7, we plot the marginal probabilities  $(\hat{\gamma}_s)_{s \in \mathcal{S}_1}$  in the univariate model and well-specified setting. In the Excitation scenario, the largest marginal probability is on the truth  $s_0 = (1, 2)$ , i.e.,  $\hat{\gamma}_s = \hat{\gamma}_{s_0}$ , and all the other marginal probabilities are negligible. Therefore, in this case, the averaged variational posterior  $\hat{Q}_{AV}$  from (26) is essentially equivalent to the mode variational posterior  $\hat{Q}_{MV}$  from (29). In the Self-inhibition scenario, we have  $\hat{s} = (1, 1)$ , but  $\hat{\gamma}_{s_0}$  is close to  $\hat{\gamma}_{\hat{s}}$ , i.e., the marginal probability on  $s_0$  is the second largest. Therefore, in this case the averaged variational posterior is essentially a mixture of the mode variational posterior  $\hat{Q}_{MV}$ , which is slightly over-regularising in this case, and the variational distribution at the true  $s_0$ ,  $\hat{Q}_{s_0}$ . We also plot the estimated intensity based on the mode variational posterior mean in Figure 10 and note that the variational posterior estimates is very close to the true intensity and the “optimal” MH estimates (see Figure 10).

In Figure 9, we compare the mode variational posterior  $\hat{Q}_{MV}$  with the posterior distribution obtained with the “optimal” MH sampler. We note that in the Excitation scenario, the variational posterior mean is very close to the posterior mean, however its 95% credible bands are significantly smaller. In the Inhibition scenario, in spite of the wrongly selected histogram depth, the estimated parameter is still not too far from the truth. In the mis-specified setting, we note in Figure 8 that the marginal probabilities are also peaked on a single value  $\hat{s}$ . Moreover, we see on Figure 11 that the true parameter is quite well estimated by  $\hat{Q}_{\hat{s}}$ . Nonetheless, the 95% credible bands are once again slightly too narrow.

The previous observations can also be made in the two-dimensional model. In the well-specified settings, the largest marginal probabilities are on the true  $s_0$  in both Excitation and Self-inhibition scenarios (see Figure 12 (b) and (c)). Therefore, both the causality structure and the dimensionality are well recovered in this case. We also note from Figures 13 and 14, that the variational posterior mean on the interaction functions approximates well the posterior mean, and thus leads to similar intensity estimates (see Figure 16). In the mis-specified setting, the continuous interaction functions are also quite well estimated, although the under-coverage phenomenon of the credible regions also appears (see Figure 15).

Finally, we note that the computational times of our fully-adaptive variational algorithm is lower than the one of the “optimal” MH sampler, although here the latter is not adaptive, in particular in the bivariate setting <sup>2</sup>, as can be seen in Table 3. This simulation therefore shows that our fully-adaptive variational algorithm enjoys several advantages in Bayesian estimation for Hawkes processes: it can infer the causality structure and provides a good approximation of the posterior mean, and is computationally efficient.

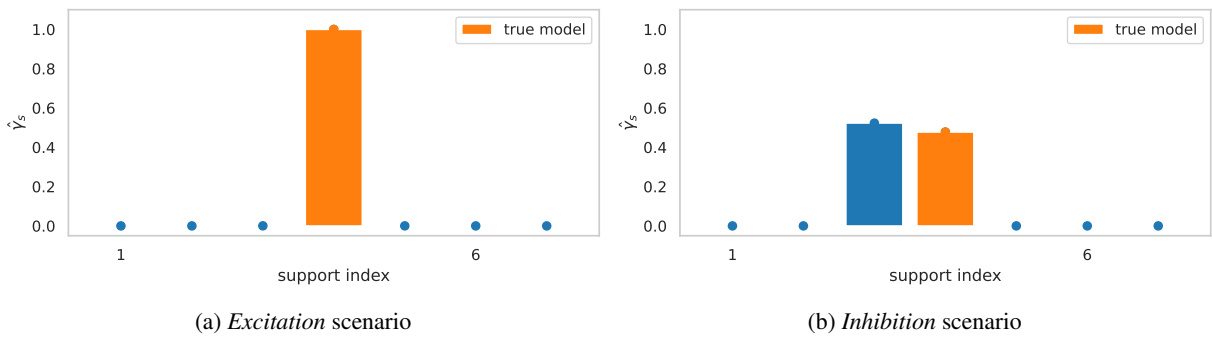


Figure 7: Marginal probabilities  $(\hat{\gamma}_s)_{s \in \mathcal{S}_1}$  in the adaptive mean-field variational posterior, in the well-specified scenario of Simulation 3 with  $K = 1$ . The left and right panels correspond to the *Excitation* (resp. *Inhibition*) setting where  $h_0 \geq 0$  (resp.  $h_0 \leq 0$ ). The elements in  $\mathcal{S}_1$  are indexed from 1 to 7, and correspond respectively to  $s = (0, 0)$ , and  $s = (1, d)$  with  $d = 0, \dots, 5$ . The marginal probability on the true  $s_0 = (1, 2)$  is colored in orange.

#### 5.4 Simulation 4: Two-step variational algorithm for multivariate sigmoid models

In this experiment, we test our two-step mean-field variational algorithm (Algorithm 3) in the multivariate sigmoid model with  $K = 2, 4, 8, 32$ . We note that to the best of our knowledge, the only Bayesian nonparametric method that has currently been tested in high-dimensional Hawkes processes is the Gaussian process model of Malem-Shinitski et al. [2021] in a sigmoid Hawkes model with time-varying background rate. We consider a well-specified setting with

<sup>2</sup>We further note that the current implementation of our algorithm has not been yet optimised.

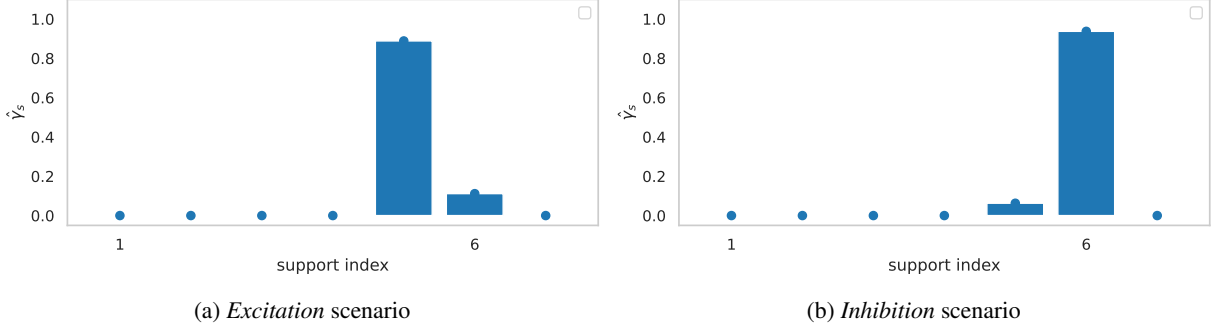


Figure 8: Marginal probabilities  $(\hat{\gamma}_s)_{s \in \mathcal{S}_1}$  in the adaptive mean-field variational posterior, in the mis-specified setting of Simulation 3 with  $K = 1$ . The left and right panels correspond to the (mostly) *Excitation* (resp. *Inhibition*) setting. The elements in  $\mathcal{S}_1$  are indexed from 1 to 7, and correspond respectively to  $s = (0, 0)$ , and  $s = (1, d)$  with  $D = 0, \dots, 5$ .

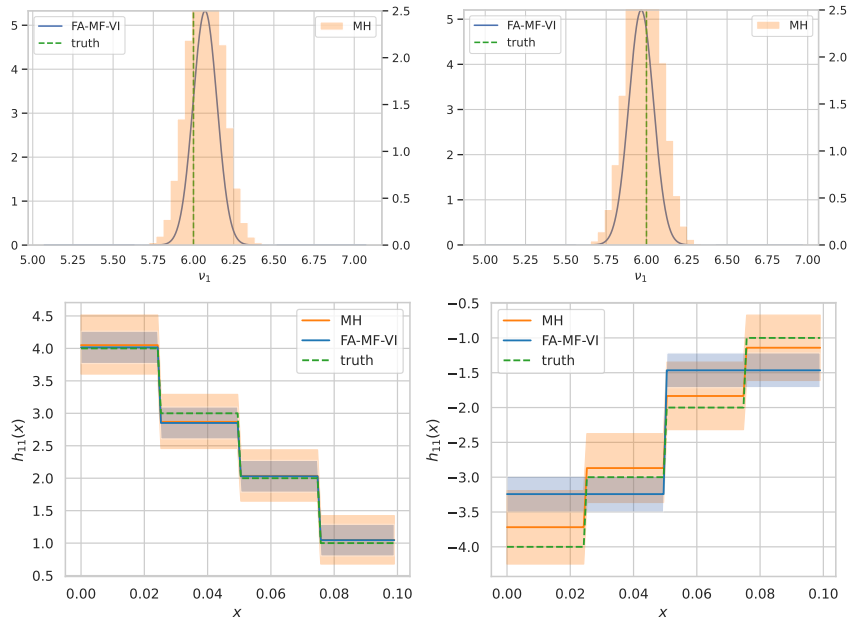


Figure 9: Posterior and mode variational posterior distributions on  $f = (\nu_1, h_{11})$  in the univariate sigmoid model and well-specified setting of Simulation 3, evaluated by the MH sampler and the fully-adaptive mean-field variational (FA-MF-VI) algorithm (Algorithm 2). The two columns correspond to the *Excitation* (left) and *Inhibition* (right) settings. The first row contains the marginal distribution on the background rate  $\nu_1$ , and the second row represents the (variational) posterior mean (solid line) and 95% credible sets (colored areas) on the (self) interaction function  $h_{11}$ . The true parameter  $f_0$  is plotted in dotted green line.

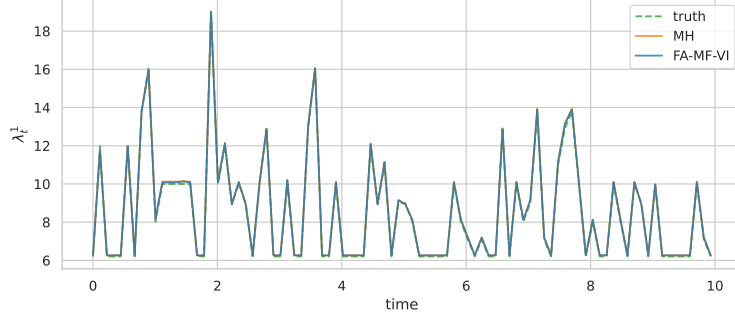
$h_0 \in \mathcal{H}_{hist}^{D_0}$  and  $D_0 = 1$ , and a *sparse* graph parameter  $\delta_0$  with  $\sum_{l,k} \delta_{lk}^0 = 2K - 1$  (see Figure 18). We also design an *Excitation* scenario and a *Self-inhibition* scenario similar to Simulation 3. We only report the results for the former in this section, and the ones for the latter can be found in Appendix D.2. We set  $T = 1000$  and report the number of events and excursions in each setting in Table 4. Here, we fix a threshold of  $\eta_0 = 0.07$  in Algorithm 3 - this choice will be further discussed below.

In Table 5, we report the performance of our method, in terms of the  $L_1$ -risk of the mode variational posterior on the parameter defined as

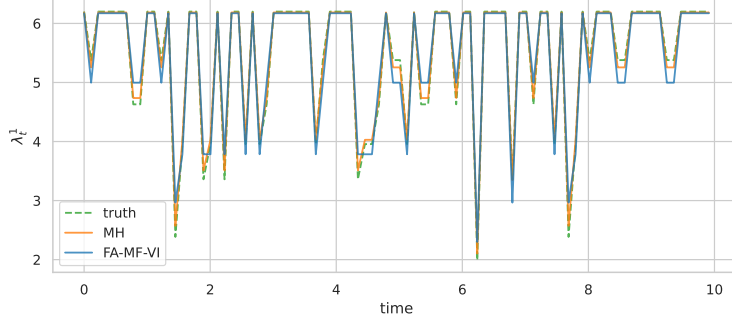
$$r_{L_1}(\hat{Q}_{MV}) := \mathbb{E}_{\hat{Q}_{MV}}[\|v - v_0\|_1] + \sum_{l,k} \mathbb{E}_{\hat{Q}_{MV}}[\|h_{lk} - h_{lk}^0\|_1]. \quad (32)$$

We note that the number of terms in the risk grows with  $K$  and the number of non-null interaction functions in  $h$  and  $h_0$ . In every setting, we obtain that  $\hat{s} = s_0 = (\delta_0, 1)$ , therefore our algorithm is able to recover the true graph  $\delta_0$  and dimensionality  $D_0$ . Moreover, we note that the risk seems to grow linearly with  $K$ , which indicates that the estimation





(a) Excitation scenario



(b) Inhibition scenario

Figure 10: Estimated intensity function based on the (variational) posterior mean, in the well-specified setting of Simulation 3 on  $[0, 10]$ , using the fully-adaptive mean-field variational (FA-MF-VI) algorithm (Algorithm 2). The true intensity  $\lambda_t^1(f_0)$  is plotted in dotted green line.

does not deteriorate with larger  $K$ . This can be also visually checked in Figure 21, where we plot the variational distribution  $\hat{Q}_s$  on a subset of the parameter  $f_2$  for each  $K$ . We note that the 95% credible bands on the background rate  $\nu_2$  increases with  $K$ , while this phenomenon does not appear on the interaction functions.

In Figure 19, we also plot the  $L_1$ -errors using  $\hat{Q}^{\delta_c}$ , i.e.,  $(\mathbb{E}_{\hat{Q}^{\delta_c}} [\|h_{lk} - h_{lk}^0\|_1])_{l,k}$  in the form of a heatmap compared to the true norms. We recall that  $\hat{Q}^{\delta_c}$  is mode variational distribution obtained after the first step of Algorithm 3, and is used to estimate the graph for the second step. We note that in all settings, these errors are relatively small, therefore allowing us to select the true graph parameter for the second step. Indeed, in Figure 20, we plot the estimated  $L_1$ -norms of the interaction functions using  $\hat{Q}^{\delta_c}$ , i.e.,  $(\mathbb{E}_{\hat{Q}^{\delta_c}} [\|h_{lk}\|_1])_{l,k}$  in increasing order of magnitude and observe a gap between the small and larger “signals”. Therefore, with our threshold of  $\eta_0 = 0.07$ , our algorithm is able to discriminate between the true signals and the noise, but in these settings, the threshold value could have been selected using the “gap” heuristic (see Section 4.4.2). Similar observation can also be made for the Self-inhibition scenario, which results are in Appendix D.2, although the estimation is slightly worse in this scenario. Finally, the computational times of our algorithm seem to scale well with  $K$  and the number of events, as can be seen in Figure 17.

This simulation in low and moderately high-dimensional settings therefore shows that our two-step procedure is able to select the causality structure and dimensionality of the process and allows to scale up variational Bayes approaches to larger number of dimensions in sparse settings. Nonetheless, we note that the choice of the threshold and heuristic approaches for this choice need to further explored.

## 6 Discussion

In this paper, we provided a theoretical study of variational Bayes methods in nonlinear Hawkes processes. We obtained variational concentration rates under easily verifiable conditions on the prior and approximating family, that we validated for estimation set-ups commonly used in practice. Our general theory holds in particular in the sigmoid Hawkes model, for which we also developed adaptive variational mean-field algorithms, that can infer the connectivity graph and the dimensionality of the parameter. Moreover, we demonstrated on simulated data that our most computationally efficient algorithm is able to scale up to high-dimensional processes.

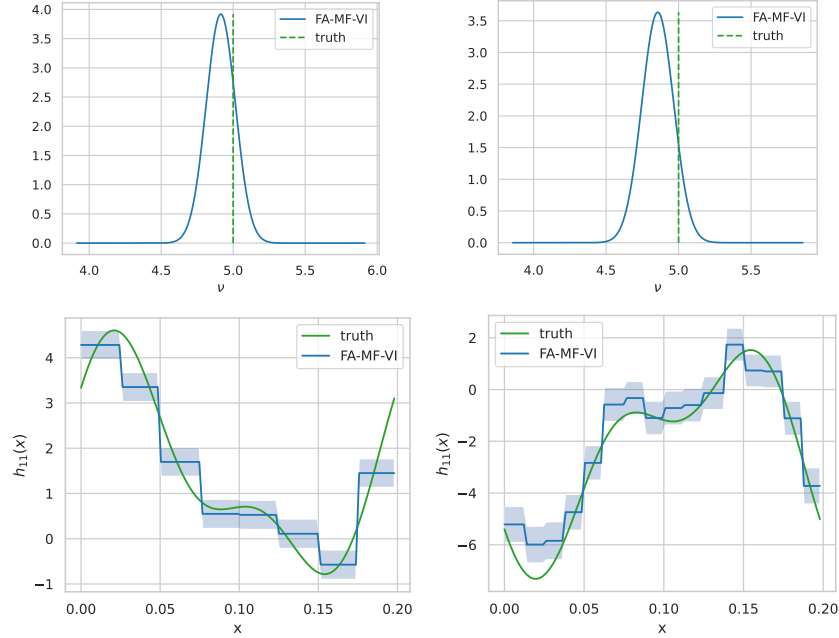


Figure 11: Mode variational posterior distributions on  $f = (\nu_1, h_{11})$  in the univariate sigmoid model and mis-specified setting of Simulation 3, evaluated by the fully-adaptive mean-field variational (FA-MF-VI) algorithm (Algorithm 2). The two columns correspond to a (mostly) *Excitation* (left) and a (mostly) *Inhibition* (right) settings. The first row contains the marginal distribution on the background rate  $\nu_1$ , and the second row represents the variational posterior mean (solid line) and 95% credible sets (colored areas) on the (self) interaction function  $h_{11}$ . The true parameter  $f_0$  is plotted in dotted green line.

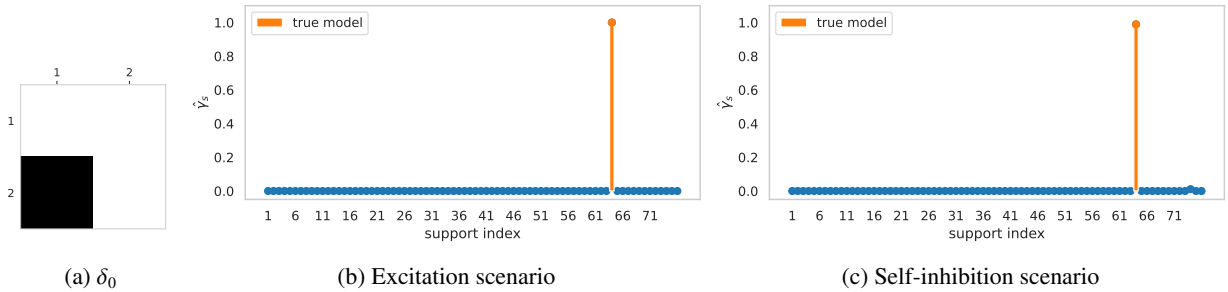


Figure 12: True graph parameter  $\delta_0$  (black=0, white=1) (a) and marginal probabilities  $(\hat{y}_s)_{s \in \mathcal{S}_2}$  in the adaptive mean-field variational posterior, in the well-specified setting of Simulation 3 with  $K = 2$ . The *Excitation* scenario (b) corresponds to  $h_0 \geq 0$ , while in the *Self-inhibition* scenario (c),  $h_{11}^0, h_{22}^0 \leq 0$ . The elements in  $\mathcal{S}_2$  are indexed from 1 to 76 and the true model corresponds to  $s_0 = (\delta_0, 2)$ .

Nonetheless, our theory does not yet cover the high-dimensional setting with  $K \rightarrow \infty$ , which is of practical interest in applications of Hawkes processes in social network analysis and neuroscience. In this limit, previous works have considered sparse models Cai et al. [2021], Bacry et al. [2020], Chen et al. [2017] and mean-field settings Pfaffelhuber et al. [2022]. We would therefore be interested in extending our results to these models.

Moreover, our empirical study shows that the credible sets of variational distributions do not always have good coverage, an observation that sometimes also holds for the posterior distribution. Therefore, it is left for future work to study the property of (variational) posterior credible regions, and potentially design post-processing methods of the latter to improve coverage in practice. Additionally, the thresholding approach for estimating the graph in our two-step adaptive variational procedure could be further explored. In particular, designing “good” heuristics to choose the threshold in a data-driven way would be of practical interest.

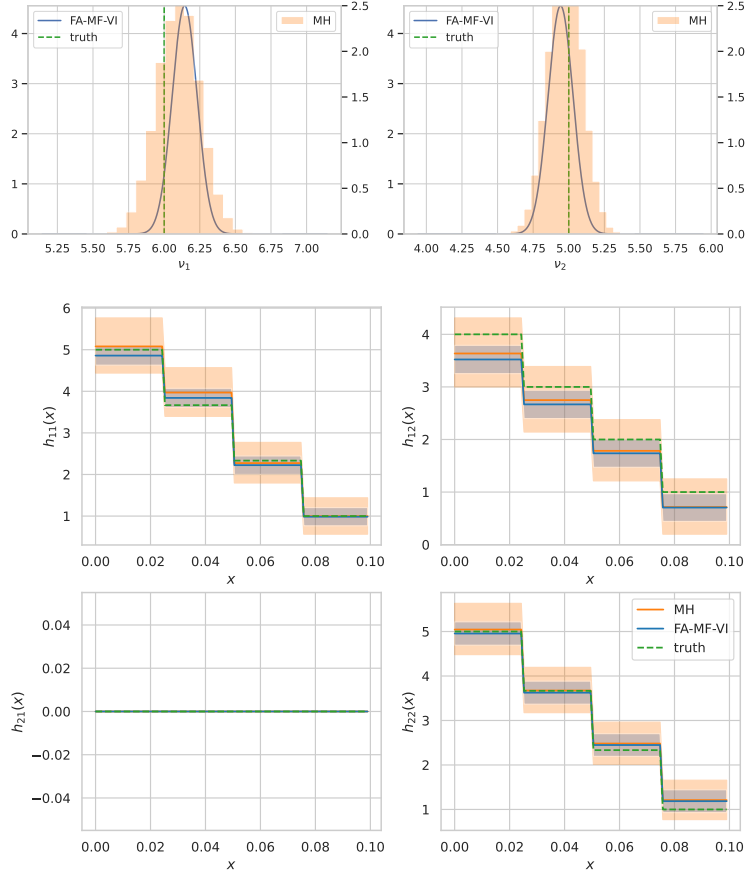


Figure 13: Posterior and mode variational posterior distributions on  $f = (v, h)$  in the bivariate sigmoid model, well-specified setting, and Excitation setting of Simulation 3, evaluated by the “optimal” MH sampler and the fully-adaptive mean-field variational (FA-MF-VI) algorithm (Algorithm 2). The first row contains the marginal distribution on the background rates  $(v_1, v_2)$ , and the second and third rows represent the (variational) posterior mean (solid line) and 95% credible sets (colored areas) on the four interaction function  $h_{11}, h_{12}, h_{21}, h_{22}$ . The true parameter  $f_0$  is plotted in dotted green line.

# dimensions	Scenario	# events	# excursions
2	Excitation	11 719	3295
	Inhibition	8335	3590
4	Excitation	25 509	2362
	Inhibition	17406	2948
8	Excitation	52 390	637
	Inhibition	35530	1043
16	Excitation	108 185	24
	Inhibition	71874	60
32	Excitation	217 320	0
	Inhibition	144741	0

Table 4: Number of observed events and excursions in the multivariate settings of Simulation 4.

Finally, it would be of practical interest to develop variational algorithms beyond the sigmoid model, e.g., the ReLU and softplus models. While in the sigmoid model, the conjugacy of the mean-field variational posterior using the

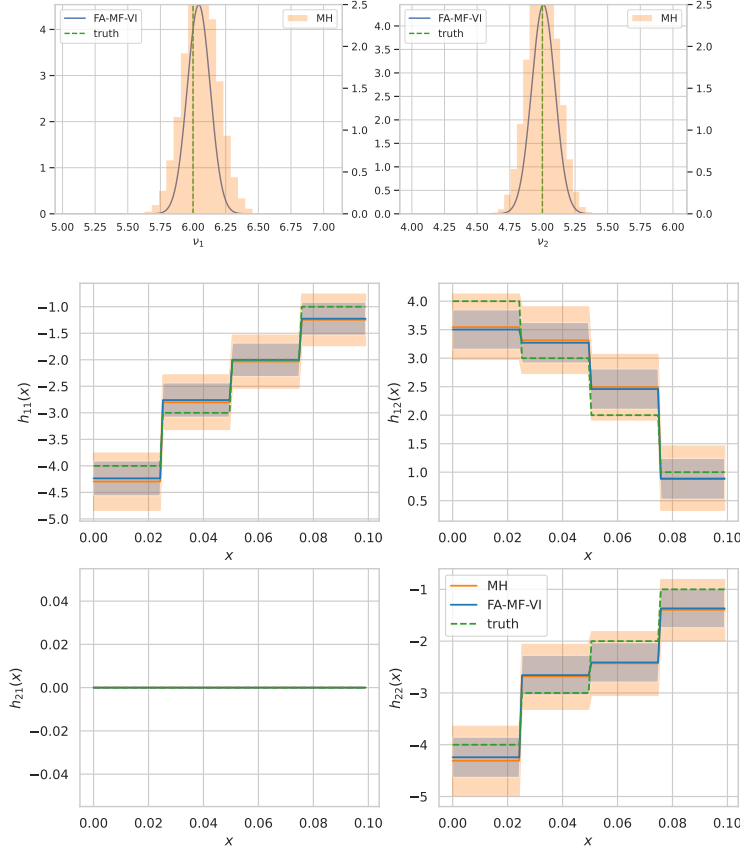


Figure 14: Posterior and mode variational posterior distributions on  $f = (v, h)$  in the bivariate sigmoid model, well-specified setting, and Self-Inhibition setting of Simulation 3, evaluated by the MH sampler and the fully-adaptive mean-field variational (FA-MF-VI) algorithm (Algorithm 2). The first row contains the marginal distribution on the background rates  $(v_1, v_2)$ , and the second and third rows represent the (variational) posterior mean (solid line) and 95% credible sets (colored areas) on the four interaction function  $h_{11}, h_{12}, h_{21}, h_{22}$ . The true parameter  $f_0$  is plotted in dotted green line.

# dimensions	Scenario	$\hat{s} = s_0$	Risk
2	Excitation	Yes	0.408
	Inhibition	Yes	0.277
4	Excitation	Yes	0.697
	Inhibition	Yes	0.767
8	Excitation	Yes	1.672
	Inhibition	Yes	2.312
16	Excitation	Yes	4.692
	Inhibition	Yes	4.688
32	Excitation	Yes	11.066
	Inhibition	Yes	12.074

Table 5: Performance of Algorithm 3 in the multivariate settings of Simulation 4. We report the risk  $r_{L_1}(\hat{Q})$  defined in (32) and if the model with largest marginal probability in  $\hat{Q}$  corresponds to the true one .

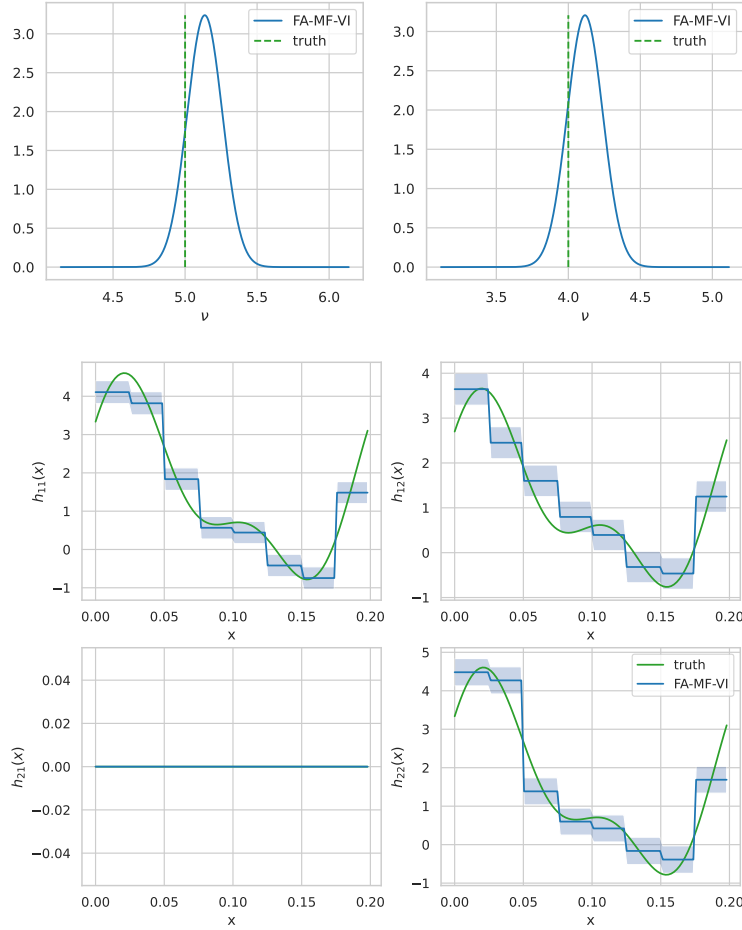
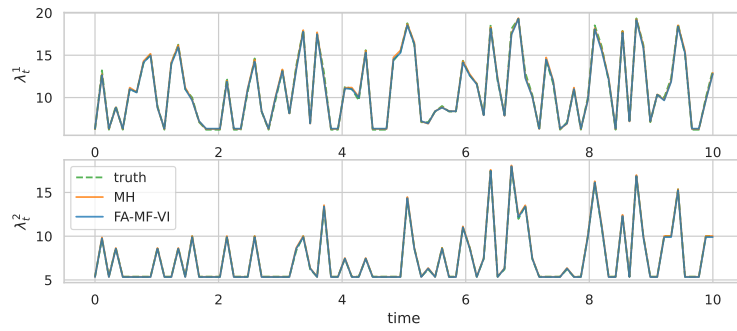
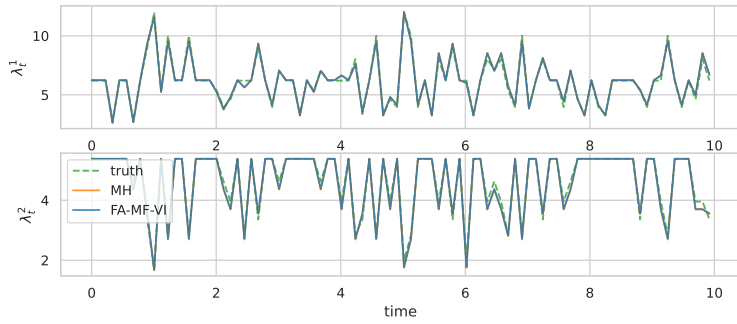


Figure 15: Mode variational posterior distributions on  $f = (\nu, h)$  in the bivariate sigmoid model, mis-specified setting, and Excitation setting of Simulation 3, computed with the fully-adaptive mean-field variational (FA-MF-VI) algorithm (Algorithm 2). The first row correspond two columns correspond to the *Excitation* (left) and *Inhibition* (right) settings. The first row contains the marginal distribution on the background rates  $(\nu_1, \nu_2)$ , and the second and third rows represent the (variational) posterior mean (solid line) and 95% credible sets (colored areas) on the four interaction function  $h_{11}, h_{12}, h_{21}, h_{22}$ . The true parameter  $f_0$  is plotted in dotted green line.

data augmentation strategy leads to particularly efficient algorithms, it is unlikely that such convenient forms could be obtained for more general models. A potential approach for other models could be to parametrise variational families with normalising flows, as it is for instance done for cut posteriors in Carmona and Nicholls [2022].



(a) Excitation scenario



(b) Self-inhibition scenario

Figure 16: Estimated intensity function based on the (variational) posterior mean, in the well-specified and bivariate setting of Simulation 3 on  $[0, 10]$ , using the fully-adaptive mean-field variational (FA-MF-VI) algorithm (Algorithm 2). The true intensity  $\lambda_t(f_0)$  is plotted in dotted green line.

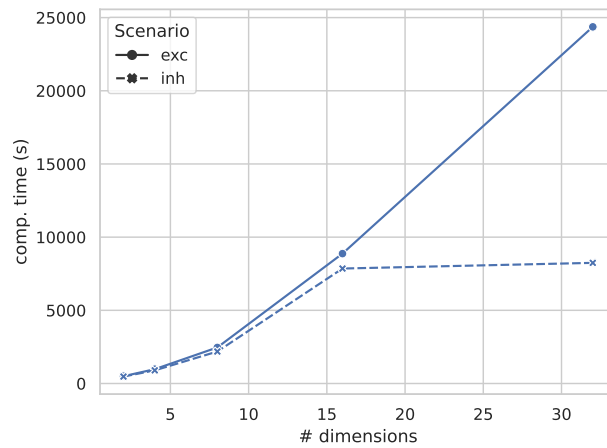


Figure 17: Computational times of our two-step mean-field variational algorithm (Algorithm 3) in the Excitation (exc) and Self-inhibition (inh) scenarios and well-specified setting of Simulation 4, for  $K = 2, 4, 8, 16, 32$ .

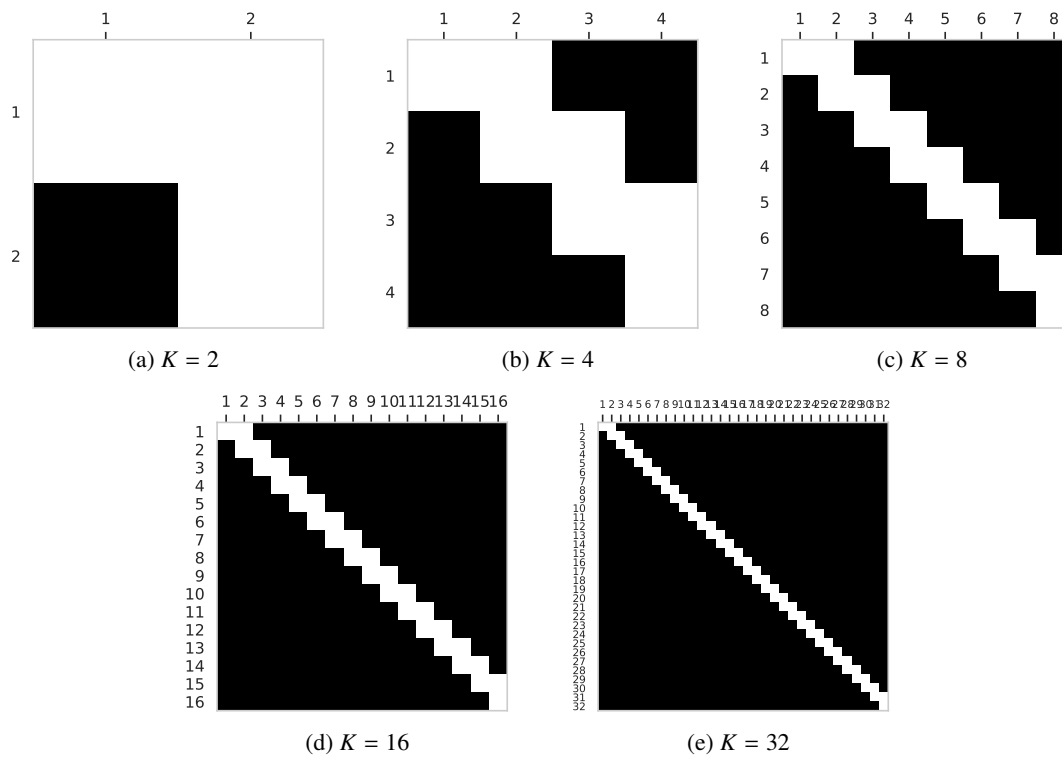


Figure 18: True graph parameter  $\delta_0$  (black=0, white=1) in the multivariate settings of Simulation 4.

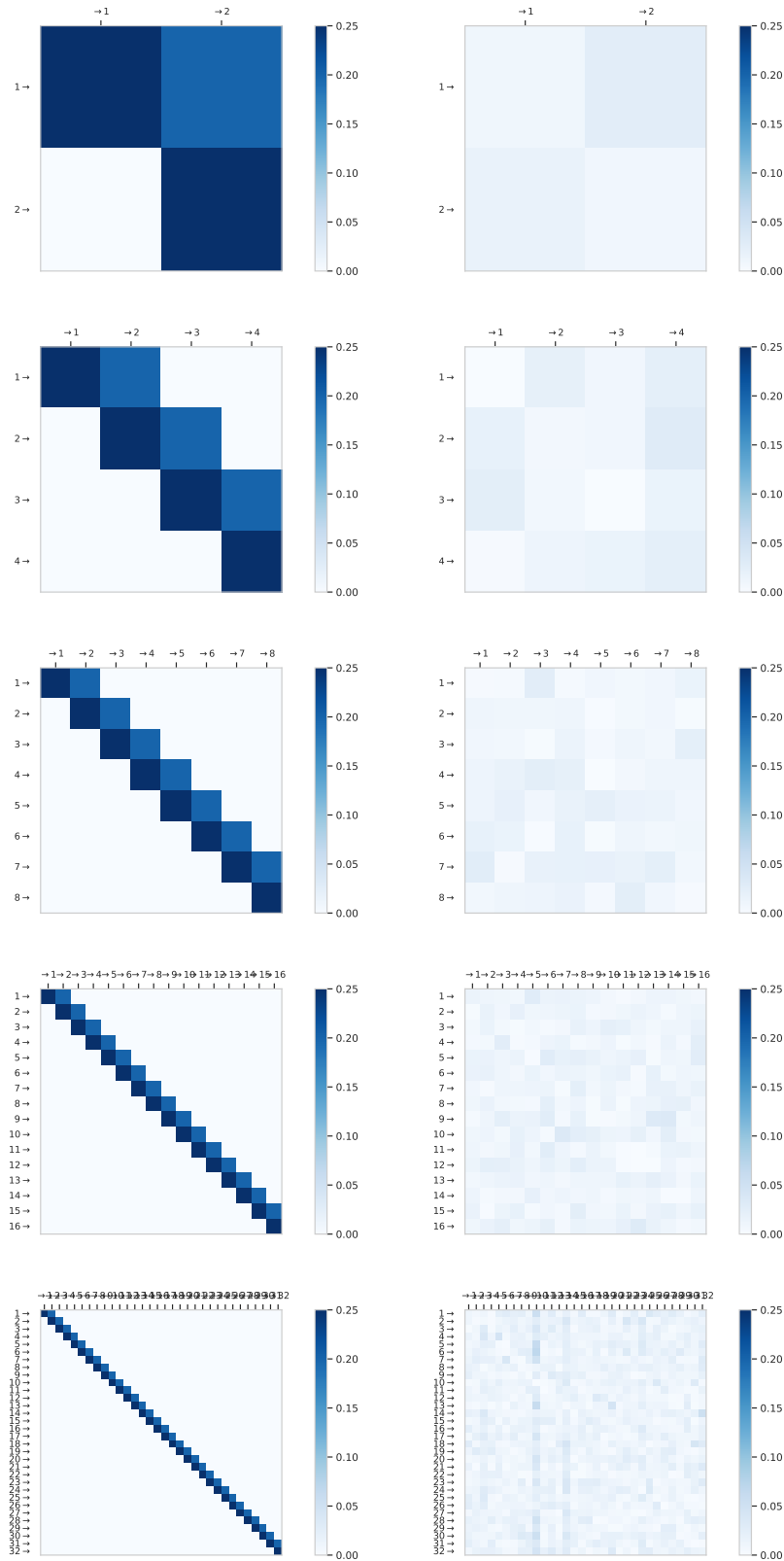
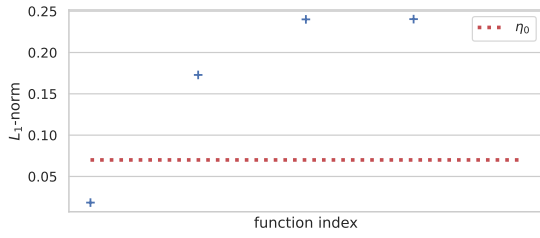
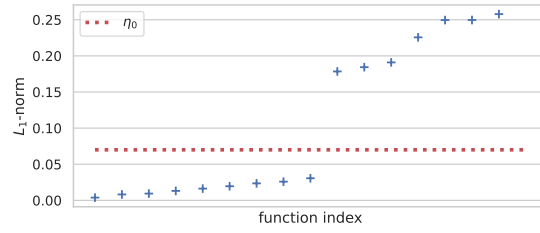


Figure 19: Heatmaps of the  $L_1$ -norms of the true parameter  $h_0$  (left column) and  $L_1$ -errors (right column) after the first step of Algorithm 3, in the Excitation scenario of Simulation 4. The rows correspond to  $K = 2, 4, 8, 16, 32$ .

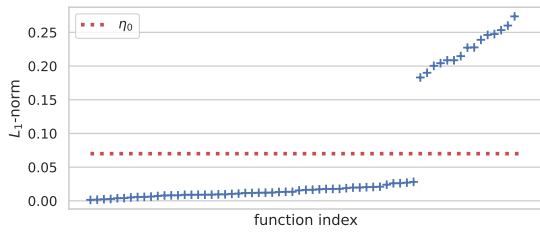




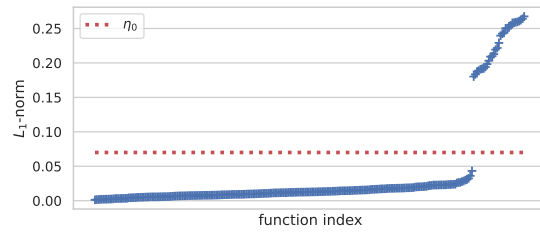
(a)  $K = 2$



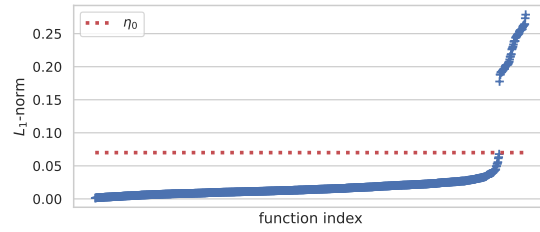
(b)  $K = 4$



(c)  $K = 8$



(d)  $K = 16$



(e)  $K = 32$

Figure 20: Estimated  $L_1$ -norms after the first step of Algorithm 3, plotted in increasing order, in the Excitation scenario of Simulation 4, for the models with  $K = 2, 4, 8, 16, 32$ . The threshold in our algorithm  $\eta_0 = 0.07$  is plotted in dotted red line.

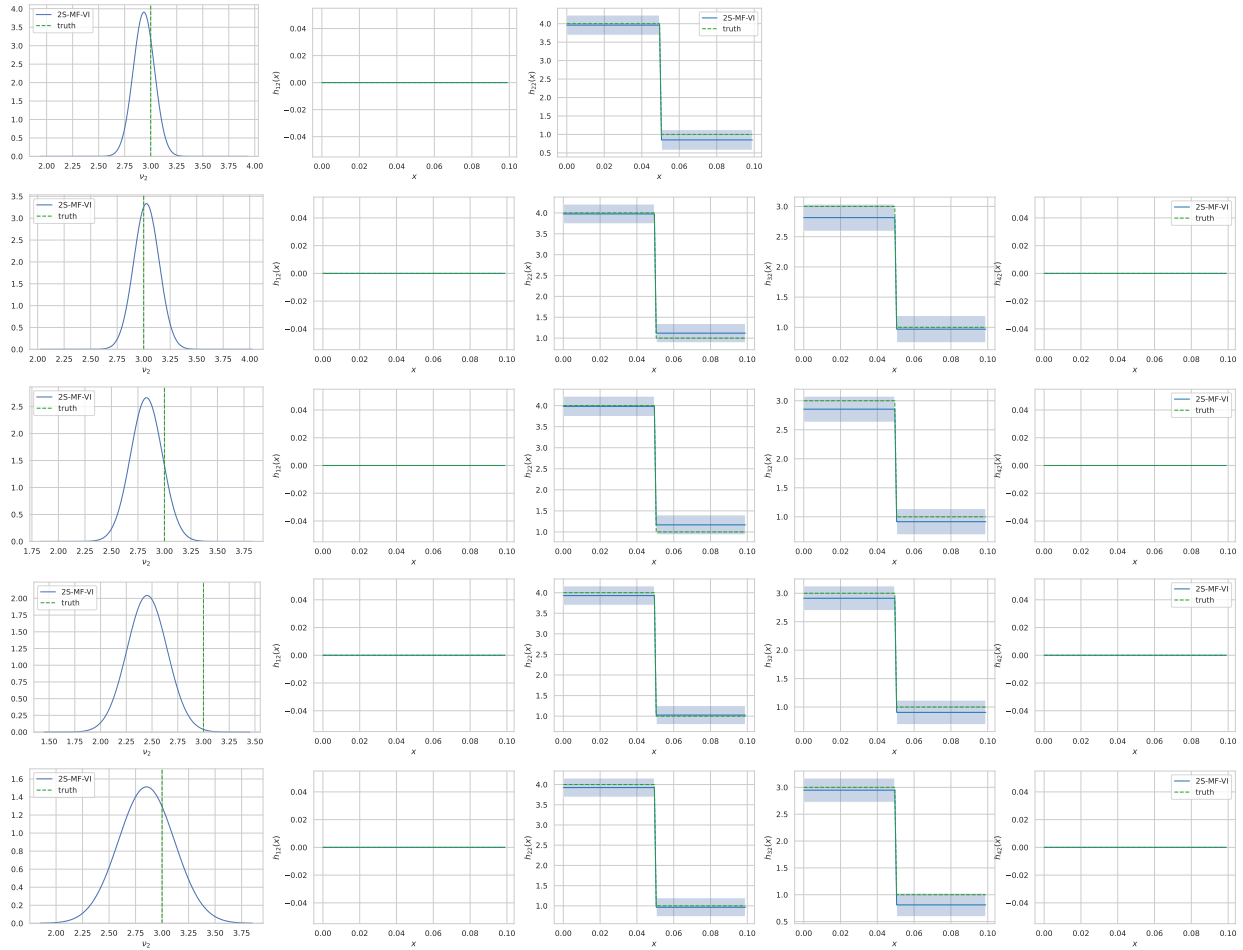


Figure 21: Mode variational posterior distributions on  $v_2$  (left column) and interaction functions  $h_{12}, h_{22}, h_{32}, h_{42}$  (second to last columns) in the Excitation scenario and multivariate sigmoid models of Simulation 4, computed with our two-step mean-field variational (2S-MF-VI) algorithm (Algorithm 3). The different rows correspond to different multivariate settings  $K = 2, 4, 8, 16, 32$ .

## References

- Ryan Prescott Adams, Iain Murray, and David J. C. MacKay. Tractable nonparametric bayesian inference in poisson processes with gaussian process intensities. In *Proceedings of the 26th Annual International Conference on Machine Learning*, ICML '09, page 9–16, New York, NY, USA, 2009. Association for Computing Machinery. ISBN 9781605585161. doi: 10.1145/1553374.1553376. URL <https://doi.org/10.1145/1553374.1553376>.
- Ifigeneia Apostolopoulou, Scott Linderman, Kyle Miller, and Artur Dubrawski. Mutually regressive point processes. *Advances in Neural Information Processing Systems*, 32, 2019.
- Emmanuel Bacry and Jean-Francois Muzy. Second order statistics characterization of hawkes processes and non-parametric estimation, 2015.
- Emmanuel Bacry, Martin Bompaire, Stéphane Gaïffas, and Jean-Francois Muzy. Sparse and low-rank multivariate hawkes processes. *Journal of Machine Learning Research*, 21(50):1–32, 2020.
- Christopher M Bishop and Nasser M Nasrabadi. *Pattern recognition and machine learning*, volume 4. Springer, 2006.
- Anna Bonnet, Miguel Martinez Herrera, and Maxime Sangnier. Maximum likelihood estimation for hawkes processes with self-excitation or inhibition. *Statistics & Probability Letters*, 179:109214, 2021.
- Pierre Bremaud and Laurent Massoulié. Stability of nonlinear hawkes processes. *The Annals of Probability*, 1996.
- Biao Cai, Jingfei Zhang, and Yongtao Guan. Latent network structure learning from high dimensional multivariate point processes, 2021.
- Chris U. Carmona and Geoff K. Nicholls. Scalable semi-modular inference with variational meta-posteriors, 2022. URL <https://arxiv.org/abs/2204.00296>.
- Lisbeth Carstensen, Albin Sandelin, Ole Winther, and Niels R Hansen. Multivariate hawkes process models of the occurrence of regulatory elements. *BMC bioinformatics*, 11(1):1–19, 2010.
- Shizhe Chen, Ali Shojaie, Eric Shea-Brown, and Daniela Witten. The multivariate hawkes process in high dimensions: Beyond mutual excitation. *arXiv:1707.04928v2*, 2017.
- Manon Costa, Carl Graham, Laurence Marsalle, and Viet Chi Tran. Renewal in hawkes processes with self-excitation and inhibition. *Advances in Applied Probability*, 52(3):879–915, 2020. doi: 10.1017/apr.2020.19.
- Daryl J Daley and David Vere-Jones. *An introduction to the theory of point processes: volume II: general theory and structure*. Springer Science & Business Media, 2007.
- Isabella Deutsch and Gordon J. Ross. Bayesian estimation of multivariate hawkes processes with inhibition and sparsity, 2022. URL <https://arxiv.org/abs/2201.05009>.
- Christian Donner and Manfred Opper. Efficient bayesian inference of sigmoidal gaussian cox processes, 2019.
- Sophie Donnet, Vincent Rivoirard, and Judith Rousseau. Nonparametric Bayesian estimation for multivariate Hawkes processes. volume 48, pages 2698 – 2727. Institute of Mathematical Statistics, 2020. doi: 10.1214/19-AOS1903. URL <https://doi.org/10.1214/19-AOS1903>.
- Michael Eichler, Rainer Dahlhaus, and Johannes Dueck. Graphical modeling for multivariate hawkes processes with nonparametric link functions. *Journal of Time Series Analysis*, 38(2):225–242, 2017.
- Felipe Gerhard, Moritz Deger, and Wilson Truccolo. On the stability and dynamics of stochastic spiking neuron models: Nonlinear hawkes process and point process glms. volume 13, page e1005390, 02 2017. doi: 10.1371/journal.pcbi.1005390.
- Gene H Golub and John H Welsch. Calculation of gauss quadrature rules. *Mathematics of computation*, 23(106): 221–230, 1969.
- Niels Richard Hansen, Patricia Reynaud-Bouret, and Vincent Rivoirard. Lasso and probabilistic inequalities for multivariate point processes. *Bernoulli*, 21(1):83–143, 2015. ISSN 1350-7265. doi: 10.3150/13-BEJ562. URL <http://dx.doi.org/10.3150/13-BEJ562>.
- J. F. C. Kingman. *Poisson processes*, volume 3 of *Oxford Studies in Probability*. The Clarendon Press Oxford University Press, New York, 1993. ISBN 0-19-853693-3. Oxford Science Publications.
- Remi Lemonnier and Nicolas Vayatis. Nonparametric markovian learning of triggering kernels for mutually exciting and mutually inhibiting multivariate hawkes processes. In *Joint European Conference on Machine Learning and Knowledge Discovery in Databases*, pages 161–176. Springer, 2014.
- Xiaofei Lu and Frédéric Abergel. High-dimensional hawkes processes for limit order books: modelling, empirical analysis and numerical calibration. *Quantitative Finance*, 18(2):249–264, 2018.

- Noa Malem-Shinitzki, Cesar Ojeda, and Manfred Opper. Nonlinear hawkes process with gaussian process self effects, 2021.
- Hongyuan Mei and Jason Eisner. The neural hawkes process: A neurally self-modulating multivariate point process, 2017.
- G. O. Mohler, M. B. Short, P. J. Brantingham, F. P. Schoenberg, and G. E. Tita. Self-exciting point process modeling of crime. *Journal of the American Statistical Association*, 106(493):100–108, 2011. doi: 10.1198/jasa.2011.ap09546. URL <https://doi.org/10.1198/jasa.2011.ap09546>.
- Dennis Nieman, Botond Szabo, and Harry van Zanten. Contraction rates for sparse variational approximations in gaussian process regression, 2021. URL <https://arxiv.org/abs/2109.10755>.
- Yoshihiko Ogata. Seismicity analysis through point-process modeling: A review. *Seismicity patterns, their statistical significance and physical meaning*, pages 471–507, 1999.
- Ilsang Ohn and Lizhen Lin. Adaptive variational bayes: Optimality, computation and applications, 2021.
- Jack Olinde and Martin B. Short. A self-limiting hawkes process: Interpretation, estimation, and use in crime modeling. In *2020 IEEE International Conference on Big Data (Big Data)*, pages 3212–3219, 2020. doi: 10.1109/BigData50022.2020.9378017.
- Peter Pfaffelhuber, Stefan Rotter, and Jakob Stiefel. Mean-field limits for non-linear hawkes processes with excitation and inhibition. *Stochastic Processes and their Applications*, 2022.
- Nicholas G. Polson, James G. Scott, and Jesse Windle. Bayesian inference for logistic models using polygamma latent variables, 2012. URL <https://arxiv.org/abs/1205.0310>.
- Kolyan Ray and Botond Szabó. Variational bayes for high-dimensional linear regression with sparse priors. *Journal of the American Statistical Association*, pages 1–12, jan 2021. doi: 10.1080/01621459.2020.1847121. URL <https://doi.org/10.1080>.
- Deborah Sulem, Vincent Rivoirard, and Judith Rousseau. Bayesian estimation of nonlinear hawkes process, 2021.
- Michalis Titsias and Miguel Lázaro-Gredilla. Spike and slab variational inference for multi-task and multiple kernel learning. In J. Shawe-Taylor, R. Zemel, P. Bartlett, F. Pereira, and K.Q. Weinberger, editors, *Advances in Neural Information Processing Systems*, volume 24. Curran Associates, Inc., 2011. URL <https://proceedings.neurips.cc/paper/2011/file/b495ce63ede0f4efc9eec62cb947c162-Paper.pdf>.
- A. van der Vaart and J. H. van Zanten. Adaptive Bayesian estimation using a Gaussian random field with inverse Gamma bandwidth. volume 37, pages 2655–2675, 2009a.
- A. W. van der Vaart and J. H. van Zanten. Adaptive bayesian estimation using a gaussian random field with inverse gamma bandwidth. *The Annals of Statistics*, 37(5B), oct 2009b. doi: 10.1214/08-aos678. URL <https://doi.org/10.1214>.
- Yichen Wang, Bo Xie, Nan Du, and Le Song. Isotonic hawkes processes. In *Proceedings of the 33rd International Conference on International Conference on Machine Learning - Volume 48, ICML’16*, page 2226–2234. JMLR.org, 2016.
- Fengshuo Zhang and Chao Gao. Convergence rates of variational posterior distributions. *arXiv: Statistics Theory*, 2017.
- Rui Zhang, Christian Walder, and Marian-Andrei Rizoiu. Variational inference for sparse gaussian process modulated hawkes process. *Proceedings of the AAAI Conference on Artificial Intelligence*, 34(04):6803–6810, Apr 2020. ISSN 2159-5399. doi: 10.1609/aaai.v34i04.6160. URL <http://dx.doi.org/10.1609/aaai.v34i04.6160>.
- Feng Zhou, Zhidong Li, Xuhui Fan, Yang Wang, Arcot Sowmya, and Fang Chen. Efficient em-variational inference for hawkes process, 2019.
- Feng Zhou, Zhidong Li, Xuhui Fan, Yang Wang, Arcot Sowmya, and Fang Chen. Efficient inference for nonparametric hawkes processes using auxiliary latent variables. *Journal of Machine Learning Research*, 21(241):1–31, 2020. URL <http://jmlr.org/papers/v21/19-930.html>.
- Feng Zhou, Quyu Kong, Yixuan Zhang, Cheng Feng, and Jun Zhu. Nonlinear hawkes processes in time-varying system, 2021a.
- Feng Zhou, Yixuan Zhang, and Jun Zhu. Efficient inference of flexible interaction in spiking-neuron networks, 2021b.

## A Proofs

In this section, we provide the proofs of our main theoretical results, Theorem 3.2 and Proposition 4.5. We first recall a set of useful lemmas from Sulem et al. [2021].

## A.1 Technical lemmas

In the first lemma, we recall the definition of excursions from Sulem et al. [2021], for stationary nonlinear Hawkes processes verifying condition (C1) or (C2). Then, Lemma A.2, corresponding to Lemma A.1 in Sulem et al. [2021], provides a control on the main event  $\tilde{\Omega}_T$  considered in the proof of Theorem 3.2. Finally, Lemma A.3 (Lemma A.4 in Sulem et al. [2021]) is a technical lemma for proving posterior concentration in Hawkes processes.

We also introduce the following notation. For any excursion index  $j \in [J_T - 1]$ , we denote  $(U_j^{(1)}, U_j^{(2)})$  the times of the first two events after the  $j$ -th renewal time  $\tau_j$ , and  $\xi_j := U_j^{(2)}$  if  $U_j^{(2)} \in [\tau_j, \tau_{j+1})$  and  $\xi_j := \tau_{j+1}$  otherwise.

**Lemma A.1** (Lemma 5.1 in Sulem et al. [2021]). *Let  $N$  be a Hawkes process with monotone non-decreasing and Lipschitz link functions  $\phi = (\phi_k)_k$  and parameter  $f = (v, h)$  such that  $(\phi, f)$  verify (C1) or (C2). Then the point process measure  $X_t(\cdot)$  defined as*

$$X_t(\cdot) = N|_{(t-A, t]}, \quad (33)$$

is a strong Markov process with positive recurrent state  $\emptyset$ . Let  $\{\tau_j\}_{j \geq 0}$  be the sequence of random times defined as

$$\tau_j = \begin{cases} 0 & \text{if } j = 0; \\ \inf \left\{ t > \tau_{j-1}; X_t \neq \emptyset, X_t = \emptyset \right\} = \inf \left\{ t > \tau_{j-1}; N|_{(t-A, t]} \neq \emptyset, N|_{(t-A, t]} = \emptyset \right\} & \text{if } j \geq 1. \end{cases}$$

Then,  $\{\tau_j\}_{j \geq 0}$  are stopping times for the process  $N$ . For  $T > 0$ , we also define

$$J_T = \max\{j \geq 0; \tau_j \leq T\}. \quad (34)$$

The intervals  $\{[\tau_j, \tau_{j+1})\}_{j=0}^{J_T-1} \cup [\tau_{J_T}, T]$  form a partition of  $[0, T]$ . The point process measures  $(N|_{[\tau_j, \tau_{j+1})})_{1 \leq j \leq J_T-1}$  are i.i.d. and independent of  $N|_{[0, \tau_1]}$  and  $N|_{[\tau_{J_T}, T]}$ ; they are called excursions and the stopping times  $\{\tau_j\}_{j \geq 1}$  are called regenerative or renewal times.

**Lemma A.2** (Lemma A.1 in Sulem et al. [2021]). *Let  $Q > 0$ . We consider  $\tilde{\Omega}_T$  defined in Section A.2. For any  $\beta > 0$ , we can choose  $C_\beta$  and  $c_\beta$  in the definition of  $\tilde{\Omega}_T$  such that  $\mathbb{P}_0[\tilde{\Omega}_T^c] \leq T^{-\beta}$ . Moreover, for any  $1 \leq q \leq Q$ ,*

$$\mathbb{E}_0 \left[ \mathbb{1}_{\tilde{\Omega}_T^c} \max_l \sup_{t \in [0, T]} \left( N^l[t - A, t] \right)^q \right] \leq 2T^{-\beta/2}.$$

**Lemma A.3** (Lemma 1.4 in Sulem et al. [2021]). *For any  $f \in \mathcal{F}_T$  and  $l \in [K]$ , let*

$$Z_{1l} = \int_{\tau_1}^{\xi_1} |\lambda_t^l(f) - \lambda_t^l(f_0)| dt,$$

Under the assumptions of Theorem 3.2, for  $M_T \rightarrow \infty$  such that  $M_T > M \sqrt{k_T}$  with  $M > 0$  and for any  $f \in \mathcal{F}_T$  such that  $\|v - v_0\|_1 \leq \max(\|v_0\|_1, \tilde{C})$  with  $\tilde{C} > 0$ , there exists  $l \in [K]$  such that on  $\tilde{\Omega}_T$ ,

$$\mathbb{E}_f[Z_{1l}] \geq C(f_0) \|f - f_0\|_1,$$

with  $C(f_0) > 0$  a constant that depends only on  $f_0$  and  $\phi = (\phi_k)_k$ .

## A.2 Proof of Theorem 3.2

We recall that in this result, we consider a general Hawkes model with known link functions  $(\phi_k)_k$ . Let  $r_0 = (r_1^0, \dots, r_k^0)$  with  $r_k^0 = \phi_k(v_k^0)$ . With  $C_\beta, c_\beta > 0$ , we first define  $\tilde{\Omega}_T \in \mathcal{G}_T$  as

$$\begin{aligned} \tilde{\Omega}_T &= \Omega_N \cap \Omega_J \cap \Omega_U, \\ \Omega_N &= \left\{ \max_{k \in [K]} \sup_{t \in [0, T]} N^k[t - A, t] \leq C_\beta \log T \right\} \cap \left\{ \sum_{k=1}^K \left| \frac{N^k[-A, T]}{T} - \mu_k^0 \right| \leq \delta_T \right\}, \\ \Omega_J &= \{J_T \in \mathcal{J}_T\}, \quad \Omega_U = \left\{ \sum_{j=1}^{J_T-1} (U_j^{(1)} - \tau_j) \geq \frac{T}{\mathbb{E}_0[\Delta\tau_1] \|r_0\|_1} \left( 1 - 2c_\beta \sqrt{\frac{\log T}{T}} \right) \right\}, \\ \mathcal{J}_T &= \left\{ J \in \mathbb{Z}_{\geq 0}; \left| \frac{J-1}{T} - \frac{1}{\mathbb{E}_0[\Delta\tau_1]} \right| \leq c_\beta \sqrt{\frac{\log T}{T}} \right\}, \end{aligned}$$

with  $J_T$  the number of excursions as defined in (34),  $\mu_k^0 := \mathbb{E}_0[\lambda_t^k(f_0)]$ ,  $\forall k$ ,  $\delta_T = \delta_0 \sqrt{\frac{\log T}{T}}$ ,  $\delta_0 > 0$  and  $\{U_j^{(1)}\}_{j=1, \dots, J_T-1}$  denoting the first events of each excursion (see Lemma A.1 for a precise definition). Secondly, we define  $A'_T \in \mathcal{G}_T$  as

$$A'_T = \left\{ \int e^{L_T(f) - L_T(f_0)} d\tilde{\Pi}(f) > e^{-C_1 T \varepsilon_T^2} \right\}, \quad \tilde{\Pi}(B) = \frac{\Pi(B \cap K_T)}{\Pi(K_T)}, \quad K_T \subset \mathcal{F},$$

with  $C_1 > 0$  and  $\varepsilon_T, M_T$  positive sequences such that  $T\varepsilon_T^2 \rightarrow \infty$  and  $M_T \rightarrow \infty$ . From Lemma A.2, we have that  $\mathbb{P}_0[\tilde{\Omega}_T^c] = o(1)$ . Thus, with  $A_T = \tilde{\Omega}_T \cap A'_T$ ,  $K_T = B_\infty(\varepsilon_T)$ , and  $\varepsilon_T = \sqrt{\kappa_T} \varepsilon_T$ , we can obtain that

$$\begin{aligned} \mathbb{P}_0[A_T^c] &\leq \mathbb{P}_0[\tilde{\Omega}_T^c] + \mathbb{P}_0[A_T^c \cap \tilde{\Omega}_T] = o(1) + \mathbb{P}_0\left[\left\{ \int_{K_T} e^{L_T(f) - L_T(f_0)} d\Pi(f) \leq \Pi(K_T) e^{-C_1 T \varepsilon_T^2} \right\} \cap \tilde{\Omega}_T\right] \\ &\leq o(1) + \mathbb{P}_0\left[\left\{ D_T \leq \Pi(K_T) e^{-C_1 T \varepsilon_T^2} \right\} \cap \tilde{\Omega}_T\right] = o(1), \end{aligned}$$

with  $C_1 > 1$ , using (A0), i.e.,  $\Pi(K_T) \geq e^{-c_1 T \varepsilon_T^2}$ , and the following intermediate result from the proof of Theorem 3.2 in Sulem et al. [2021]

$$\mathbb{P}_0\left[\left\{ D_T \leq \Pi(B_\infty(\varepsilon_T)) e^{-\kappa_T T \varepsilon_T^2} \right\} \cap \tilde{\Omega}_T\right] = o(1).$$

Therefore, we can conclude that

$$\mathbb{P}_0[A_T] \xrightarrow{T \rightarrow \infty} 1.$$

We now define the stochastic distance  $\tilde{d}_{1T}$  and stochastic neighborhoods around  $f_0$  as

$$\tilde{d}_{1T}(f, f') = \frac{1}{T} \sum_{k=1}^K \int_0^T \mathbb{1}_{A_2(T)}(t) |\lambda_t^k(f) - \lambda_t^k(f')| dt, \quad A_2(T) = \bigcup_{j=1}^{J_T-1} [\tau_j, \xi_j] \quad (35)$$

$$A_{d_1}(\varepsilon) = \{f \in \mathcal{F}; \tilde{d}_{1T}(f, f_0) \leq \varepsilon\}, \quad \varepsilon > 0,$$

where for each  $j \in [J_T]$ ,  $U_j^{(2)}$  is the first event after  $U_j^{(1)}$ , and  $\xi_j := U_j^{(2)}$  if  $U_j^{(2)} \in [\tau_j, \tau_{j+1})$  and  $\xi_j := \tau_{j+1}$  otherwise. Let  $\eta_T$  be a positive sequence and  $\hat{Q}$  be the variational posterior as defined in (5). Using Markov's inequality, we have

$$\mathbb{E}_0[\hat{Q}(A_{d_1}(\eta_T)^c)] \leq \mathbb{P}_0[A_T^c] + \mathbb{E}_0[\hat{Q}(A_{d_1}(\eta_T)^c) \mathbb{1}_{A_T}]. \quad (36)$$

We first bound the second term on the RHS of (36) using the following technical lemma, which is an adaptation of Theorem 5 of Ray and Szabó [2021] and Lemma 13 in Nieman et al. [2021].

**Lemma A.4.** *Let  $B_T \subset \mathcal{F}$ ,  $A_T \in \mathcal{G}_T$ , and  $Q$  be a distribution on  $\mathcal{F}$ . If there exist  $C, u_T > 0$  such that*

$$\mathbb{E}_0[\Pi(B_T|N) \mathbb{1}_{A_T}] \leq C e^{-u_T}, \quad (37)$$

*then, we have that*

$$\mathbb{E}_0[Q(B_T) \mathbb{1}_{A_T}] \leq \frac{2}{u_T} \left( \mathbb{E}_0[KL(Q||\Pi(\cdot|N)) \mathbb{1}_{A_T}] + C e^{-u_T/2} \right).$$

*Proof.* We follow the proof of Ray and Szabó [2021] and use the fact that, for any  $g : \mathcal{F} \rightarrow \mathbb{R}$  such that  $\int_{\mathcal{F}} e^{g(f)} d\Pi(f|N) < +\infty$ , it holds true that

$$\int_{\mathcal{F}} g(f) dQ \leq KL(Q||\Pi(\cdot|N)) + \log \int_{\mathcal{F}} e^{g(f)} \Pi(f|N).$$

Applying the latter inequality with  $g = \frac{1}{2} u_T \mathbb{1}_{B_T}$ , we obtain

$$\begin{aligned} \frac{1}{2} u_T Q(B_T) &\leq KL(Q||\Pi(\cdot|N)) + \log(1 + e^{\frac{1}{2} u_T} \Pi(B_T|N)) \\ &\leq KL(Q||\Pi(\cdot|N)) + \frac{1}{2} u_T \Pi(B_T|N). \end{aligned}$$

Then, multiplying both sides of the previous inequality by  $\mathbb{1}_A$  and taking expectation wrt to  $\mathbb{P}_0$ , using (37), we finally obtain

$$\frac{1}{2} u_T \mathbb{E}_0[Q(B_T) \mathbb{1}_{A_T}] \leq \mathbb{E}_0[KL(Q||\Pi(\cdot|N)) \mathbb{1}_{A_T}] + C e^{-\frac{1}{2} u_T}.$$

□

We thus apply Lemma A.4 with  $B_T = A_{d_1}(\eta_T)^c$ ,  $\eta_T = M'_T \varepsilon_T$ ,  $Q = \hat{Q}$ , and  $u_T = M_T T \varepsilon_T^2$  with  $M'_T \rightarrow \infty$ . We first check that (37) holds, i.e., we show that there exists  $C, M_T, M'_T > 0$  such that

$$\mathbb{E}_0 \left[ \mathbb{1}_{A_T} \Pi[\tilde{d}_{1T}(f, f_0) > M'_T \varepsilon_T | N] \right] \leq C \exp(-M_T T \varepsilon_T^2). \quad (38)$$

For any test  $\phi$ , we have the following decomposition

$$\mathbb{E}_0 \left[ \mathbb{1}_{A_T} \Pi[\tilde{d}_{1T}(f, f_0) > M'_T \varepsilon_T | N] \right] \leq \underbrace{\mathbb{E}_0 [\phi \mathbb{1}_{A_T}]}_{(I)} + \underbrace{\mathbb{E}_0 [(1 - \phi) \mathbb{1}_{A_T} \Pi[A_{d_1}(M'_T \varepsilon_T)^c | N]]}_{(II)}.$$

Note that we have

$$\begin{aligned} (II) &= \mathbb{E}_0 [(1 - \phi) \mathbb{1}_{A_T} \Pi[A_{d_1}(M'_T \varepsilon_T)^c | N]] = \mathbb{E}_0 \left[ \int_{A_{d_1}(M \varepsilon_T)^c} \mathbb{1}_{A_T} (1 - \phi) \frac{e^{L_T(f) - L_T(f_0)}}{D_T} d\Pi(f) \right] \\ &\leq \Pi(K_T) e^{C_1 T \varepsilon_T^2} \mathbb{E}_0 \left[ \sup_{f \in \mathcal{F}_T} \mathbb{E}_f \left[ \mathbb{1}_{A_{d_1}(M \varepsilon_T)^c} \mathbb{1}_{A_T} (1 - \phi) | \mathcal{G}_0 \right] \right], \end{aligned} \quad (39)$$

since on  $A_T$ ,  $D_T \geq \Pi(K_T) e^{C_1 T \varepsilon_T^2}$ . Using the proof of Theorem 5.5 in Sulem et al. [2021], we can directly obtain that for  $T$  large enough, there exist  $x_1, M, M' > 0$  such that

$$\begin{aligned} (I) &\leq 2(2K + 1) e^{-x_1 M^2 T \varepsilon_T^2} \\ (II) &\leq 2(2K + 1) e^{-x_1 M^2 T \varepsilon_T^2 / 2}, \end{aligned}$$

which imply that

$$\mathbb{E}_0 \left[ \mathbb{1}_{A_T} \Pi[\tilde{d}_{1T}(f, f_0) > M'_T \varepsilon_T | N] \right] \leq 4(2K + 1) e^{-x_1 M'^2 T \varepsilon_T^2 / 2},$$

and (38) with  $M_T = x_1 M'^2 / 2$  and  $C = 2(2K + 1)$ . Applying Lemma A.4 thus leads to

$$\mathbb{E}_0 \left[ \hat{Q}(A_{d_1}(\eta_T)^c) \mathbb{1}_{A_T} \right] \leq 2 \frac{KL(\hat{Q} | \Pi(\cdot | N)) + C e^{-M_T T \varepsilon_T^2 / 2}}{M_T T \varepsilon_T^2} \leq 2C e^{-M_T T \varepsilon_T^2 / 2} + 2 \frac{KL(\hat{Q} | \Pi(\cdot | N))}{M_T T \varepsilon_T^2}.$$

Moreover, from (A2) and Remark 3.4, it holds that  $KL(\hat{Q} | \Pi(\cdot | N)) = O(T \varepsilon_T^2)$ , therefore we obtain the following intermediate result

$$\mathbb{E}_0 \left[ \hat{Q}(A_{d_1}(\eta_T)^c) \right] = o(1).$$

Now, with  $M_T > M'_T$ , we note that

$$\mathbb{E}_0 \left[ \hat{Q}(\|f - f_0\|_1 > M_T \varepsilon_T) \right] = \mathbb{E}_0 \left[ \hat{Q}(\tilde{d}_{1T}(f, f_0) > M'_T \varepsilon_T) \right] + \mathbb{E}_0 \left[ \hat{Q}(\|f - f_0\|_1 > M_T \varepsilon_T, \tilde{d}_{1T}(f, f_0) < M'_T \varepsilon_T) \mathbb{1}_{A_T} \right] + \mathbb{P}_0[A_T^c].$$

Therefore, it remains to show that

$$\mathbb{E}_0 \left[ \hat{Q}(\|f - f_0\|_1 > M_T \varepsilon_T, \tilde{d}_{1T}(f, f_0) < M'_T \varepsilon_T) \mathbb{1}_{A_T} \right] = \mathbb{E}_0 \left[ \hat{Q}(A_{L_1}(M_T \varepsilon_T)^c \cap A_{d_1}(M'_T \varepsilon_T)) \mathbb{1}_{A_T} \right] = o(1).$$

For this, we apply again Lemma A.4 with  $B_T = A_{L_1}(M_T \varepsilon_T)^c \cap A_{d_1}(M'_T \varepsilon_T)$  and  $u_T = T M_T^2 \varepsilon_T^2$ . We have

$$\mathbb{E}_0 \left[ \mathbb{1}_{A_T} \Pi(A_{L_1}(M_T \varepsilon_T)^c \cap A_{d_1}(M'_T \varepsilon_T) | N) \right] \leq \Pi(K_T) e^{C_1 T \varepsilon_T^2} \mathbb{E}_0 \left[ \mathbb{E}_f \left[ \mathbb{1}_{A_T} \mathbb{1}_{A_{L_1}(M_T \varepsilon_T)^c \cap A_{d_1}(M'_T \varepsilon_T)} | \mathcal{G}_0 \right] \right].$$

Let  $f \in A_{L_1}(M_T \varepsilon_T)^c \cap A_{d_1}(M'_T \varepsilon_T)$ . For any  $j \in [J_T - 1]$  and  $l \in [K]$ , let

$$Z_{jl} = \int_{\tau_j}^{\xi_j} |\lambda_j^l(f) - \lambda_j^l(f_0)| dt, \quad j \in [J_T - 1], \quad l \in [K]. \quad (40)$$

Using Lemma A.3, for any  $f \in A_{L_1}(M_T \varepsilon_T)^c$ , we have

$$\begin{aligned} \mathbb{E}_f \left[ \mathbb{1}_{A_T} \mathbb{1}_{A_{d_1}(M'_T \varepsilon_T)} | \mathcal{G}_0 \right] &\leq \mathbb{P}_f \left[ \sum_{j=1}^{J_T-1} Z_{jl} \leq T M'_T \varepsilon_T | \mathcal{G}_0 \right] \\ &\leq \sum_{j \in \mathcal{J}_T} \mathbb{P}_f \left[ \sum_{l=1}^{J-1} Z_{jl} - \mathbb{E}_f [Z_{jl}] \leq T M'_T \varepsilon_T - \frac{T}{2 \mathbb{E}_0 [\Delta \tau_1]} C(f_0) M_T \varepsilon_T | \mathcal{G}_0 \right] \\ &\leq \sum_{j \in \mathcal{J}_T} \mathbb{P}_f \left[ \sum_{l=1}^{J-1} Z_{jl} - \mathbb{E}_f [Z_{jl}] \leq -\frac{T}{4 \mathbb{E}_0 [\Delta \tau_1]} C(f_0) M_T \varepsilon_T | \mathcal{G}_0 \right], \end{aligned}$$

for any  $M_T \geq 4\mathbb{E}_0[\Delta\tau_1]M'_T$ . Similarly to the proof of Theorem 3.2 in Sulem et al. [2021]), we apply Bernstein's inequality for each  $J \in \mathcal{J}_T$  and obtain that

$$\mathbb{E}_f \left[ \mathbb{1}_{A_T} \mathbb{1}_{A_{d_1}(M_T \varepsilon_T)} | \mathcal{G}_0 \right] \leq \exp\{-c(f_0)'T\}, \quad \forall f \in A_{L_1}(M_T \varepsilon_T)^c.$$

Therefore, we can conclude that

$$\mathbb{E}_0 \left[ \hat{Q}(A_{L_1}(M_T \varepsilon_T)^c \cap A_{d_1}(M_T \varepsilon_T)) \mathbb{1}_{A_T} \right] \leq \frac{2}{M_T T \varepsilon_T^2} \mathbb{E}_0 \left[ KL(\hat{Q} \| \Pi(\cdot|N)) \right] + \exp\{-c(f_0)'T/2\} = o(1),$$

since  $\mathbb{E}_0 \left[ KL(\hat{Q} \| \Pi(\cdot|N)) \right] = O(T \varepsilon_T^2)$  by assumption (A2). This leads to our final conclusion

$$\mathbb{E}_0 \left[ \hat{Q}(\|f - f_0\|_1 > M_T \varepsilon_T) \right] = o(1).$$

## B Additional proofs

### B.1 Proof of Lemma 4.3

Using the proof of Proposition 2.3 in Sulem et al. [2021], we can easily obtain that  $N =^D N'$  implies that

$$\frac{\theta_k}{\theta'_k} = \frac{\tilde{\sigma}(v'_k)}{\tilde{\sigma}(v_k)} = \frac{\tilde{\sigma}(h'_{lk})}{\tilde{\sigma}(h_{lk})}, \quad \forall l, k.$$

Now, using Assumption 4.1 and the proof of Proposition 2.3 in Sulem et al. [2021], one can show that

$$\begin{aligned} \mathbb{P}[\sup_{t \geq 0} \lambda_t^k(f) = \theta_k] &= 1 \\ \mathbb{P}[\sup_{t \geq 0} \lambda_t^k(f') = \theta'_k] &= 1. \end{aligned}$$

Then, one can conclude that  $\theta = \theta'$ , implying also that  $h = h'$  and  $v = v'$ .

## C Additional derivation in the sigmoid Hawkes model with data augmentation

### C.1 Updates of the fixed-dimension mean-field variational algorithm

In this section, we derive the analytic forms of the conditional updates in Algorithm 1, the mean-field variational algorithm with fixed dimensionality described in Section 4.3. For ease of exposition, we drop the indices  $k$  and  $s$  and use the notation  $Q_1, Q_2$  for the variational factors. In the following computation, we use the notation  $c$  to denote a generic constant which value can vary from one line to the other. We also define  $\alpha := 0.1$  and  $\eta = 10$ .

From the definition of the augmented posterior (21), we first note that

$$\begin{aligned} \log p(f, N, \omega, \bar{N}) &= \log \Pi(f, \omega, \bar{N}|N) + \log p(N) = L_T(f, \omega, \bar{N}; N) + \log \Pi(f) + \log p(N) + c \\ &= \log p(\omega|f, N) + \log p(\bar{N}|f, N) + \log \Pi(f) + \log p(N) + c. \end{aligned} \quad (41)$$

In the previous equality we have used the facts that  $p(\omega|f, N, \bar{N}) = p(\omega|f, N)$  and  $p(\bar{N}|f, N, \omega) = p(\bar{N}|f, N)$ . We recall our notation  $H(t) = (H^0(t), H^1(t), \dots, H^K(t)) \in \mathbb{R}^{KJ+1}$ ,  $t \in \mathbb{R}$ , where for  $k \in [K]$ ,  $H^k(t) = (H_j^k(t))_{j=1, \dots, J}$  and  $H_j^k$  defined in (25). We have that

$$\begin{aligned} \mathbb{E}_{Q_2}[\log p(\omega|f, N)] &= \mathbb{E}_{Q_2} \left[ \sum_{i \in [N]} g(\omega_i, \tilde{\lambda}_{T_i}(f)) \right] + c = \mathbb{E}_{Q_2} \left[ \sum_{i \in [N]} -\frac{\omega_i \tilde{\lambda}_{T_i}(f)^2}{2} + \frac{\tilde{\lambda}_{T_i}(f)}{2} \right] + c \\ &= \mathbb{E}_{Q_2} \left[ \sum_{i \in [N]} -\frac{\omega_i \alpha^2 (f^T H(T_i) H(T_i)^T f - 2\eta H(T_i)^T f + \eta^2)}{2} + \frac{\alpha H(T_i)^T f}{2} \right] + c \\ &= \mathbb{E}_{Q_2} \left[ -\frac{1}{2} \sum_{i \in [N]} \left\{ \omega_i \alpha^2 f^T H(T_i) H(T_i)^T f - \alpha(2\omega_i \alpha \eta + 1) H(T_i)^T f + \omega_i \alpha^2 \eta^2 \right\} \right] + c \\ &= -\frac{1}{2} \sum_{i \in [N]} \left\{ \mathbb{E}_{Q_2}[\omega_i] \alpha^2 f^T H(T_i) H(T_i)^T f - \alpha(2\mathbb{E}_{Q_2}[\omega_i] \alpha \eta + 1) H(T_i)^T f + \mathbb{E}_{Q_2}[\omega_i] \alpha^2 \eta^2 \right\} + c. \end{aligned}$$



Moreover, we also have that

$$\begin{aligned}
\mathbb{E}_{Q_2}[\log p(\bar{N}|f, N)] &= \mathbb{E}_{Q_2} \left[ -\frac{1}{2} \sum_{j \in [\bar{N}]} \left\{ \bar{\omega}_j \alpha^2 f^T H(\bar{T}_j) H(\bar{T}_j)^T f - \alpha(2\bar{\omega}_j \alpha \eta - 1) H(\bar{T}_j)^T f + \bar{\omega}_j \alpha^2 \eta^2 \right\} \right] + c \\
&= \int_0^T \int_0^\infty \left[ -\frac{1}{2} \left( \bar{\omega} \alpha^2 f^T H(t) H(t)^T f - \alpha(2\bar{\omega} \alpha \eta - 1) H(t)^T f + \bar{\omega} \alpha^2 \eta^2 \right) \right] \Lambda(t, \bar{\omega}) d\bar{\omega} dt + c \\
&= -\frac{1}{2} \left[ f^T \left( \alpha^2 \int_0^T \int_0^\infty \bar{\omega} H(t) H(t)^T \Lambda(t, \bar{\omega}) d\bar{\omega} dt \right) f + f^T \left( \alpha \int_0^T \int_0^\infty (2\bar{\omega} \alpha \eta - 1) H(t)^T \Lambda(t, \bar{\omega}) d\bar{\omega} dt \right) \right] + c.
\end{aligned}$$

Besides, we have  $\mathbb{E}_{Q_2}[\log \Pi(f)] = -\frac{1}{2} f^T \Sigma^{-1} f + f^T \Sigma^{-1} \mu + c$ . Therefore, using (23), we obtain that

$$\begin{aligned}
\log Q_1(f) &= -\frac{1}{2} \left[ f^T \left( \alpha^2 \sum_{i \in [N]} \mathbb{E}_{Q_2}[\omega_i] H(T_i) H(T_i)^T + \alpha^2 \int_0^T \int_0^\infty \bar{\omega} H(t) H(t)^T \Lambda(t, \bar{\omega}) d\bar{\omega} dt + \Sigma^{-1} \right) f \right. \\
&\quad \left. - f^T \left( \alpha \sum_{i \in [N]} (2\mathbb{E}_{Q_2}[\omega_i] \alpha \eta + 1) H(T_i)^T + \alpha \int_0^T \int_0^\infty (2\bar{\omega} \alpha \eta - 1) H(t)^T \Lambda(t, \bar{\omega}) d\bar{\omega} dt + 2\Sigma^{-1} \mu \right) \right] + c \\
&=: -\frac{1}{2} (f - \tilde{\mu})^T \tilde{\Sigma}^{-1} (f - \tilde{\mu}) + c,
\end{aligned}$$

therefore  $Q_1(f)$  is a normal distribution with mean vector  $\tilde{\mu}$  and covariance matrix  $\tilde{\Sigma}$  given by

$$\tilde{\Sigma}^{-1} = \alpha^2 \sum_{i \in [N]} \mathbb{E}_{Q_2}[\omega_i] H(T_i) H(T_i)^T + \alpha^2 \int_0^T \int_0^\infty \bar{\omega} H(t) H(t)^T \Lambda(t, \bar{\omega}) d\bar{\omega} dt + \Sigma^{-1}, \quad (42)$$

$$\tilde{\mu} = \frac{1}{2} \tilde{\Sigma} \left[ \alpha \sum_{i \in [N]} (2\mathbb{E}_{Q_2}[\omega_i] \alpha \eta + 1) H(T_i)^T + \alpha \int_0^T \int_0^\infty (2\bar{\omega} \alpha \eta - 1) H(t)^T \Lambda(t, \bar{\omega}) d\bar{\omega} dt + 2\Sigma^{-1} \mu \right]. \quad (43)$$

For  $Q_2(\omega, \bar{N})$ , we first note that using (24) and (41), we have  $Q_2(\omega, \bar{N}) = Q_{21}(\omega) Q_{22}(\bar{N})$ . Using the same computation as Donner and Opper [2019] Appendices B and D, one can then show that

$$\begin{aligned}
Q_{21}(\omega) &= \prod_{i \in [N]} p_{PG}(\omega_i | 1, \underline{\lambda}_T), \\
\underline{\lambda}_t &= \sqrt{\mathbb{E}_{Q_1}[\tilde{\lambda}_t(f)^2]} = \alpha^2 \sqrt{H(t)^T \tilde{\Sigma} H(t) + (H(t)^T \tilde{\mu})^2 - 2\eta H(t)^T \tilde{\mu} + \eta^2}, \quad \forall t \in [0, T],
\end{aligned}$$

and that  $Q_{22}$  is a marked Poisson point process measure on  $[0, T] \times \mathbb{R}^+$  with intensity

$$\begin{aligned}
\Lambda(t, \bar{\omega}) &= \theta e^{\mathbb{E}_{Q_1}[\eta(\bar{\omega}, -\tilde{\lambda}_t(f))]} p_{PG}(\bar{\omega}; 1, 0) = \theta \frac{\exp(-\frac{1}{2} \mathbb{E}_{Q_1}[\tilde{\lambda}_t(f)])}{2 \cosh \frac{\tilde{\lambda}_t(f)}{2}} p_{PG}(\bar{\omega} | 1, \underline{\lambda}_t(f)) \\
&= \theta \sigma(-\underline{\lambda}_t) \exp \left\{ \frac{1}{2} (\underline{\lambda}_t(f) - \mathbb{E}_{Q_1}[\tilde{\lambda}_t(f)]) \right\} p_{PG}(\bar{\omega} | 1, \underline{\lambda}_t) \\
\mathbb{E}_{Q_1}[\tilde{\lambda}_t(f)] &= \alpha (H(t)^T \tilde{\mu} - \eta).
\end{aligned}$$

Therefore, we have that

$$\mathbb{E}_{Q_1}[\omega_i] = \frac{1}{2 \underline{\lambda}_{T_i}} \underline{\lambda}_{T_i}, \quad \forall i \in [N].$$

## C.2 Analytic form of the ELBO

In this section, we provide the derivation of the  $ELBO(\hat{Q}_s)$  in our adaptive mean-field variational algorithm, Algorithm 2, for each  $s = (\delta, D)$ . For ease of expositions, we will drop the subscript  $s$ . From (28), we have

$$\begin{aligned}
ELBO(\hat{Q}) &= \mathbb{E}_{\hat{Q}} \left[ \log \frac{p(f, \omega, \bar{N}, N)}{\hat{Q}_1(f) \hat{Q}_2(\omega, \bar{N})} \right] \\
&= \mathbb{E}_{Q_2} [-\log \hat{Q}_2(\omega, \bar{N})] + \mathbb{E}_{Q_2} [\mathbb{E}_{\hat{Q}_1} [\log p(f, \omega, \bar{N}, N)]] + \mathbb{E}_{\hat{Q}_1} [-\log \hat{Q}_1(f)].
\end{aligned}$$

Now using the notation of Section 4.3, we first note that defining  $K(t) := H(t)H(t)^T$ , we have that

$$\begin{aligned}\mathbb{E}_{\hat{Q}_1}[\tilde{\lambda}_{T_i}(f)^2] &= \text{tr}(K(t)\tilde{\Sigma}) + \tilde{\mu}^T K(t)\tilde{\mu} \\ \mathbb{E}_{\hat{Q}_1}[\log \mathcal{N}(f; \mu, \Sigma)] &= -\frac{1}{2}\text{tr}(\Sigma^{-1}\tilde{\Sigma}) - \frac{1}{2}\tilde{\mu}^T \Sigma^{-1}\tilde{\mu} + \tilde{\mu}^T \Sigma^{-1}\mu - \frac{1}{2}\mu^T \Sigma^{-1}\mu - \frac{1}{2}\log |2\pi\Sigma|.\end{aligned}$$

Moreover, we have

$$\mathbb{E}_{\hat{Q}_1}[\log \hat{Q}_1(f)] = -\frac{|m|}{2} - \frac{1}{2}\log |2\pi\tilde{\Sigma}|.$$

Using that for any  $c > 0$ ,  $p_{PG}(\omega; 1, c) = e^{-c^2\omega/2} \cosh(c/2)p_{PG}(\omega; 1, 0)$ , we also have

$$\begin{aligned}\mathbb{E}_{\hat{Q}_2}[-\log \hat{Q}_{2D}(\omega, \bar{N})] &= \sum_k \sum_{i \in [N_k]} -\mathbb{E}_{\hat{Q}_2}[\log p_{PG}(\omega_i^k, 1, 0)] + \frac{1}{2}\mathbb{E}_{\hat{Q}_2}[\omega_i^k]\mathbb{E}_{\hat{Q}_1}[\tilde{\lambda}_{T_i}(f)^2] - \log \cosh\left(\frac{\lambda_{T_i}(f)}{2}\right) \\ &\quad - \int_{t=0}^T \int_0^{+\infty} [\log \Lambda(t, \bar{\omega})]\Lambda(t, \bar{\omega})d\bar{\omega}dt + \int_{t=0}^T \int_0^{+\infty} \Lambda(t, \bar{\omega})d\bar{\omega}dt \\ &= \sum_k \sum_{i \in [N_k]} -\mathbb{E}_{\hat{Q}_2}[\log p_{PG}(\omega_i^k, 1, 0)] + \frac{1}{2}\mathbb{E}_{\hat{Q}_2}[\omega_i^k]\mathbb{E}_{\hat{Q}_{1D}}[\tilde{\lambda}_{T_i}(f)^2] - \log \cosh\left(\frac{\lambda_{T_i}(f)}{2}\right) \\ &\quad - \int_{t=0}^T \int_0^{+\infty} \left[ \log \theta_k - \frac{1}{2}\mathbb{E}_{\hat{Q}_1}[\tilde{\lambda}_{T_i}(f)] - \log 2 - \log \cosh\left(\frac{\lambda_{T_i}(f)}{2}\right) - \frac{1}{2}\mathbb{E}_{\hat{Q}_{1D}}[\tilde{\lambda}_{T_i}(f)^2]\bar{\omega} \right. \\ &\quad \left. + \log \cosh\left(\frac{1}{2}\lambda_{T_i}(f)\right) + \log p_{PG}(\bar{\omega}; 1, 0) - 1 \right] \Lambda^k(t)p_{PG}(\bar{\omega}; 1, \lambda_{T_i}(f))d\bar{\omega}dt \\ &= \sum_k \sum_{i \in [N_k]} -\mathbb{E}_{\hat{Q}_2}[\log p_{PG}(\omega_i^k, 1, 0)] + \frac{1}{2}\mathbb{E}_{\hat{Q}_2}[\omega_i^k]\mathbb{E}_{\hat{Q}_{1D}}[\tilde{\lambda}_{T_i}(f)^2] - \log \cosh\left(\frac{\lambda_{T_i}(f)}{2}\right) \\ &\quad - \int_{t=0}^T \left[ \log \theta_k - \frac{1}{2}\mathbb{E}_{\hat{Q}_1}[\tilde{\lambda}_{T_i}(f)] - \log 2 - \frac{1}{2}\mathbb{E}_{\hat{Q}_1}[\tilde{\lambda}_{T_i}(f)^2]\mathbb{E}_{\hat{Q}_2}[\bar{\omega}] - 1 \right] \Lambda^k(t)dt \\ &\quad - \int_{t=0}^T \int_0^{+\infty} \log p_{PG}(\omega; 1, 0)\Lambda^k(t)p_{PG}(\omega; 1, \lambda_{T_i}(f))d\omega dt.\end{aligned}$$

$$\text{with } \Lambda^k(t) = \theta_k \int_0^{+\infty} \Lambda^k(t, \bar{\omega})d\bar{\omega} = \frac{e^{-\frac{1}{2}\mathbb{E}_{\hat{Q}_1}[\tilde{\lambda}_{T_i}(f)]}}{2 \cosh\left(\frac{\lambda_{T_i}(f)}{2}\right)}.$$

$$\begin{aligned}\mathbb{E}_{\hat{Q}_2}[\mathbb{E}_{\hat{Q}_1}[\log p(f_k, \omega, \bar{N}, N)]] &= \sum_k \sum_{i \in [N_k]} \left\{ \log \theta_k + \mathbb{E}_{\hat{Q}_2}[\mathbb{E}_{\hat{Q}_1}[g(\omega_i^k, \tilde{\lambda}_{T_i}(f))] + \log p_{PG}(\omega_i^k; 1, 0)] \right\} \\ &\quad + \sum_k \log \theta_k + \mathbb{E}_{\hat{Q}_2}[\mathbb{E}_{\hat{Q}_1}[g(\bar{\omega}_i, -\tilde{\lambda}_{T_i}(f))] + \log p_{PG}(\bar{\omega}_i; 1, 0)] + \mathbb{E}_{\hat{Q}_1}[\log \mathcal{N}(f_k; \mu_k, \Sigma_k)] \\ &= \sum_k \sum_{i \in [N_k]} \log \theta_k - \log 2 - \frac{1}{2}\mathbb{E}_{\hat{Q}_1}[\tilde{\lambda}_{T_i}(f)^2]\mathbb{E}_{\hat{Q}_2}[\omega_i^k] + \frac{1}{2}\mathbb{E}_{\hat{Q}_1}[\tilde{\lambda}_{T_i}(f)] + \mathbb{E}_{\hat{Q}_2}[\log p_{PG}(\omega_i^k; 1, 0)] \\ &\quad + \int_0^T \int_0^{+\infty} \left[ \log \theta_k - \log 2 - \frac{1}{2}\mathbb{E}_{\hat{Q}_1}[\tilde{\lambda}_{T_i}(f)^2]\bar{\omega} - \frac{1}{2}\mathbb{E}_{\hat{Q}_1}[\tilde{\lambda}_{T_i}(f)] + \log p_{PG}(\bar{\omega}; 1, 0) \right] \Lambda^k(t)p_{PG}(\omega; 1, \lambda_{T_i}(f))d\omega dt \\ &\quad + \mathbb{E}_{\hat{Q}_1}[\log \mathcal{N}(f_k; \mu_k, \Sigma_k)] - \theta_k T \\ &= \sum_k \sum_{i \in [N_k]} \log \theta_k - \log 2 - \frac{1}{2}\mathbb{E}_{\hat{Q}_1}[\tilde{\lambda}_{T_i}(f)^2]\mathbb{E}_{\hat{Q}_2}[\omega_i^k] + \frac{1}{2}\mathbb{E}_{\hat{Q}_1}[\tilde{\lambda}_{T_i}(f)] + \mathbb{E}_{\hat{Q}_2}[\log p_{PG}(\omega_i^k; 1, 0)] \\ &\quad + \int_0^T \left[ \log \theta_k - \log 2 - \frac{1}{2}\mathbb{E}_{\hat{Q}_1}[\tilde{\lambda}_{T_i}(f)^2]\mathbb{E}_{\hat{Q}_2}[\bar{\omega}] - \frac{1}{2}\mathbb{E}_{\hat{Q}_1}[\tilde{\lambda}_{T_i}(f)] \right] \Lambda^k(t)dt \\ &\quad + \int_0^T \int_0^{+\infty} \log p_{PG}(\bar{\omega}; 1, 0)\Lambda^k(t)p_{PG}(\bar{\omega}; 1, \lambda_{T_i}(f))d\bar{\omega}dt + \mathbb{E}_{\hat{Q}_1}[\log \mathcal{N}(f_k; \mu_k, \Sigma_k)] - \theta_k T.\end{aligned}$$

Therefore, with  $c > 0$  a constant that does not depend on the size of the model, with zero mean prior  $\mu = 0$ ,

$$\begin{aligned} ELBO(\hat{Q}) &= \frac{|m|}{2} + \frac{1}{2} \log |2\pi\tilde{\Sigma}| - \frac{1}{2} \text{tr}(\Sigma^{-1}\tilde{\Sigma}) - \frac{1}{2} \tilde{\mu}^T \Sigma^{-1} \tilde{\mu} - \frac{1}{2} \log |2\pi\Sigma| \\ &+ \sum_k \sum_{i \in [N_k]} \log \theta_k - \log 2 + \frac{\mathbb{E}_{\hat{Q}_i} [\tilde{\lambda}_{T_i}^k(f)]}{2} - \log \cosh \left( \frac{\tilde{\lambda}_{T_i}^k(f)}{2} \right) \\ &+ \int_{t=0}^T \int_0^{+\infty} \Lambda(t, \bar{\omega}) d\bar{\omega} dt - \theta_k T. \end{aligned}$$

### C.3 Gibbs sampler

From the augmented posterior  $\Pi_A(f, \omega, \bar{N})$  defined in (21) and using the Gaussian prior family described in Section 4.2, similar computation as Appendix C.1 can provide analytic forms of the conditional posterior distributions  $\Pi_A(f|\omega, \bar{N}, N)$ ,  $\Pi_A(\omega|N, f)$  and  $\Pi_A(\bar{N}|f, N)$ . This allows to design a Gibbs sampler algorithm that sequentially samples the parameter  $f$ , the latent variables  $\omega$  and Poisson process  $\bar{N}$ . With the notation of Appendix C.1, such procedure can be defined as

For every  $k \in [K]$ ,

(Sample latent variables)  $\omega_i^k | N, f_k \sim p_{PG}(\omega_i^k; 1, \tilde{\lambda}_{T_i}^k(f))$ ,  $\forall i \in [N_k]$

$\tilde{N}^k | f_k$ , a Poisson process on  $[0, T]$  with intensity  $\Lambda^k(t, \bar{\omega}) = \theta_k \sigma(-\tilde{\lambda}_t^k(f)) p_{PG}(\bar{\omega}; 1, \tilde{\lambda}_t^k(f))$

(Update hyperparameters)  $R_k = \tilde{N}^k[0, T]$

$H_k = [H_{N^k}, H_{\tilde{N}^k}]$ ,  $[H_{N^k}]_{id} = H_j(T_i^k)$ ,  $[H_{\tilde{N}^k}]_{jd} = H_b(\bar{T}_j^k)$ ,  $d = 0, \dots, KJ$ ,  $i \in [N_k]$ ,  $j \in [R_k]$

$D_k = \text{Diag}([\omega_i^k]_{i \in [N^k]}, [\bar{\omega}_j^k]_{j \in [R^k]})$

$\tilde{\Sigma}_k = [\beta^2 H_k D_k (H_k)^T + \Sigma^{-1}]^{-1}$

$\tilde{\mu}_k = \tilde{\Sigma}_k (H_k [\beta v_k + \beta^2 \eta u_k] + \Sigma^{-1} \mu)$ ,  $v_k = 0.5[\mathbb{1}_{N_k}, -\mathbb{1}_{R_k}]$ ,  $u_k = [[\omega_i^k]_{i \in [N_k]}, [\bar{\omega}_j^k]_{j \in [R_k]}]$

(Sample parameter)  $f_k | N, \tilde{N}^k, \omega^k \sim \mathcal{N}(f_k; \tilde{m}_k, \tilde{\Sigma}_k)$ .

These steps are summarised in Algorithm 4. We note that in this algorithm, one does not need to perform a numerical integration, however, sampling the latent Poisson process is computationally intensive. In our numerical experiments, we use the Python package `polygamma`<sup>3</sup> to sample the Polya-Gamma variables and a thinning algorithm to sample the inhomogeneous Poisson process.

## D Additional details and results of the simulation study

### D.1 Hyperparameters

We approximate integrals using the Gaussian quadrature method with  $n_{GQ} = 2^{D+1}T/A$  points in the univariate settings (Simulation 1,2 and 3). In Simulation 4, we set  $n_{GQ}$  to reduce the computational time.

### D.2 Self-inhibition scenarios of Simulation 4

<sup>3</sup><https://pypi.org/project/polygamma/>

---

**Algorithm 4** Gibbs sampler in the sigmoid Hawkes model with data augmentation

---

**Input:**  $N, n_{iter}, \mu, \Sigma$ .

**Output:** Samples  $S = (f_i)_{i \in [n_{iter}]}$  from the posterior  $\Pi_A(f|N)$ .

Precompute  $(H_k(T_i^k))_i, k \in [K]$ .

Initialise  $f \sim \mathcal{N}(f, \mu, \Sigma)$  and  $S = []$ .

**for**  $t \leftarrow 1$  to  $n_{iter}$  **do**

**for**  $k \leftarrow 1$  to  $K$  **do**

**for**  $i \leftarrow 1$  to  $N_k$  **do**

      Sample  $\omega_i^k \sim p_{PG}(\omega_i^k; 1, \tilde{\lambda}_{T_i^k}^k(f))$

**end for**

    Sample  $(\bar{T}_j^k)_{j=1, R_k}$  a Poisson temporal point process on  $[0, T]$  with intensity  $\theta_k \sigma(-\tilde{\lambda}_t^k(f))$

**for**  $j \leftarrow 1$  to  $R_k$  **do**

      Sample  $\bar{\omega}_j^k \sim p_{PG}(\omega; 1, \tilde{\lambda}_{\bar{T}_j^k}^k(f))$

**end for**

    Update  $\tilde{\Sigma}_k = [\beta^2 H_k D_k (H_k)^T + \Sigma^{-1}]^{-1}$

    Update  $\tilde{\mu}_k = \tilde{\Sigma}_k (H_k [\beta v_k + \beta^2 \eta u_k] + \Sigma^{-1} \mu)$

    Sample  $f_k \sim \mathcal{N}(f_k; \tilde{\mu}_k, \tilde{\Sigma}_k)$

**end for**

  Add  $f = (f_k)_k$  to  $S$ .

**end for**

---

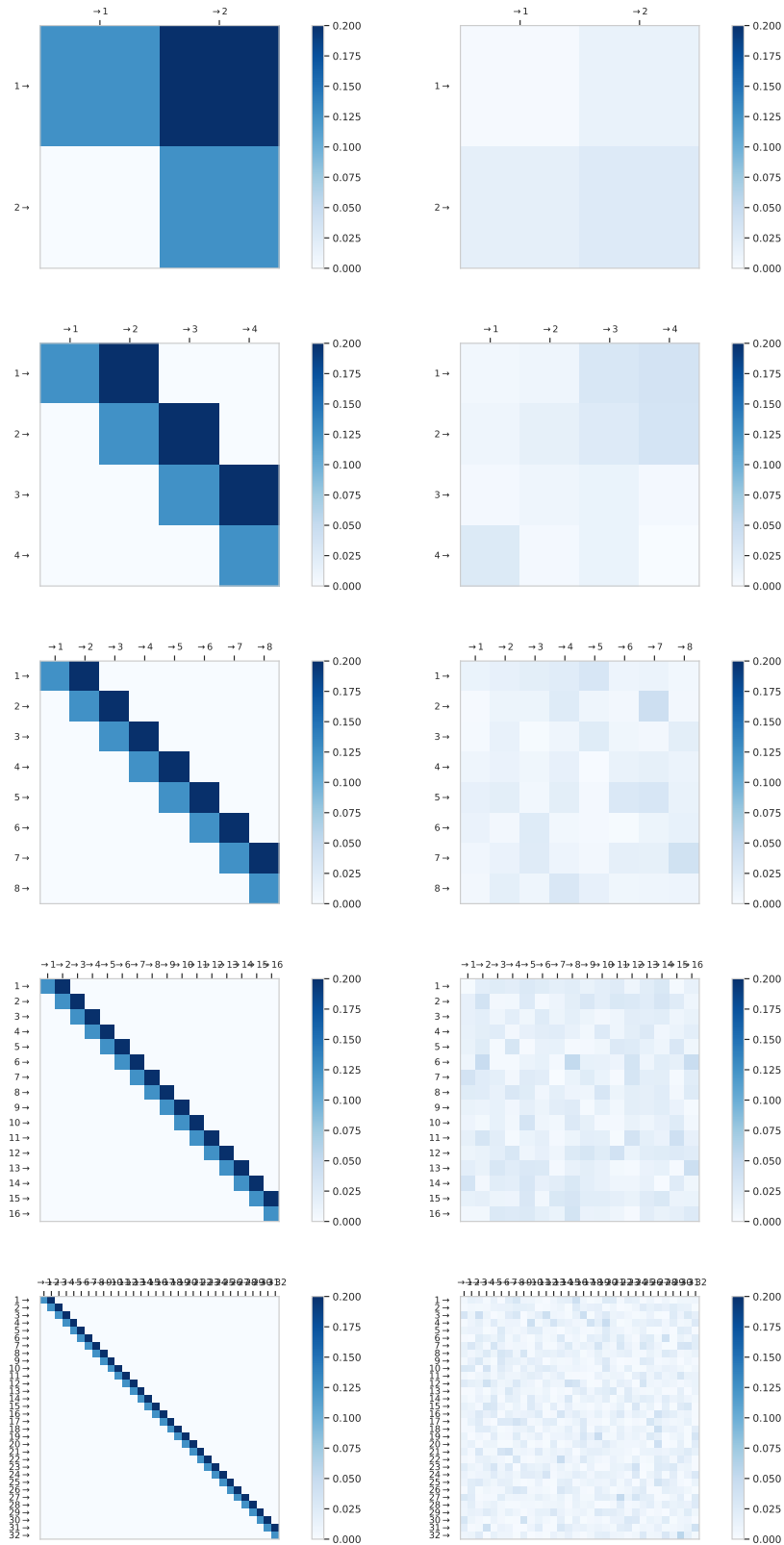


Figure 22: Heatmaps of the  $L_1$ -norms of the true parameter  $h_0$  (left column) and  $L_1$ -errors (right column) after the first step of Algorithm 3, in the Self-inhibition scenario of Simulation 4. The rows correspond to  $K = 2, 4, 8, 16, 32$ .

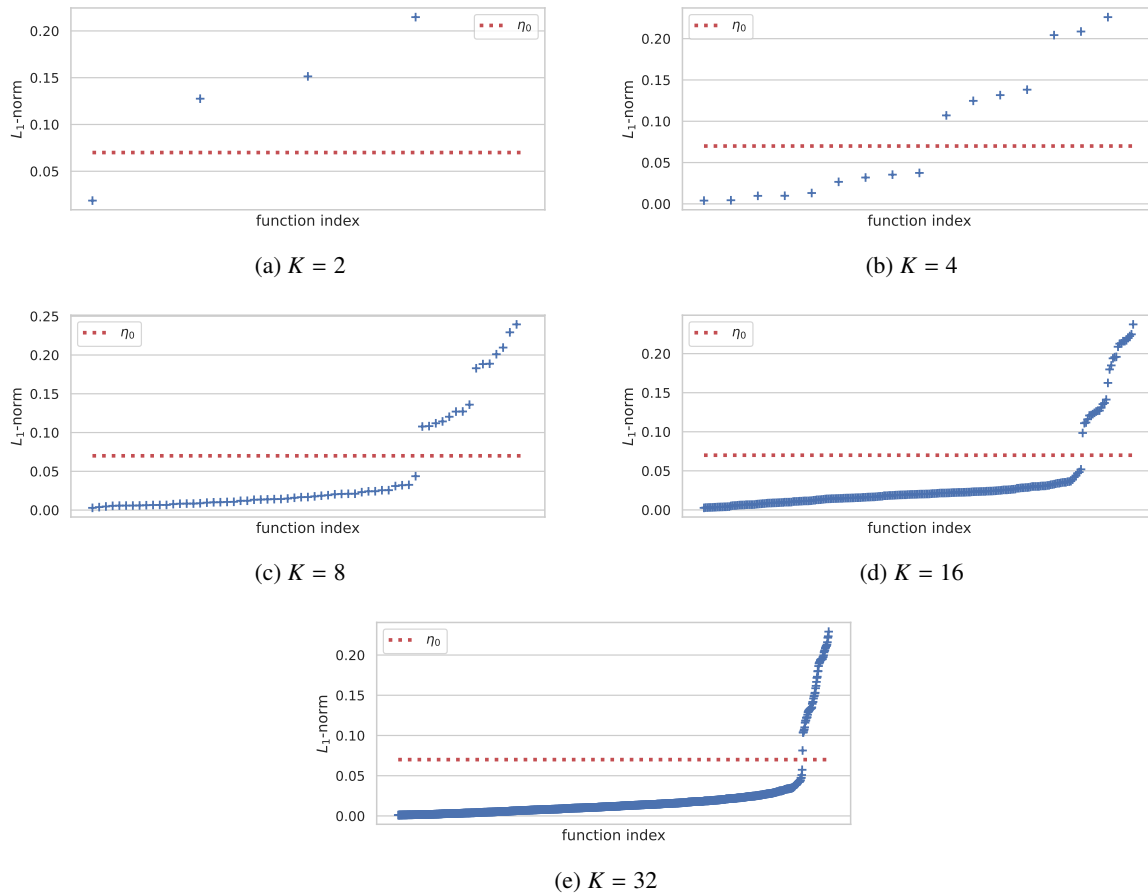


Figure 23: Estimated  $L_1$ -norms after the first step of Algorithm 3, plotted in increasing order, in the Inhibition scenario of Simulation 4, for the models with  $K = 2, 4, 8, 16, 32$ . The threshold in our algorithm  $\eta_0 = 0.07$  is plotted in dotted red line.

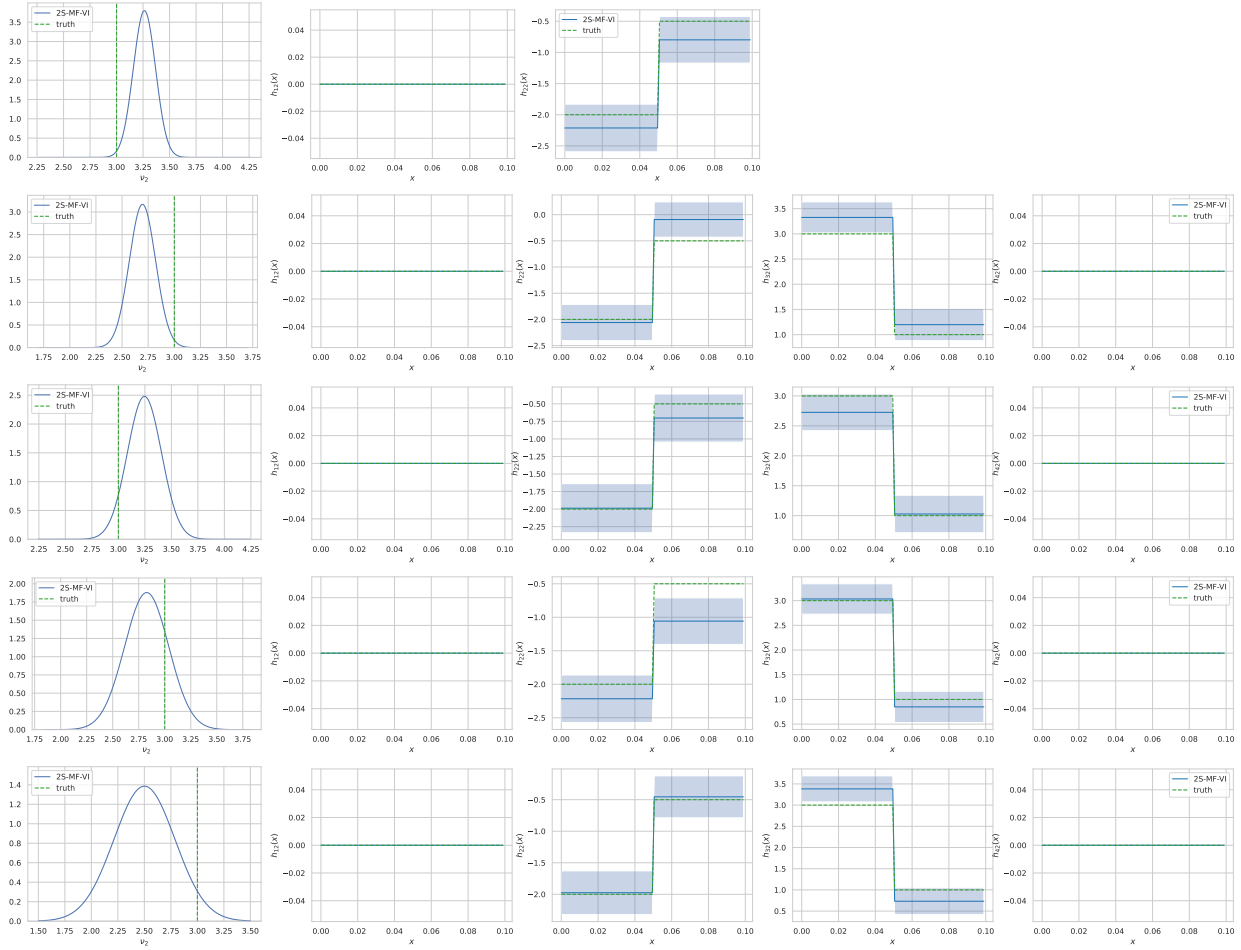


Figure 24: Mode variational posterior distributions on  $v_2$  (left column) and interaction functions  $h_{12}, h_{22}, h_{32}, h_{42}$  (second to last columns) in the Self-inhibition scenario and multivariate sigmoid models of Simulation 4, computed with our two-step mean-field variational (2S-MF-VI) algorithm (Algorithm 3). The different rows correspond to different multivariate settings  $K = 2, 4, 8, 16, 32$ .